Functionalized Cellulose Nanocrystals with Enhanced Mucoadhesive Properties

by

Fatemah Haji

A thesis
presented to the University of Waterloo
in fulfillment of the
thesis requirement for the degree of
Master of Applied Science
in
Chemical Engineering (Nanotechnology)

Waterloo, Ontario, Canada, 2021

AUTHOR'S DECLARATION

I hereby declare that I am the sole author of this thesis. This is a true copy of the thesis, including any required final revisions, as accepted by my examiners.

I understand that my thesis may be made electronically available to the public.

Abstract

Salmon farms across Canada face millions of dollars in losses every year due to sea lice infestations, which is a cause for growing concern. The current treatment methods are limited and have adverse effects on the aquatic ecosystem. Sustainable mucoadhesive drug delivery systems offer a viable alternative to existing treatments. The primary goal of the work presented in this thesis was to fabricate cellulose nanocrystal-based mucoadhesive materials for targeted delivery to fish mucosal membranes.

Cellulose nanocrystals (CNCs) can interact with mucin glycoproteins via hydrogen bonding. However, their mucoadhesive properties are weak compared to other well-known mucoadhesives. CNCs were modified with natural compounds such as tannic acid (CNC-TA) and catechol (CPC-cat) to enhance their mucoadhesive capabilities. The fabricated nanomaterials were colloidally stable at pH 7 and had small particle sizes ranging from 200 to 300 nm. Turbidity titrations and rheological measurements revealed that the modified CNCs had stronger interactions with mucin compared to pristine CNCs. Modification with tannic acid introduced additional functional groups for hydrogen bond formation, resulting in a slight (2.5-fold) increase in the $\eta_{relative}$ compared to CNCs. CPC-cat nanoparticles displayed the strongest mucoadhesion, with a 60-fold enhancement in the $\eta_{relative}$, which was attributed to electrostatic interactions and possible covalent bond formation. The enhanced mucoadhesive capabilities of these materials show great promise for sustainable drug delivery practices in aquaculture.

Acknowledgements

I would like to thank my supervisor, Dr. Michael Tam, for his support and guidance throughout the course of my degree here at the University of Waterloo. This work would not have been possible without his invaluable insight.

I would also like to thank my committee members, Dr. Brian Dixon and Dr. Boxin Zhao, for their time and effort through the defense process.

Thank you to Mishi Groh for training and helping me with the transmission electron microscope. Thank you also to Dr. Juewen Liu for access to his lab for zeta potential and size analysis. It would not have been possible to fully characterize my materials without these instruments.

I'd like to thank my friend, Ramis, for the constant motivation and for always being there to cheer me up. A special thanks to Iflah for her friendship and support throughout. To her, and to all my other labmates at the Tam group, thank you for a memorable two years!

Table of Contents

List of Figures

List of Tables

Chapter 1. Introduction

1.1 Project Motivation

The aquaculture industry has experienced enormous growth over the years owing to increases in the world population and a rising demand for protein. However, this development comes with associated problems, such as acidification of soils, destruction of natural ecosystems, and chemical contamination [1]. The rapid growth has also resulted in fish farms becoming increasingly crowded and prone to the outbreak of disease. Salmon louse (*Lepeophtheirus salmonis*) have emerged as a serious problem in the farming of Atlantic salmon in the Northern hemisphere [2]. Sea lice are crustacean parasites that attach to the mucus membrane and epidermis tissue of the host salmon, feeding off the blood, skin, and mucus. They can cause fish to become stressed, affecting their growth and performance, as well as making them more susceptible to secondary infections [3]. Outbreaks of sea lice can also cause significant declines in wild salmon populations and huge losses of production to fish farmers [4].

Several strategies have been employed to combat the sea lice outbreaks. In addition to general husbandry methods, such as using single year-class sites and area management coordination of stocking and fallowing, the administration of chemotherapeutants has been relied on to manage the sea lice infestations [5]. Depending on the therapeutant, the method of delivery is either bath treatments or in-feed treatment. However, these treatments are becoming less effective due to the increased resistance developed by sea lice to these treatments. Additionally, the chemical agents used are toxic and contaminate the aquatic environment in addition to posing a risk to non-target organisms due to drug leaching [6]. This work aims to

address the growing need for a cost-effective and environmentally friendly approach to sea lice management.

Nanotechnology has been recently employed in aquaculture for the delivery of nutrients and drugs. The use of nanocarriers offers several advantages over traditional treatment methods such as controlled delivery of the active agent, improved solubility of hydrophobic compounds, improved bioavailability, reduced frequency of dosage, and reduction in toxic effects [7]. Nanocarriers can also be functionalized to target the site of infection. The motivation for this work was to develop a nano-drug delivery system for the treatment of sea lice that utilizes sustainable and biocompatible materials, and is able to target fish mucosa, where the sea lice are present. Mucoadhesive drug delivery systems (MDDS) can be employed for the targeted delivery to the exterior mucosa of fish, which improves the bioavailability and efficacy. Additionally, since the MDDS remains adhered to the mucosa, non-target organisms remain protected.

Cellulose nanocrystals (CNCs) have shown enormous potential in various applications due to their excellent mechanical strength, abundant surface hydroxyl groups, colloidal stability, biocompatibility, and biodegradability [8]. The excellent physicochemical properties of CNCs make them promising for biomedical applications such as controlled and targeted drug delivery [9]. Additionally, a recent study has shown that CNCs display mucoadhesive properties [10], therefore they can be employed for the fabrication of a MDDS. However, the mucoadhesive performance of CNC is weak compared to second-generation mucoadhesive polymers that have been chemically modified to enhance their mucoadhesive properties. This work aims to enhance the mucoadhesive capabilities of CNCs by modifying them with

environmentally friendly phenolic compounds such as tannic acid and catechol. The modified CNCs can be employed as mucoadhesive nanocarriers for the treatment of sea lice in Atlantic salmon farms.

1.2 Project Goals and Outcomes

The overall goal of this project was to fabricate cellulose nanocrystal-based mucoadhesive materials with enhanced mucoadhesive abilities for applications in drug delivery. The project design and material selection were based on several criteria that were deemed essential to the final application. Criteria considered included colloidal stability, surface charge, particle size, and the presence of mucoadhesive functional groups. Colloidal stability is an important requirement for drug delivery applications. The formulations should have good storage stability as well as be able to disperse well in water without aggregating as this could interfere with the drug release process [11]. Taking this into account, the stability of the modified cellulose nanocrystals (CNCs) was monitored over several months, and zeta potential and particle sizes were measured to ensure they were in accordance with stability requirements. Additionally, zeta potential measurements allowed for the surface charge of the particles to be determined, which is an important parameter to consider to initiate strong interactions with mucous membranes. Particles with a positive surface charge are able to interact with the negatively charged mucous via electrostatic interactions. On the other hand, anionic materials typically interact via hydrogen bond formation or hydrophobic interactions. The surface charge of the modified CNCs was measured, and in the case of a negative surface charge, tests were performed to detect mucoadhesive functionalities. Furthermore, since the pores of the mucous membrane display size selectivity [12], it was important to ensure that the

final formulations had a small particle size. Typically, sizes between 100 and 500 nm are preferred for mucoadhesive nanoparticles. CNCs were chosen as a substrate due to their nanosize and the average particle sizes of the modified CNCs were optimized to ensure they met this criteria. All measurements were performed at neutral pH to mimic conditions in aquaculture farms as closely as possible. The material selection was driven by two main criteria. Firstly, the chosen materials were evaluated for mucoadhesive capabilities. Since the goal of the project was to enhance the mucoadhesion of CNCs, it was essential to ensure the chosen materials had well-documented mucoadhesive properties. The second criteria was for materials to be environmentally friendly in order to promote sustainable aquaculture practices and reduce environmental impact. To address this, materials derived from natural sources were preferred. The material selection is discussed in more detail in Section 2.4.

Two different approaches were taken to functionalize CNCs with phenolic groups to enhance mucoadhesion. The first part of this thesis focuses on the synthesis and characterization of these materials. Optimal mass ratios for each synthesis were determined and the colloidal stability at relevant pH values was evaluated. The aforementioned properties such as surface charge and particle size were measured and the presence of mucoadhesive functional groups was confirmed. The first approach taken was physical adsorption, where tannic acid was coated onto the cellulose nanocrystals to enhance the mucoadhesive properties. The second approach involved chemical modification, where chitosan was functionalized with catechol groups and then coated onto CNCs via electrostatic gelation.

The second section explores the mucoadhesive abilities and mechanisms of mucoadhesion for the two synthesized materials and compares them with pristine CNCs. The

mucoadhesive properties of the nanomaterials were analyzed using porcine mucin. Methods employed to evaluate the mucoadhesion included rheology, turbidimetric titrations and adhesive force measurement between mucin and the mucoadhesive polymers. These tests were performed in aqueous conditions at pH 7 to ensure adhesion would be able to occur when the particles were applied for fish treatment. It was found that the mucoadhesive capability was enhanced as compared to cellulose nanocrystals for both the materials, with the catechol-functionalized material having higher mucoadhesive performance compared to CNC coated with tannic acid. Investigation of the mechanisms of interaction with mucin revealed that tannic-acid coated CNCs displayed non-specific binding, such as hydrogen bonding while the catechol-bearing material was able to bind specifically by forming covalent bonds with functional groups on mucin in addition to non-specific electrostatic interactions.

1.3 Thesis Outline

This thesis consists of six chapters. The first chapter provides an introduction to the research project and summarizes the motivation and outcomes of this work. The second chapter reviews the recent literature on mucoadhesive materials in drug delivery, including physical and chemical modifications to enhance the mucoadhesion of well-known mucoadhesives, as well as methods to evaluate mucoadhesive properties. The materials chosen for this work including CNCs, tannic acid, chitosan, and catechol are also discussed in Chapter two. Chapter three details the physical modification of CNCs by coating them with tannic acid. Optimal synthesis conditions are explored and the characterization performed to confirm successful modification is presented. Chapter four discusses the functionalization of CNCs with the catechol group, including the optimal synthesis conditions and characterization performed.

Chapter five explores the mucoadhesive properties of the functionalized nanomaterials and evaluates the enhancement in their mucoadhesive ability compared to pristine CNCs. The mechanisms of interaction of the fabricated materials with mucin are also investigated in this chapter. The sixth chapter includes the project conclusions and the recommendations for future work.

Chapter 2. Literature Review

2.1 Introduction to Mucoadhesive Drug Delivery Systems (MDDS)

Conventional drug delivery systems are associated with an immediate release and rapid absorption of the active pharmaceutical ingredient (APIs). These systems have been found to have several limitations such as low bioavailability, and the need for higher dosage and more frequent application [13]. Adverse effects as serious as overdose have been associated with traditional dosage forms, prompting researchers to search for alternatives.

Controlled drug delivery systems were developed that are able to release drugs over a prolonged period, thus achieving the desired therapeutic effects at a lower drug dosage [14]. These novel systems make use of carrier technology such as microspheres, nanoparticles, and liposomes, which control the release and absorption characteristics of the APIs, and can further be functionalized to target specific biological sites [15]. However, the success of these systems is limited by their short residence time at the site of absorption. Mucoadhesion has been explored as a way to prolong the residence time by providing an intimate contact between the carrier and the absorbing membrane, thereby improving the bioavailability and promoting local and systemic effects [16].

2.1.1 Mucous Membrane

Mucous membranes or mucosae are tissue linings that cover the exterior surfaces of various internal cavities and canals such as the gastrointestinal, respiratory, buccal, nasal, and vaginal tracts [17]. The membrane comprises of single or multiple layers of epithelial cells and a sub-layer of connective tissue (*lamina propria*) as shown in the schematic in Figure 2-1A. Esophageal glands in multi-layered epithelia and goblet cells in single-layered epithelia are responsible for secreting mucus onto the outer epithelial layer, forming a protective barrier for

the underlying organs [18]. The secreted mucus layers are viscous gels comprising mostly of water (~95%), extracellular glycoproteins, lipids, and inorganic salts [19].

Mucin glycoproteins (Figure 2-1B) contained in the outer mucous layer provide the main structure-forming characteristics of the gel. Mucins comprise of a linear protein core which makes up 20% of their molecular mass and contains cysteine-rich terminal regions involved in disulphide bond formation. A highly glycosylated central region makes up the remaining 80%, which consists of partially branched carbohydrate chains and serine and threonine residues [20]. The glycoproteins have an overall negative charge at physiological pH values due to the presence of terminal sialic acid and sulphate groups [21].

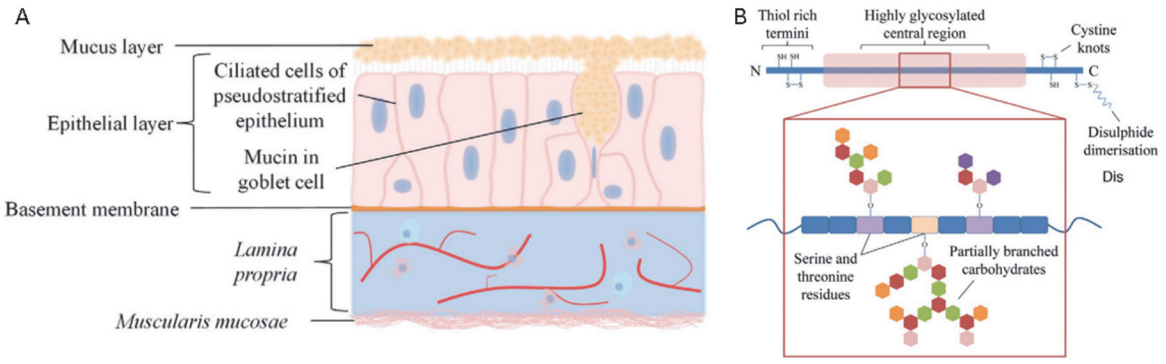

Figure 2-1. Schematic representation of A) mucous membrane, and B) mucin glycoprotein. (adapted from Brannigan et al. [17])

2.1.2 Mechanisms of Mucoadhesion

The phenomenon of "mucoadhesion" refers to the adherence of natural or synthetic polymers to mucosal membranes for extended periods of time with the help of interfacial forces [18]. The mechanism by which this occurs is generally divided into two stages, namely the

contact stage and the consolidation stage (Figure 2-2). During the contact stage, an intimate contact (wetting) occurs between the mucous membrane and the mucoadhesive polymer. This is followed by the consolidation stage, where various physical or chemical interactions take place at the interface, resulting in interpenetration, which promotes the adhesion [22].

The process of mucoadhesion has been widely studied and numerous theories have been proposed to explain the fundamental mechanisms involved. Due to the relatively complex nature of the process, it is likely that the phenomenon cannot be described by a single theory. The five main theories of mucoadhesion are briefly described below.

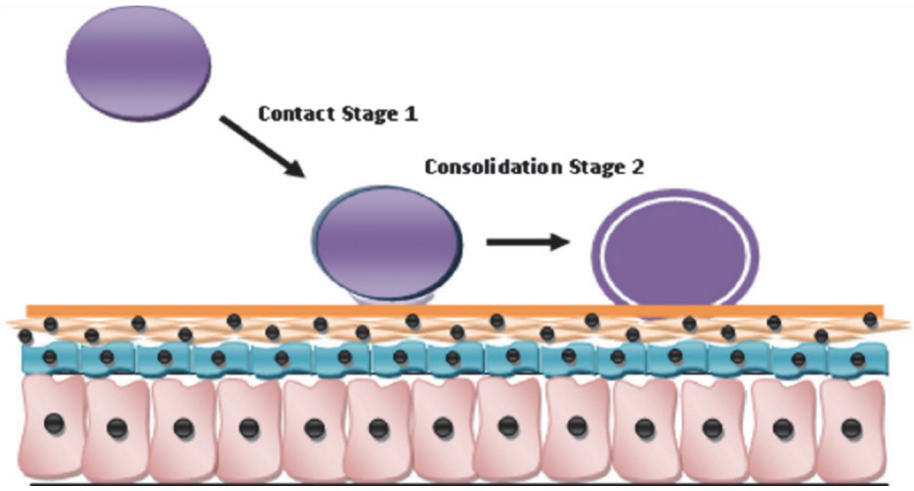

Figure 2-2. The two step basic mechanistic approach of mucoadhesion (adapted from Mansuri et al. [23])

2.1.2.1 Wettability Theory

The wettability theory is based on the ability of a mucoadhesive polymer to spread on the mucous membrane and is generally applied to low viscosity mucoadhesive systems. In order to spread, the mucoadhesive must overcome the surface tension present at the interface.

If there is adequate spreading, the mucoadhesive is able to penetrate into the surface deformations, harden and adhere to the mucus layer because of the changes in the interfacial energy [23]. The ability of the mucoadhesive to spread is given by the spreadability coefficient, S, which is related to the interfacial tensions (γ) by the following formula.

$$S=\gamma_{ML}-(\gamma_{PM}+\gamma_{PL});$$

where P=polymer, M=mucous, and L=liquid. The spreadability coefficient must be positive for mucoadhesion to occur.

2.1.2.2 Adsorption Theory

The adsorption theory states that after the initial contact, the mucoadhesive polymer adheres to the mucosal membrane due to the formation of primary or secondary chemical bonds acting between the atoms on the two surfaces [24]. Secondary bonds could include electrostatic interactions, van der Waal's forces, hydrogen bonding, and hydrophobic interactions, depending on the functional groups on the polymer backbone.

2.1.2.3 Electronic Theory

The electronic theory assumes that the electronic structures of the mucous membrane and the mucoadhesive polymer are different in character. Therefore, when the two surfaces come into contact with each other, a transfer of electrons occurs in order to balance the Fermi levels. As a result, an electric double layer is formed at the interface of the mucosal layer and the polymer, and the attractive forces across this layer hold the two components together [18].

2.1.2.4 Diffusion Theory

The diffusion theory suggests that the presence of a concentration gradient acts as a driving force for the diffusion of polymer chains into the mucin chains and vice versa. This inter-diffusion continues until an equilibrium penetration depth is reached. If there is sufficient penetration, an adhesive bond is formed between the two surfaces, which grows stronger with the degree of penetration [25]. The penetration depth can be increased by reducing the crosslinking density, increasing temperature or choosing longer polymer chains, all of which would improve the mucoadhesive capability of the polymer.

2.1.2.5 Fracture Theory

According to the fracture theory, the strength of the adhesive bond is directly related to the force required to separate the surfaces from each other. Longer polymer chains and a low degree of crosslinking have been found to result in greater fracture strength and stronger mucoadhesive bonds [23]. The fracture strength (σ) required to fully detach the two surfaces can be related to the Young's modulus of elasticity (E), the fracture energy (ε), and the critical crack length according to the following equation.

$$\sigma=\sqrt{E\varepsilon/L}$$

2.1.3 Materials for MDDS

Mucoadhesive drug delivery systems can be used to administer drugs through routes that are lined by mucosal layers including the buccal [26], vaginal [27], nasal [28], ocular [29], and gastrointestinal [30] tracts. Mucoadhesive polymers have been incorporated within drug formulations to promote adhesion to mucosal membranes, providing targeted and controlled delivery of APIs. Polymer characteristics such as molecular weight, chain length, degree of

cross-linking, concentration, and swelling ability affect their mucoadhesive abilities and are taken into consideration during the design of MDDS [31]. First-generation mucoadhesive polymers that bind non-specifically with mucosa can be further classified by their source, charge, hydrophilicity, and mechanism of mucoadhesion. Figure 2-3 provides an overview of the classification of various materials that are commonly employed for MDDS.

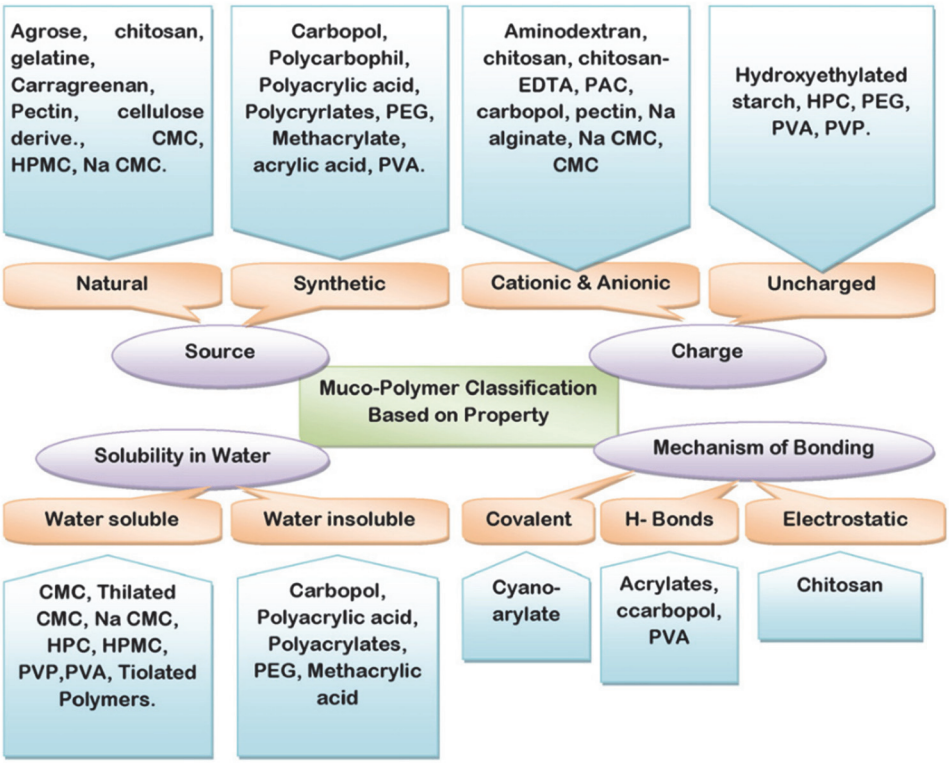

Figure 2-3. Classification of mucoadhesive polymers based on various properties (adapted from Mansuri et al. [23])

In terms of their sources, mucoadhesive polymers can be classified into synthetic or natural. In recent years, there has been an increased focus on the use of natural polymers such as chitosan, cellulose, pectin, and alginate due to their biocompatibility, biodegradability, and

low toxicity [32]. Further classification may be based on the presence of functional groups, as well as the surface charge, which determine the nature of the interaction between the mucous membrane and the polymer. Anionic polymers typically contain carboxyl and sulphate functional groups that can form strong hydrogen bonds with the mucin glycoproteins. Polyacrylic acid is the most common anionic mucoadhesive due to its high water solubility and minimal cytotoxicity [23]. Cationic polymers interact with mucosa primarily by electrostatic interactions. Chitosan, a widely occurring natural polysaccharide, is the most widely used cationic mucoadhesive. The positive surface charge, in addition to hydrogen bonding and hydrophobic interactions allows for chitosan to effectively and non-specifically bind to mucosal membranes [33]. There are also uncharged mucoadhesive polymers such as polyvinyl alcohol and polyvinyl pyrrolidone that have been utilized for MDDS, although they demonstrate much weaker mucoadhesive ability [23].

2.2 Strategies to Enhance Mucoadhesive Ability

The first-generation mucoadhesives discussed in the previous section can be chemically modified to create second-generation mucoadhesives that have enhanced mucoadhesive capabilities. Recent literature has reported different synthetic methodologies to conjugate polymeric materials with functional groups that are able to bind specifically to mucin proteins. Some of the most prominent strategies undertaken to enhance mucoadhesion are discussed here along with their reported limitations.

2.2.1 Thiol Functionalization

The conjugation of free thiol groups onto polymer backbones is the most commonly used strategy to enhance mucoadhesive performance. Thiol bearing polymers are able to form disulphide bonds with cysteine residues present on the surface of the mucosal membrane [34]. However, since thiols are prone to oxidation, unwanted cross-linking may occur, which can hinder their interaction with mucin [17].

Traditionally, thiol groups are conjugated onto first-generation mucoadhesives by sulfhydryl immobilization. The resulting "thiomers" may be cationic or anionic in nature, depending on the base polymer. Frequently used sulfhydryl immobilization routes involve carbodiimide coupling between amines and carboxylic acids or periodate treatment followed by reductive amination of a cysteamine Schiff-base adducts [17].

Anitha et al. developed thiolated chitosan nanoparticles using thioglycolic acid and chitosan by a carbodiimide coupling reaction for applications in mucoadhesive drug delivery (Figure 2-4). The degree of thiol substitution was found to be 60%, which significantly enhanced the mucoadhesive ability [35].

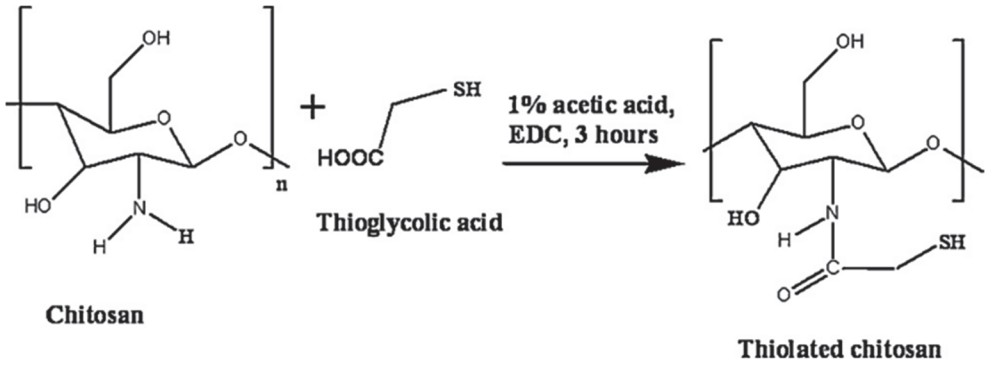

Figure 2-4. Reaction scheme for synthesis of thiolated chitosan (adapted from Anitha et al. [35])

Sharma et al. functionalized pectin, an anionic mucoadhesive, with thiol groups by esterification with thioglycolic acid in the presence of hydrochloric acid. The mucoadhesive properties of pectin and thiolated pectin beads were compared by performing a wash-off test with goat intestinal mucosa. It was found that thiolated pectin adhered to the mucosa for 5 hours compared to 2.5 hours for unmodified pectin, indicating enhanced mucoadhesive properties. Furthermore, release studies with metformin showed that thiolation did not significantly affect the drug release profile [36].

Khalid et al. prepared thiolated sodium alginate (TSA) by esterification with thioglycolic acid for the controlled release of metformin. TSA showed a greater increase in the dynamic viscosity after incubation in the mucus compared to sodium alginate (SA), indicating enhanced mucoadhesive properties. Wash-off tests showed that TSA had double the adherence to mucosa than SA due to disulphide bond formation. The TSA conjugates also showed increased swelling compared to the original polymer, which contributes towards stronger adherence to mucosa [37]. The key results from the study are summarized in Figure 2-5.

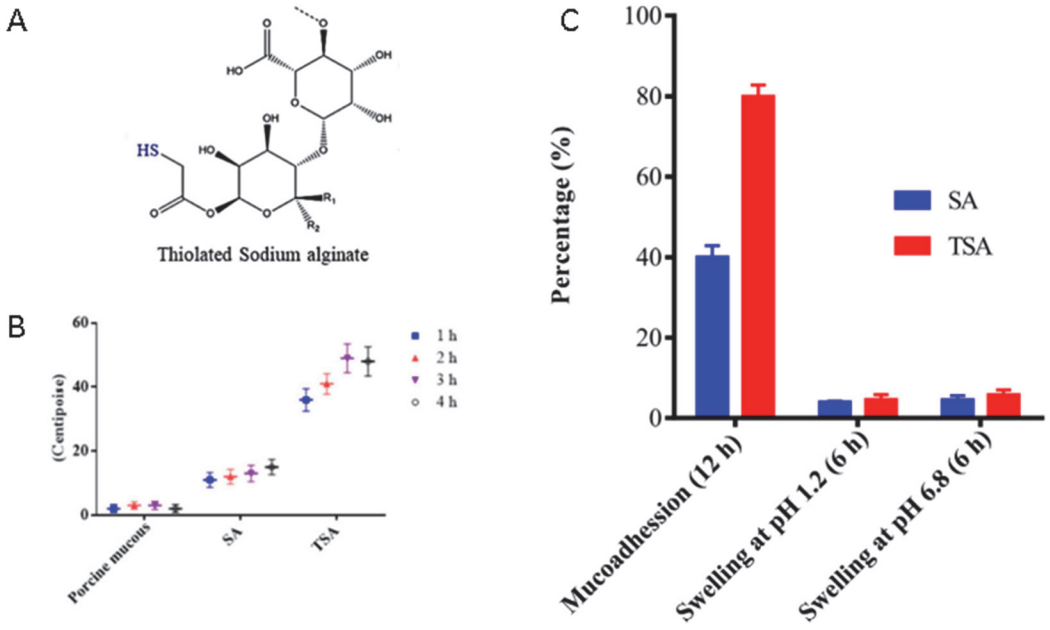

Figure 2-5. A) Chemical structure of TSA, B) Dynamic viscosity of SA and TSA after incubation in mucus, and C) %Mucoadhesion and %swelling of SA and TSA (adapted from Khalid et al. [37])

2.2.2 Catechol Functionalization

Catechol is found in nature as a side chain of L-3,4-dihydroxyphenylalinine (DOPA), an amino acid that is crucial in the underwater adhesion of mussels [38]. There has been an increased interest in the use of catechols (Figure 2-6) to enhance adhesive properties by chemical modification of natural and synthetic polymers. Catechols interact by forming strong covalent bonds with thiol and amine groups on mucin. However, they are prone to oxidation at physiological pH, which can result in color changes and a possible reduction in their mucoadhesive ability [39].

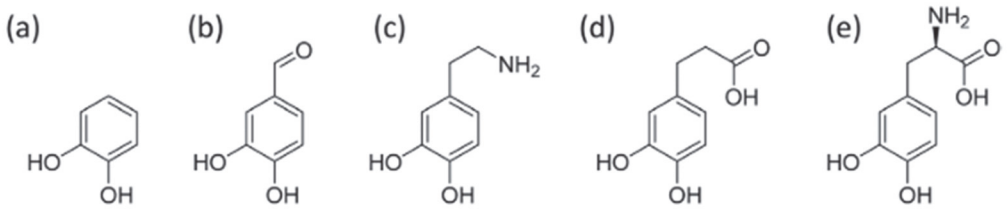

Figure 2-6. Examples of catechol-bearing molecules for modification of polymers; a) pyrocatechol, b) 3,4-dihydroxy benzaldehyde, c) dopamine, d) hydrocaffeic acid, and e) L-3,4-dihydroxyphenylalanine (adapted from Brannigan et al. [17])

The use of catechol has been mostly restricted to the enhancement of the mucoadhesive ability of chitosan (Cat-Chit). Synthetic routes to functionalize chitosan with catechol can involve amide bond formation with carboxylic acid-containing catechols through carbodiimide coupling chemistry or reductive amination of aldehyde-containing catechols [17]. The positively charged Cat-Chit formulations promote transient mucoadhesion by electrostatic forces followed by catechol-mediated covalent bond formation during the consolidation stage. This is discussed further in Section 2.4.

Research aimed at expanding the use of catechol to enhance the mucoadhesive abilities of other polymers has been conducted in recent years. Sahatsapan et al. developed catechol-functionalized alginate (Cat-Alg) nanoparticles as mucoadhesive carriers for treating bladder cancer. Wash-off tests showed that 45% of Cat-Alg nanoparticles remained adhered to porcine bladder tissue after 1 hour compared to 20% for alginate nanoparticles [40]. Pornpitchanarong et al. [41] synthesized catechol-functionalized hyaluronic acid (HAcat) by carbodiimide coupling and then combined it with cat-functionalized succinyl chitosan to prepare mucoadhesive nanoparticles for delivery of doxorubicin to oral cancer cells. The modified

nanoparticles showed superior mucoadhesive capability compared to unmodified particles and showed sustained release of the drug, indicating promise as a drug carrier for local treatment of oral cancer.

2.2.3 Acrylated Materials

Acrylated polymers have been highlighted as a novel class of mucoadhesive materials due to their ability to covalently bind with cysteine residues in mucin by Michael-type addition reactions (Figure 2-7). The first example of an acrylated mucoadhesive polymer, polyethylene glycol di-acrylate (PEG-DA), was reported by Davidovich-Pinhas and Bianco-Peled [42]. The terminal groups of polyethylene glycol (PEG) were reacted with acryloyl chloride under basic conditions. The mucoadhesive properties were found to be comparable to other second-generation mucoadhesives. Another novel mucoadhesive polymer, alginate-polyethylenglycol acrylate (alginate-PEGAc) was developed by the same group, which showed enhanced mucoadhesive capability compared to unmodified alginate as well as alginate-thiol [43].

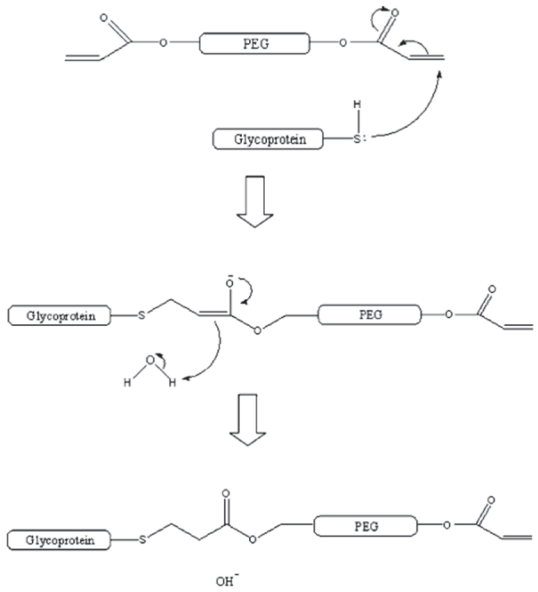

Figure 2-7. Schematic illustration of Michael type addition between PEG- DA molecule and a glycoprotein's thiol end group (adapted from Davidovich-Pinhas and Bianco-Peled [42] **)**

2.2.4 Boronate-bearing Materials

Boronic acid derivatives such as phenylboronic acid (PBA) and its derivatives have been reported as interesting functionalities to enhance mucoadhesion through interactions with the carbohydrate fragments of mucins. Boronate-bearing polymers show enhanced mucoadhesive abilities due to the formation of cyclic boronic ester linkages with 1,2-cis-diols [44]. Analogous to the catechol functionalization of chitosan, PBA derivatives can be grafted to polymer scaffolds by reductive amination and carbodiimide mediated coupling chemistry, achieving high levels of conjugation. However, there are possible limitations imposed on the mucoadhesive ability of these materials as the optimal pH required for boronate-sugar interactions is often above physiological ranges [17].

Liu et al. reported PBA-modified mucoadhesive nanoparticles to prolong the precorneal residence time of encapsulated drugs to treat eye diseases. The nanoparticles were formed from the self-assembly of block copolymers composed of poly (D, L-lactide) and Dextran, which were modified with 3-aminophenylboronic acid by reductive amination. The increased residence time revealed the potential of reducing the frequency of administration of drug with no adverse effects on efficacy [45].

Kolawole et al. reported on the synthesis of boronated chitosan by reacting chitosan with 4-carboxyphenylboronic acid. Tensile tests performed to evaluate the force of detachment and work of adhesion revealed that increasing the degree of boronation greatly strengthened the interaction with mucosa compared to unmodified chitosan [46].

2.2.5 Maleimide Functionalization

Maleimide functional groups have a similar mode of action to acrylates and thiomers, where they bind to the free thiols of mucin glycoproteins by maleimide-thiol click-like reactions. While there are only a few reported examples of maleimide-bearing polymers in the literature, these materials have been shown to exhibit excellent mucoadhesive capabilities. Not only do they show better storage stability compared to thiomers, but they also have no tendency for cross-linking, which enhances their mucoadhesive properties [17].

Sahatsapan et al. [47] synthesized a new generation mucoadhesive polymer, 6-maleimidohexanoic acid-grafted chitosan (MHA-CS) and evaluated its mucoadhesive ability compared to cysteine grafted chitosan (Cys-CS) and unmodified chitosan (CS). Rheological testing was used to evaluate the mucoadhesive behavior. MHA-CS mixtures with mucin showed the highest viscosity at a shear rate of 1 s^{-1}, exhibiting superior mucoadhesion

compared to Cys-CS, a well-known second-generation mucoadhesive. Mucoadhesive force measurements using a texture analyzer confirmed these results, with about 22-fold enhancement compared to CS, and about 4-fold enhancement compared to Cys-CS being observed for MHA-CS.

Shtenberg et al. [48] functionalized alginate with maleimide groups in a two-step synthesis. Thiolated alginate (alg-SH) was synthesized first and further modified with polyethylene glycol dimaleimide to obtain maleimide-functionalized alginate (alg-PEGM). Mucoadhesion studies by rotating cylinder and tensile assays showed a 2.8-fold enhanced retention time and a 3.6-fold enhanced detachment force compared to unmodified alginate. Alg-PEGM was also superior to the thiolated alginate, a modification frequently performed to enhance mucoadhesion. The synthesis schemes and key results are presented in Figure 2-8.

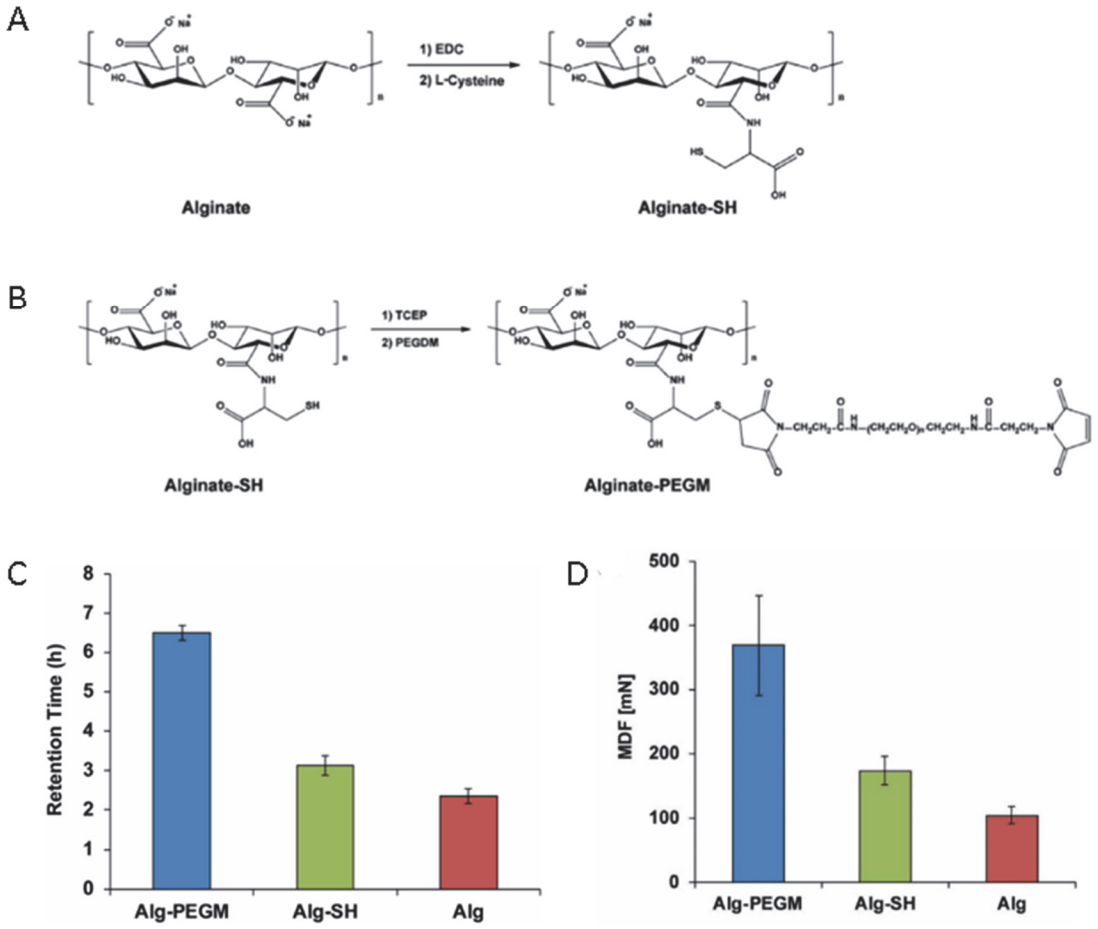

Figure 2-8. Synthesis schemes for A) Alg-SH, and B) Alg-PEGM; C) Retention time on porcine intestinal mucosa via rotating cylinder method, and D) Maximum detachment force measured by tensile assays (adapted from Shtenberg et al. [48])

2.2.6 Aminated Cellulose

While chitosan is the most widely utilized cationic mucoadhesive polymer, it displays weak mucoadhesion above pH 6. Cationic alternatives such as polyallyl amine or polyethylenimine are synthetic polymers that display severe toxicity. Due to the structural similarities of chitosan and cellulose, cationic modification of cellulose was proposed as a

viable alternative. Jelkmann et al. [49] synthesized aminated cellulose by oxidative cleavage of the 1,2-diols and subsequent reductive amination using ammonia (Figure 2-9A). The positively charged primary amine groups on the backbone of cellulose could interact via ionic interaction with the negatively-charged side chains of mucus independent of pH. Aminated cellulose showed up to a 14-fold increase in residence time on porcine intestinal mucosa as compared to chitosan. Up to a 7-fold enhancement was reported in the total work of adhesion compared to unmodified cellulose and a 2-fold enhancement compared to chitosan. The cellulose derivative with the highest degree of amination was comparable to chitosan in terms of the maximum detachment force. The results of the mucoadhesive tests are summarized in Figure 2-9. The synthesized aminocellulose is an interesting starting point for further development in the field of mucoadhesive drug delivery.

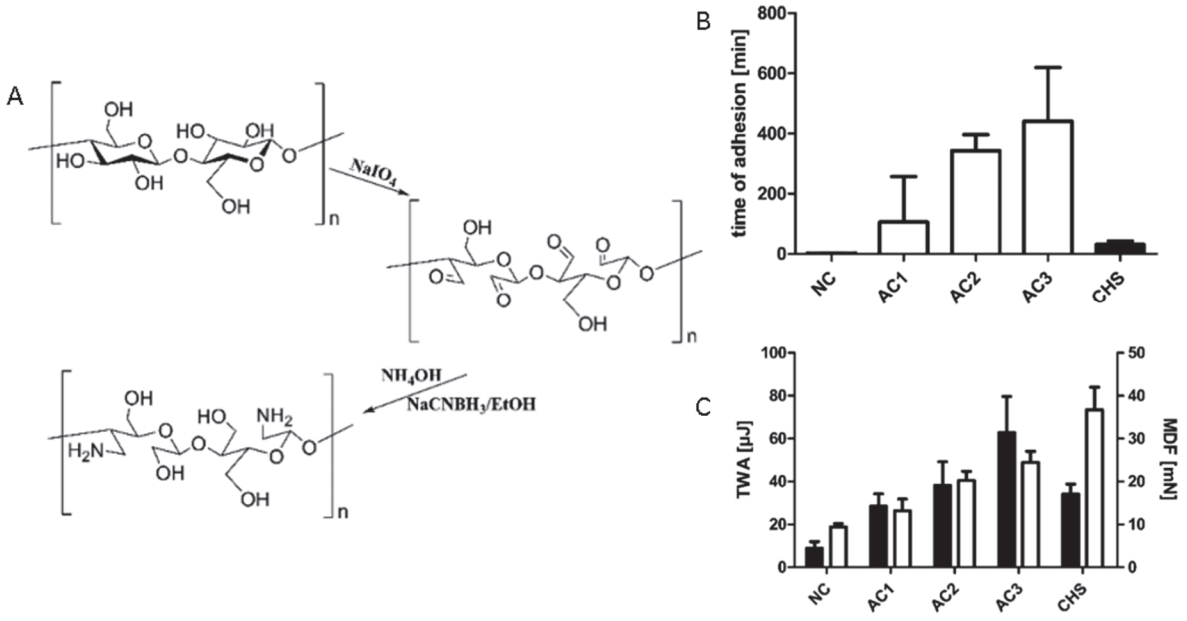

Figure 2-9. A) Two-step synthesis scheme for cationic cellulose derivative, B) Mucoadhesive properties of chitosan (CHS), native (NC), and cationic cellulose derivatives (AC) by the rotating cylinder method, and C) Total work of adhesion (black bars) and maximum detachment force (white bars) for CHS, NC and AC (adapted from Jelkmann et al. [49])

2.3 Methods to Evaluate Mucoadhesion

A crucial step in developing a new mucoadhesive system is verifying its ability to adhere to the mucus membrane. Several characterization methods have been developed by various research groups, and these can largely be classified into direct and indirect methods. Direct methods typically measure the force required to detach the mucoadhesive from a mucosal surface or the time that it can remain adhered to the substrate. This can include tensile assays to measure maximum detachment force and work of adhesion [50][51], rotating cylinder

tests to determine mucoadhesion time [52], continuous flow assays or wash-off tests [53], atomic force microscopy [54][55], and in vivo studies [56]. Indirect methods examine the interactions between the mucoadhesive polymer and mucin type glycoproteins. Rheological methods [57], spectroscopic methods [58][59], contact angle measurements [60], or zeta potential measurements [61] may be employed.

This study makes use of indirect methods due to easier access to mucin glycoproteins than fresh mucosal surfaces. The methods chosen were turbidimetric titration, rheology, and the Du Nouy ring method for measurement of adhesive force, and are detailed below.

2.3.1 Turbidimetric Titration

The turbidity of a mixture of mucin with a mucoadhesive polymer is a well-documented and simple indirect method to evaluate mucoadhesive properties. Polymers with a strong affinity to mucin particles cause aggregation, inducing the solutions to become turbid. The extent of interaction can be quantified by measuring the absorbance at a wavelength not characteristic to the absorbance of mucin particles or the polymer being tested, typically 500 or 600 nm [62][39]. The absorbance of mucin is generally measured as a control, and the turbidity, τ, can be calculated according to Equation 1 [63].

$$\tau = -\frac{1}{L}\ln\left(\frac{I}{I_0}\right) \qquad (1)$$

where L is the path length, I is the intensity of light transmitted through the sample, and I_0 is the intensity of light transmitted through the solvent.

The method involves preparation of polymer and mucin solutions in suitable buffers and combining them at different mass ratios. In the case of no interaction between mucin and

the polymer, the absorbance decreases with increasing amounts of polymer added, as the mucin is diluted further. However, if there is an interaction, the absorbance increases due to aggregate formation and increased scattering of light.

2.3.2 Rheological Methods

Hassan and Gallo [57] developed a simple procedure to assess the force of bioadhesion by monitoring viscometric changes in a system comprising porcine gastric mucin and polymers in solution. The viscosity of a mucin colloidal dispersion results from the resistance to flow exerted by chain entanglement and intermolecular interactions such as electrostatic interactions, hydrogen bonding, and hydrophobic interactions. Identical forces are involved in the process of mucoadhesion between mucin and polymers, allowing the mucoadhesive forces to be monitored by changes in viscosity. Chain interlocking, conformational changes, and chemical interactions between a mucoadhesive polymer and mucin increase the resistance to flow of a polymer-mucin mixture [64]. Thus, the viscosity of the mixture can be considered as a reflection of the strength of the mucoadhesive joint.

The proposed method involves preparing solutions of polymer, mucin, and a mixture of the two, and performing rheological measurements. The viscosity increase due to mucoadhesive interactions, $\eta_{enhancement}$, can be obtained from Equation 2 below.

$$\eta_{enhancement} = \eta_t - (\eta_m + \eta_p) \qquad (2)$$

where η_t is the viscosity of the mixture, and η_m and η_p are the individual viscosities of mucin and polymer respectively.

For the equation to be valid, the viscosities should be measured at the same concentration, temperature, time, and rate of shear. $\eta_{enhancement}$ is considered a direct estimate

of the force of mucoadhesion and at a constant rate of shear, it can be a useful parameter for comparisons between mucoadhesive materials.

2.3.3 Du Nouy Ring Method for Determination of Adhesive Force

The Du Nouy ring method (Figure 2-10), typically used to measure the surface tension of liquids, can be adapted to measure the adhesive force between a polymer film and a mucin solution. The film is placed on a moving stage while a droplet of solution is placed on a platinum ring, known as the Du Nouy ring. The stage is moved upwards to bring the film and ring into contact, until the solution penetrates the film to a specified depth, causing a small negative force to be registered. Mucoadhesive interactions between the polymer and the mucin are initiated when they come into contact. The stage is then moved downwards to separate the polymer from the mucin, causing the measured force to increase. The maximum force is registered when there is complete separation between the film and the polymer. This measured force is taken as the force of adhesion, and can be used as a measure of the strength of the mucoadhesive interaction.

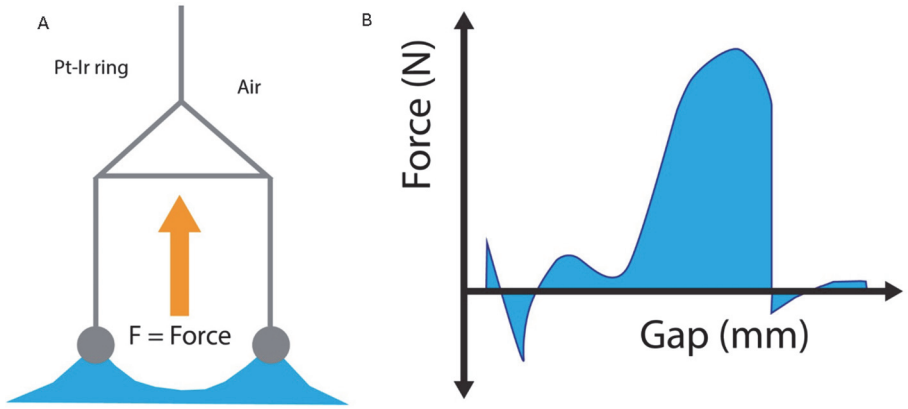

Figure 2-10. Schematic of A) Experimental setup, and B) Typical data for the Du Nouy ring method

2.4 Material Selection for this Work

2.4.1 Cellulose Nanocrystals (CNCs)

Cellulose nanocrystals (CNCs) are derived from cellulose, the most abundant and renewable polysaccharide found in nature. CNCs are extracted from pulp cellulose fibers by an acid hydrolysis process (Figure 2-11), which disrupts the hydrogen bonds and cleaves the amorphous domains leaving behind highly crystalline rod-like nanoparticles [8]. Acid hydrolysis can be performed using sulfuric acid or hydrochloric acid, however CNCs obtained from sulfuric acid hydrolysis show better dispersibility in aqueous suspensions due to the presence of negatively charged sulfate ester groups on their surface [65]. CNCs also possess excellent physical and chemical properties such as a high surface area (~250 m^2/g), a high tensile strength (7500 MPa), high stiffness, and an abundance of surface hydroxyl groups, which offer the potential for various types of chemical modifications. The desirable properties

of CNC have facilitated their application in various industries including biomedical, wastewater treatment, energy, and electronics.

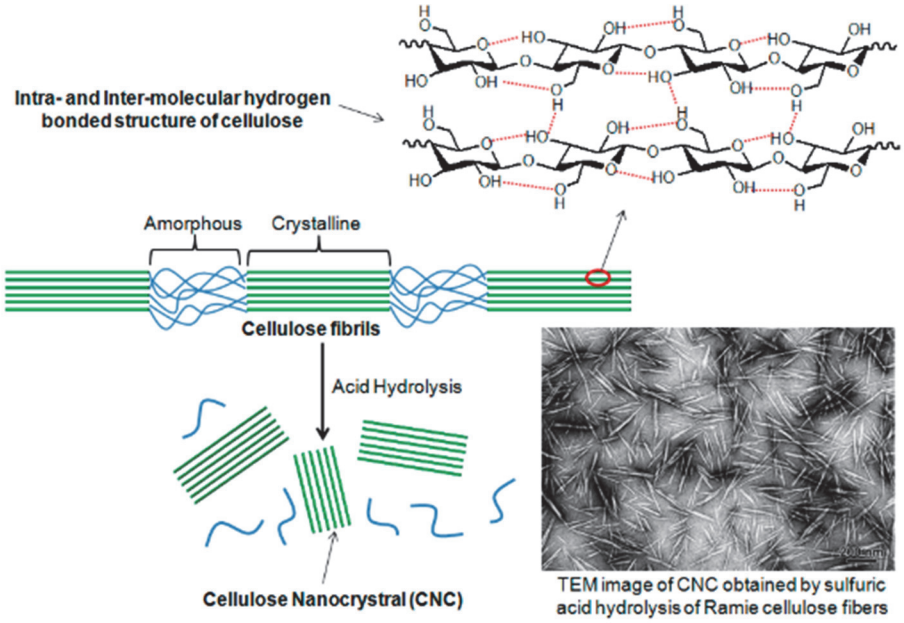

Figure 2-11. Preparation of CNC by acid hydrolysis and the corresponding TEM image (adapted from Chakrabarty and Teramoto [65])

A recent study by Lin et al. investigated the mucoadhesive potential of CNCs [10]. The interaction between CNCs and mucus was studied both in vitro (by rheology) and ex vivo (by flow-through assays). Confocal microscopy results from the flow-through assays showed that CNCs were able to homogenously spread on the mucosal tissue in simulated gastric and intestinal conditions (Figure 2-12A, B). Viscometric measurements (Figure 2-12C, D) revealed that CNC and mucin mixtures possessed an enhanced viscosity in simulated gastric and intestinal conditions at shear rates typical of digestion. The viscosity enhancements were comparable to other first-generation mucoadhesives like pectin and Carbomer.

While there have been several studies conducted on enhancing the mucoadhesive properties of polymers such as chitosan and alginate, there is little available literature on CNCs as mucoadhesives and strategies to enhance their mucoadhesion. Vakili et al. [66] grafted poly(acrylic acid) on CNCs at different ratios to prepare a mucoadhesive hydrogel with superior properties. This thesis aims to enhance the mucoadhesive ability of CNCs using natural materials instead of synthetic polymers.

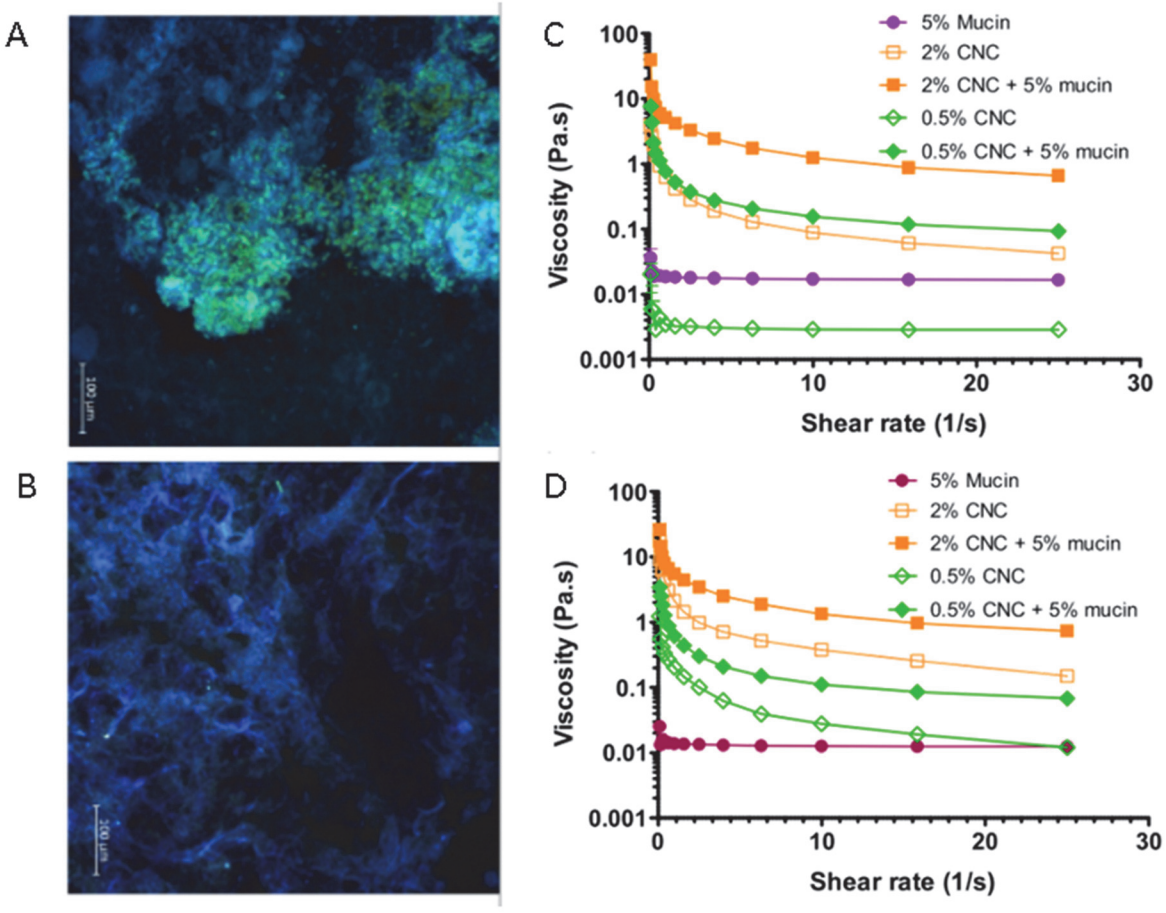

Figure 2-12. Confocal microscopy images of CNCs in A) Simulated gastric fluid (SGF), and B) Simulated intestinal fluid (SIF); Viscosity of various concentrations of CNCs and their mixtures with 5% mucin in C) SGF, and D) SIF (adapted from Lin et al. [10])

2.4.2 Tannic Acid

Tannins are plant polyphenols with anti-oxidant, anti-mutagenic, anti-carcinogenic, and anti-bacterial properties [67]. Tannic acid is a hydrolysable tannin with high affinity for various proteins such as proline-rich salivary proteins [68]. It contains pyrogallol functional groups with excellent wet-resistant properties [69]. Additionally, tannic acid is approved by the US Food and Drug Association, making it a good candidate for developing MDDS.

Shin et al. [62] studied the intermolecular interaction of tannic acid and mucin by turbidimetric titration at pH 2 and 7. Tannic acid displayed high mucoadhesion at neutral pH, indicated by the increasing turbidity of solutions due to the formation of complexes with mucin. However, in acidic conditions, the interaction between tannic acid and mucin was much weaker due to the hydrolysis of esters. Thus, the mucoadhesive abilities of tannic acid display pH dependency, which should be taken into account when incorporating it into drug delivery systems.

2.4.3 Chitosan-catechol

Chitosan (CS) is derived from chitin, the second most abundant natural polymer, by deacetylation. CS has been widely studied for biomedical applications such as antimicrobial, wound dressing, drug delivery, and bio imaging [33]. CS has also found applications in the field of mucoadhesive drug delivery, as one of the only natural cationic polymers that can interact with mucosal surfaces by electrostatic interactions. However, CS is limited by its low solubility above pH 6.3, where the amino groups on the surface are deprotonated and the positive surface charge is lost.

The grafting of phenolic acids on to the backbone of chitosan has been investigated as a strategy to improve its solubility at physiological pH without affecting its physicochemical properties. Phenolic compounds are grafted onto chitosan mainly by carbodiimide coupling reactions between the primary amino groups and carboxylic acids. Catechol, found in nature as a side chain of DOPA, has emerged as an excellent candidate for the modification of chitosan. Kim et al. functionalized chitosan with catechol (Chi-C) to prepare a novel polymer with long-lasting mucoadhesive properties [39]. The adherence of Chi-C to mucosa at pH 7 was vastly improved compared to chitosan. The mechanism of interaction of Chi-C with mucin is summarized in Figure 2-14. The catechol group can form covalent linkages with amine and cysteine residues of mucin in the consolidation stage, allowing it to remain adhered to mucosal layers for extended periods of time. The enhanced mucoadhesion of Chi-C has been utilized in this work to further enhance the mucoadhesive ability of CNCs.

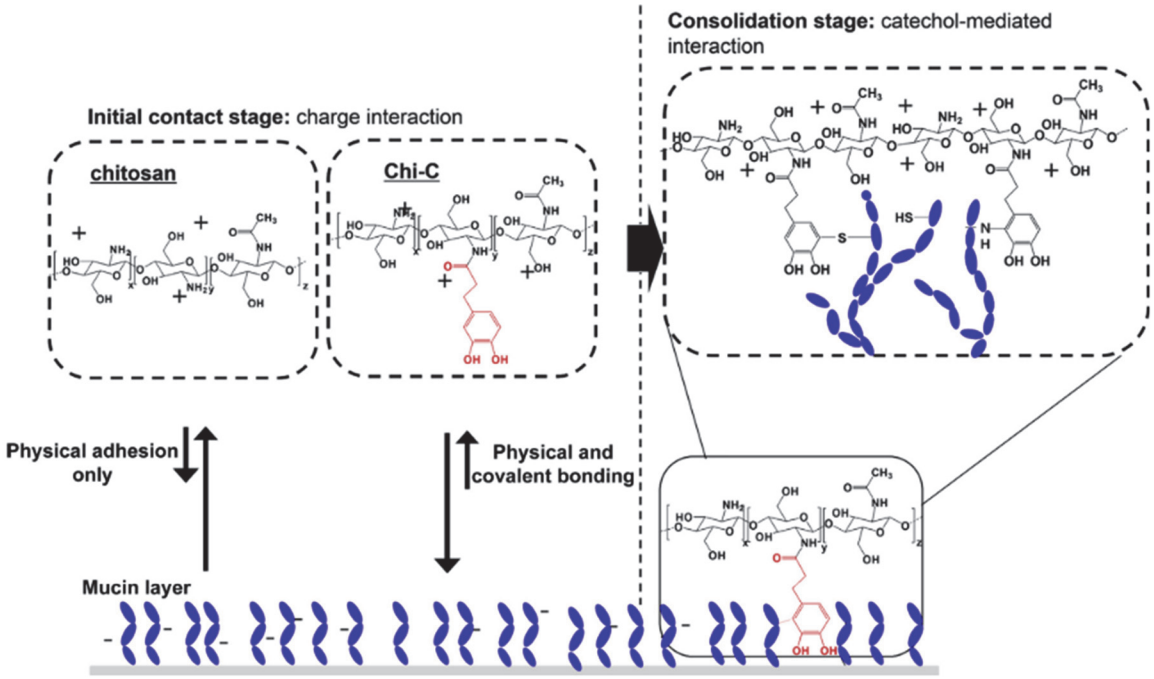

Figure 2-13. A schematic summary of the physicochemical differences in mucin binding between chitosan and Chi-C (adapted from Kim et al. [39])

2.5 Mucoadhesives in Aquaculture

The rapid growth of the aquaculture industry globally has resulted in overcrowded fish farms prone to disease outbreaks and an alarming reduction in productivity [70]. There has been an increased use of antibiotics and parasiticides to prevent diseases, resulting in antibiotic resistance and interference with aquatic ecosystems [1]. The need for a sustainable and rational approach to circumvent this issue while promoting economic growth has been highlighted in recent years.

Fish external layers are rich in mucus, playing an important role in protecting them from pathogens by acting as a barrier between by the fish and the environment [71]. However, mucoadhesion and controlled drug delivery systems are largely unexplored as strategies to

combat the aforementioned issues. There are only a limited number of publications that have fabricated and evaluated mucoadhesive nanoparticles for applications in aquaculture.

Costa et al. tested the mucoadhesive properties of chitosan using tambaqui fish as an animal model. Results showed that fluorescent chitosan nanoparticles were able to adhere to fish skin, gills, and the initial portions of the small intestine [72]. Another study conducted by Charlie-Silva et al. studied the interaction of chitosan-coated poly lactic-co-glycolic acid (PLGA) nanoparticles with fish external mucus using zebrafish as an animal model [73]. The fish were exposed to the fluorescence-tagged nanoparticles, transferred to clean water and fluorescence intensity was measured over time (Figure 2-14). Results showed that the nanoparticles could adhere to the external mucus of zebrafish for up to 3 hours with minimal residual effect on the water.

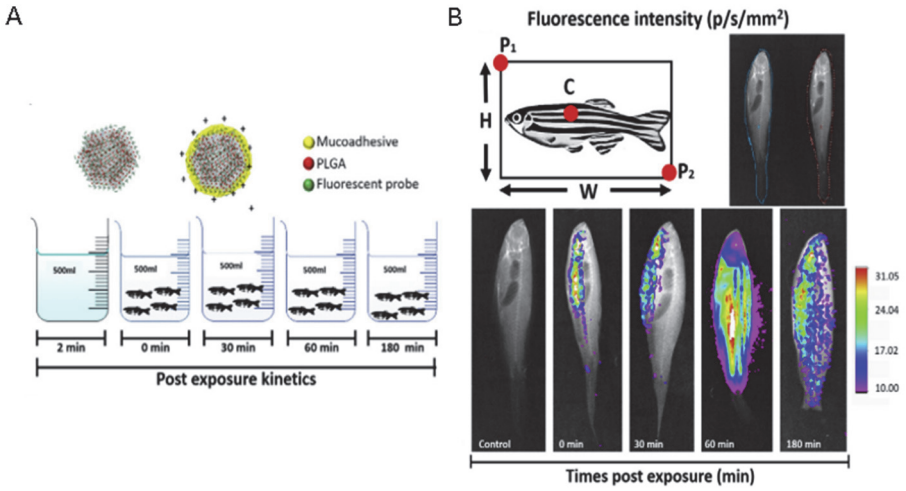

Figure 2-14. Mucoadhesive system in zebrafish. A) preparation of mucoadhesive studies for zebrafish, and B) Green fluorescence image of zebra fish at different exposure times *(p/s/mm^2)= photon/second/millimeter^2 (adapted from Charlie-Silva et al. [73])

More recently, Ferreira et al. prepared mucoadhesive chitosan-coated zein nanoparticles for application of anesthetics in Nile tilapia. The positively-charged particles successfully adhered to fish mucus and reduced the amount of anesthetic required by about 50% due to controlled release [74]. There has also been work surrounding mucoadhesive vaccines for fish. Kitiyodum et al. prepared a chitosan-complexed nanovaccine (CS-NE) and experimentally vaccinated red tilapia with the nanoparticles by immersion. The results of the study showed that the CS-NE particles displayed better adsorption on the mucosal surfaces of the fish and exhibited great vaccine efficacy compared to conventional vaccines [75].

2.6 Conclusions

An overview of the literature on mucoadhesive drug delivery systems and the strategies to enhance mucoadhesive properties of various polymers has been presented in this chapter. While numerous publications have addressed chemical modifications of first-generation mucoadhesives such as chitosan, alginate, and pectin, limited studies have been conducted on cellulose nanocrystals in the field of mucoadhesive drug delivery. Cellulose nanocrystals are attractive candidates for application in MDDS due to their capacity to spread homogenously on mucosa and their ability to act as drug carriers. This work aims to develop strategies to enhance the mucoadhesive abilities of CNCs using natural compounds. The designed systems have been optimized to ensure colloidal stability and the ability to interact with mucin has been thoroughly investigated.

Chapter 3. Optimized Synthesis of Cellulose Nanocrystals Coated with Tannic Acid (CNC-TA)

3.1 Introduction

Nanotechnology-based drug delivery systems have received much attention in recent years due to their ability to provide a controlled release of active ingredients. The use of nanocarriers can improve the colloidal stability and solubility of drugs, provide efficient and targeted delivery, and protect the drug from degradation in harsh environments [76]. The residence time of drug carriers can be improved by introducing mucoadhesive properties. Mucoadhesive drug delivery systems (MDDS) comprise of mucoadhesive polymers that are able to adhere to mucosal target sites. This prolongs the residence time of the drug, improving the bioavailability and reducing the need for frequent application [16].

Nano-polysaccharides possess favorable characteristics such as biocompatibility, biodegradability, excellent mechanical properties, and colloidal stability, which make them attractive candidates for biomedical applications. Cellulose nanocrystals (CNCs) are nano-polysaccharides derived from cellulose fibers by strong acid hydrolysis. CNCs are cheap, readily available, and can be easily modified due to the presence of hydroxyl groups on their surface [77]. The hydroxyl groups on CNCs can interact with mucin glycoproteins via the formation of hydrogen bonds. A recent study conducted by Lin et al. [10] found that CNCs can spread homogenously on mucosal layers. However, there is limited literature available on the application of CNCs in MDDS. Furthermore, CNCs display relatively weak mucoadhesion compared to other commonly utilized mucoadhesive nanomaterials. To address this, we modified CNCs with tannic acid, a plant polyphenol with mucoadhesive properties. Tannic acid is rich in pyrogallol groups that can form strong interactions with mucin proteins at neutral pH [62].

In this chapter, CNCs were coated with tannic acid (TA) via a one-step green synthesis. The optimal mass ratio for the synthesis was investigated and the coated CNCs were evaluated for colloidal stability, which is important for drug delivery applications. The size of the CNC-TA nanoparticles was also determined to ensure good penetration of mucosal membranes and the chemical structure was examined to detect functional groups that can interact with mucin.

3.2 Materials and Methods

3.2.1 Materials

Tannic acid (ACS reagent), HEPES 4-(2-Hydroxyethyl)-1-piperazineethanesulfonic acid, sodium hydroxide (NaOH) pellets, and potassium bromide (anhydrous, powder, 99.95% metals basis) were purchased from Sigma Aldrich. Cellulose nanocrystals (CNCs) were supplied by Celluforce Inc. Milli-Q water (generated by a Millipore Mill-A purification system) was used as the solvent for all the procedures.

3.2.2 One-pot Synthesis of CNC-TA Nanoparticles

2.0 g of CNCs were homogenously dispersed in 100 mL of Milli-Q water and probe sonicated for 5 minutes. 0.476 g of HEPES buffer was dissolved in the CNC dispersion under magnetic stirring at 200 rpm. The pH of the solution was then adjusted to 8 by slow drop-wise addition of previously prepared 1M NaOH. Various amounts of tannic acid were dissolved in Milli-Q water under magnetic stirring at 200 rpm. The tannic acid solutions were slowly added drop-wise to the CNC dispersions and left to stir at 200 rpm at room temperature until a dark color was obtained. The final solutions were dialyzed for five days against deionized water, and then freeze-dried to obtain powder for further characterization.

3.2.3 UV-Visible Spectroscopy

UV-Visible spectroscopy was used to confirm successful coating of tannic acid on the surface of the cellulose nanocrystals. A stock solution of tannic acid (200 ppm) was prepared in Milli-Q water at pH 7. The stock solution was diluted to prepare various concentrations of tannic acid (10 to 100 ppm) for preparation of a calibration curve. UV-Vis spectra for the various concentrations of tannic acid and the prepared CNC-TA nanoparticles (various CNC:TA mass ratios) were measured using a Cary 100 Bio UV-Visible spectrophotometer. All samples were prepared in Milli-Q water at a 0.1 wt% concentration, and probe sonicated for 2 minutes prior to measurement. The scans were performed at room temperature at pH 7. The amount of tannic acid in each sample was calculated using the generated calibration curve based on absorbance at 276 nm.

3.2.4 Hydrodynamic Size and Zeta Potential

The hydrodynamic size and zeta potential of CNC-TA nanoparticles (various CNC:TA mass ratios) were measured to evaluate the colloidal stability and optimize the mass ratio for future syntheses. Size and zeta potential of CNC was also measured for comparative purposes. The samples were diluted to a 0.1 mg/mL concentration in Milli-Q water and bath sonicated for 2 minutes prior to the measurements that were performed using a Malvern Nano-ZS90 Zetasizer at room temperature. 4 measurements (15 runs each) were taken for each sample and the average is presented.

3.2.5 Transmission Electron Microscopy (TEM)

A Philips CM 10 transmission electron microscope was used to image the CNC and CNC-TA particles at an accelerating voltage of 60 kV. The samples were diluted to a

concentration of 0.01 wt% in Milli-Q water and bath sonicated for 5 minutes to ensure full dispersion. 20 μL of sample was placed onto a carbon-coated copper grid (200 mesh) and left to dry overnight in ambient conditions. Image analysis was performed using the ImageJ software. Particle sizes presented were obtained from the analysis of a minimum of 100 particles.

3.2.6 Fourier Transform Infrared (FTIR) Spectroscopy

The functional groups present in CNCs, tannic acid, and CNC-TA were analyzed using a Bruker Tensor 27 FTIR spectrometer. Powdered samples of each were ground in a mortar along with potassium bromide and compressed using a hydraulic press to produce homogenous pellets. The FTIR spectra were recorded between 4000 cm^{-1} and 400 cm^{-1} at a resolution of 4 cm^{-1} with 32 scans performed at each wavenumber.

3.3 Results and Discussion

3.3.1 Synthesis of CNC-TA nanoparticles

Cellulose nanocrystals were successfully coated with tannic acid following the one-pot green synthesis proposed by Hu et al. [78]. Previously, in-situ oxidative polymerization of catechol-based compounds in alkaline conditions was discovered as a universal route for polydopamine deposition on any type of surface[38]. A similar route can be used to deposit plant polyphenols such as tannic acid onto surfaces, owing to their analogous structures to polydopamine. The reaction mechanism for tannic acid deposition on CNCs is expected to follow previously reported mechanisms for plant polyphenol and polydopamine coatings on other substrates [79]. While the exact mechanism is not understood fully, it has been shown

that the oxidized phenolic moieties of tannic acid can interact with substrates such as CNCs through covalent bonds, hydrogen bonds or π- π interactions [38].

Alkaline conditions and the presence of dissolved oxygen were essential for the reaction to occur. Therefore, the pH of the CNC dispersion was adjusted to 8 and monitored regularly. Plant polyphenols are known to oxidize and oligomerize under these conditions, which results in the formation of a less soluble, higher molecular weight species. It is presumed that the reduction in the solubility of the tannic acid and its inherent affinity towards surfaces causes it to deposit on the surface of the CNCs [79]. The dark color of the solution after the reaction indicated successful oxidation (Figure 3-1A). After dialysis and freeze-drying, a light yellow colored powder was obtained (Figure 3-1B), which showed colloidal stability when re-dispersed in Milli-Q water at a concentration of 0.5 wt% (Figure 3-1C).

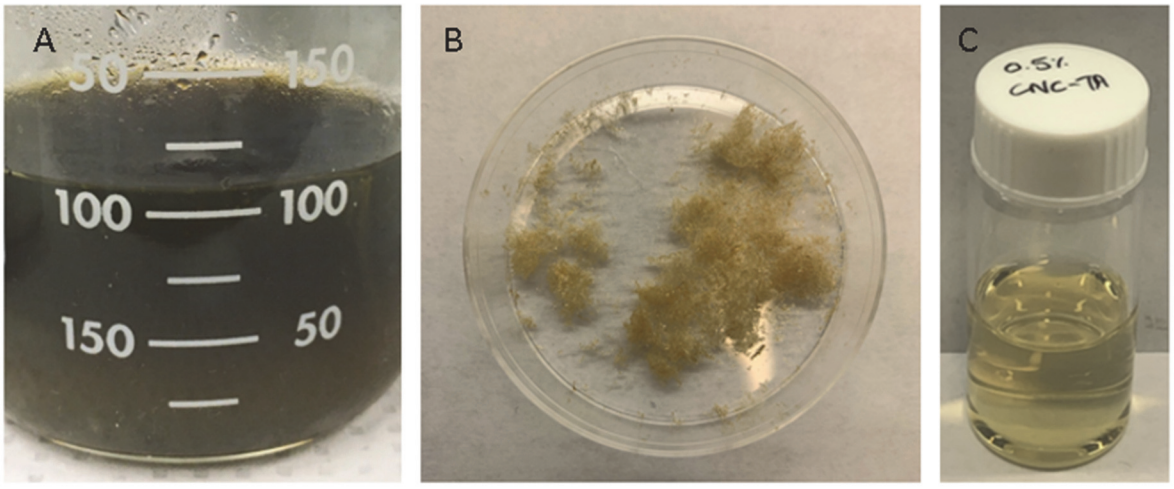

Figure 3-1. A) CNC-TA solution after reaction completion, B) Freeze-dried CNC-TA nanoparticles, and C) CNC-TA re-dispersed in Milli-Q water (0.5 wt%)

The reaction was repeated at four different mass ratios (CNC:TA w/w) in order to determine the optimal mass ratio for the synthesis. The concentration of the CNC dispersions was maintained at 2 wt% and the concentration of tannic acid added was varied as shown in Table 1.

Table 1. Mass ratio between tannic acid and CNC

Sample	**CNC-TA1**	**CNC-TA2**	**CNC-TA3**	**CNC-TA4**
CNC (wt %)	2	2	2	2
TA (wt %)	0.05	0.1	0.2	0.4
Mass ratio (CNC:TA)	40:1	20:1	10:1	5:1

*Working volume = 20 mL (10 mL of each solution)

3.3.2 Optimization and Characterization of CNC-TA

3.3.2.1 Particle Size and Zeta Potential Measurements

The particle size and zeta potential of the CNC-TA nanoparticles (Figure 3-2) were measured to evaluate their colloidal behavior and determine the optimal mass ratio for future syntheses. The average particle size of pristine CNCs was around 100 nm. After coating with tannic acid at a ratio of 40:1 CNC:TA, the average particle size increased to 192 nm, confirming that the CNCs were coated successfully. As can be seen in Figure 3-2, increasing the amount of tannic acid in the system increased the particle size further till a mass ratio of 10:1 was reached. The increase in particle size corresponded with an increase in the zeta potential up to a mass ratio of 10:1.

Pristine CNCs had a zeta potential of -41 mV, indicating high colloidal stability. This is attributed to electrostatic repulsion between the negatively charged sulfate half ester groups on their surface. However, coating the CNCs with tannic acid covers these groups, which could have implications on the colloidal stability. Hu et al. [78] used conductometric titrations to show this reduction in accessible sulfate groups due to the presence of a layer of tannic acid on the surface. The zeta potential results for CNC-TA (Figure 3-2) revealed that the negative surface charge was indeed reduced as more tannic acid was added and the CNC surface was covered. However, the highest zeta potential (-30 mV) observed at a mass ratio of 10:1 is still considered as highly colloidally stable.

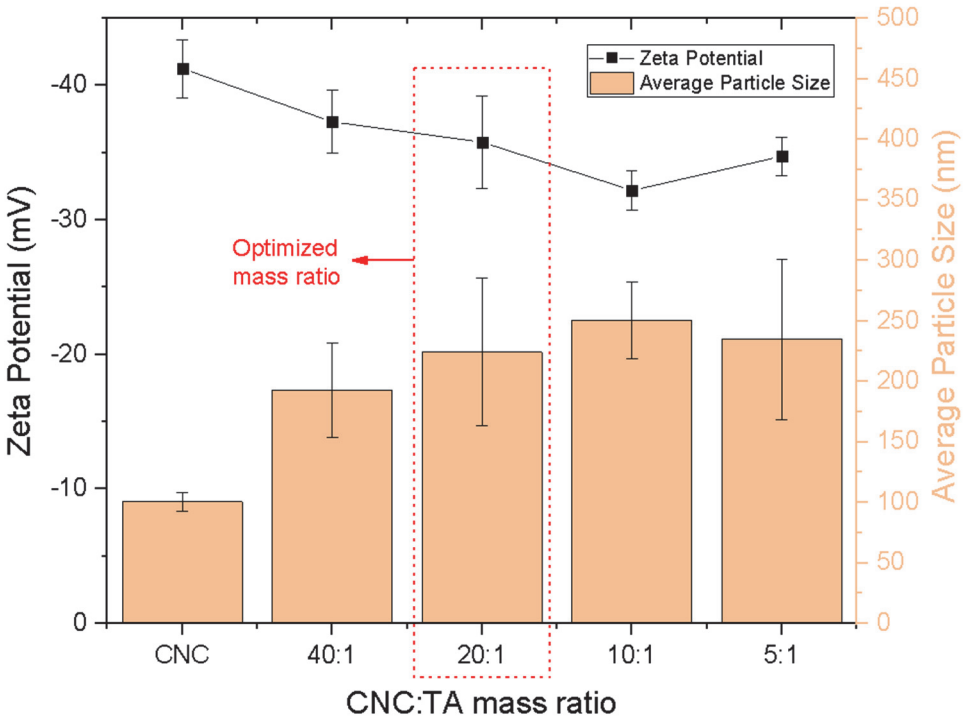

Figure 3-2. The average particle sizes and zeta potentials of unmodified CNCs and CNC-TA synthesized at various mass ratios

Increasing the mass ratio further to 5:1 resulted in a slight improvement in the colloidal stability. A 15 nm decrease was observed in the particle size, corresponding to a decrease in the zeta potential to -35 mV. The increased colloidal stability can be attributed to the oxidation of the hydroxyl groups of tannic acid to form quinones during the synthesis. Quinones have a negative charge due to the lone pairs on the oxygen atoms. At a ratio of 5:1, there are enough of these groups present on the surface of the CNC-TA to enhance the electrostatic repulsion and improve the colloidal stability. It is expected that increasing the mass ratio further would result in smaller particles with lower zeta potentials.

Despite the promising colloidal stability at a mass ratio of 5:1, a ratio of 20:1 was selected as the optimal synthesis condition. This was largely due to the fact that the stirring time required for sufficient oxidation of the tannic acid was 6 days at a ratio of 5:1, which would not be optimal for scaled-up production. Overnight stirring was sufficient for a mass ratio of 20:1. While a mass ratio of 40:1 had a smaller particle size and higher zeta potential, a mass ratio of 20:1 was favored to ensure that there was enough tannic acid present to interact with the mucous layer.

3.3.2.2 UV-Visible Spectroscopy

The presence of tannic acid in the CNC-TA nanoparticles was confirmed by UV-visible spectroscopy. The UV-visible spectrum of tannic acid is highly pH dependent, and at pH 7, it shows two characteristic peaks around 213 nm and 276 nm [80]. These peaks are associated with the absorbance of phenols, which typically occurs at around 211 and 270 nm. The UV-Vis spectra of tannic acid at pH 7 for concentrations between 5 and 50 ppm are depicted in Figure 3-3A. All the spectra show the characteristic peaks at 213 nm and 276 nm, with

increasing intensity as the tannic acid concentration was increased. A calibration curve for tannic acid (Figure 3-3B) was plotted according to the Beer-Lambert law based on absorbance at 276 nm. The law states that there is a linear relationship between the absorbance and concentration of the solution, enabling unknown concentrations to be determined by measuring the absorbance. The calibration curve for tannic acid had an absorptivity coefficient of 0.0435 and could be used to determine the concentrations of tannic acid in the synthesized CNC-TA nanoparticles between 5 and 50 ppm.

Figure 3-4 illustrates the UV-Vis spectra of CNC-TA nanoparticles at various mass ratios (CNC:TA). The spectra at all 4 mass ratios depict the characteristic peaks at 213 nm and 276 nm, confirming the presence of tannic acid in the nanoparticles. The intensity of the peak increased as the mass ratio was increased, indicating a greater concentration of tannic acid was coated onto the surface of the CNCs. At a mass ratio of 40:1, the peaks observed were not clear, further confirming that there was not enough tannic acid present in that sample. This was used to rationalize the selection of the 20:1 mass ratio as the optimal one, in addition to the zeta potential and size data.

Evidence of the oxidation of tannic acid is also depicted in the UV-Visible spectra. In addition to the characteristic absorbance of the phenol groups at 213 nm and 276 nm, new peaks were observed around 250 nm and 360 nm. These peaks were relatively broad for the 40:1 sample, but increased in intensity and sharpness as the concentration of tannic acid was increased. Absorbance peaks at these wavelengths are typically associated with benzoquinones, which were formed due to the oxidation of the phenol groups at alkaline pH during the synthesis.

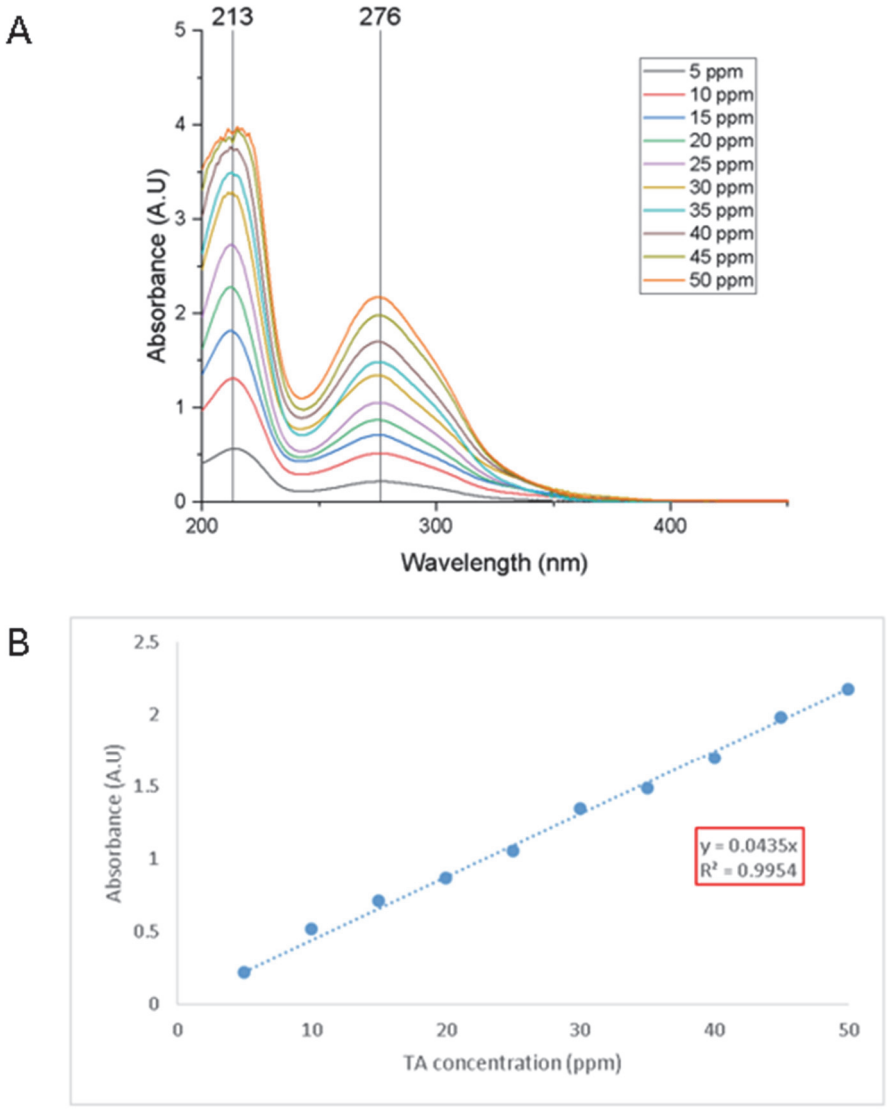

Figure 3-3. A) UV-Visible Spectra of tannic acid (5 to 50 ppm), and B) Tannic acid calibration curve based on absorbance at 276 nm

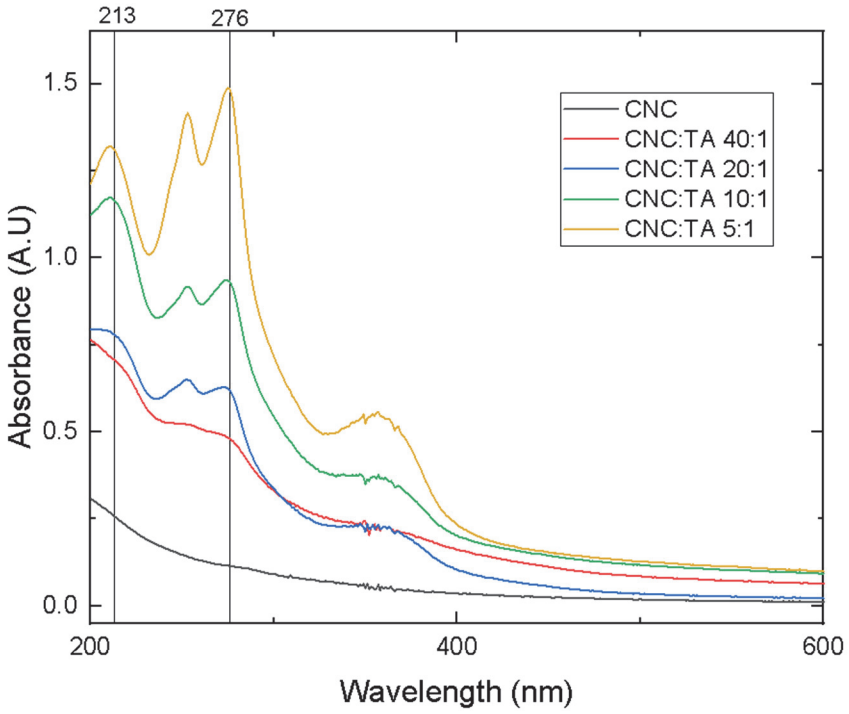

Figure 3-4. UV-Visible spectra of unmodified CNC and CNC-TA synthesized at various mass ratios

3.3.2.3 Transmission Electron Microscopy (TEM)

TEM was employed to measure the cross-sections and lengths, as well as to observe the morphology of CNC and CNC-TA nanoparticles. The TEM images of CNC (Figure 3-5A) and CNC-TA (Figure 3-5B) show that the rod morphology of CNCs was maintained after modification with tannic acid. The average length remained unaffected by modification as well, with both CNC and CNC-TA depicting average lengths of about 190 ± 40 nm. However, the cross-sections increased from 20 ± 5 nm for unmodified CNCs to 26 ± 6 nm for CNC-TA, which further illustrated successful coating. Similar observations regarding the maintenance of the rod morphology and increase in thickness of the CNCs upon coating were made by Hu et al [78], indicating that the synthesized CNC-TA showed good agreement with literature.

Furthermore, the enhanced dark contrast in the TEM image for CNC-TA (Figure 3-5B) is believed to be due to the aromatic groups of tannic acid [78].

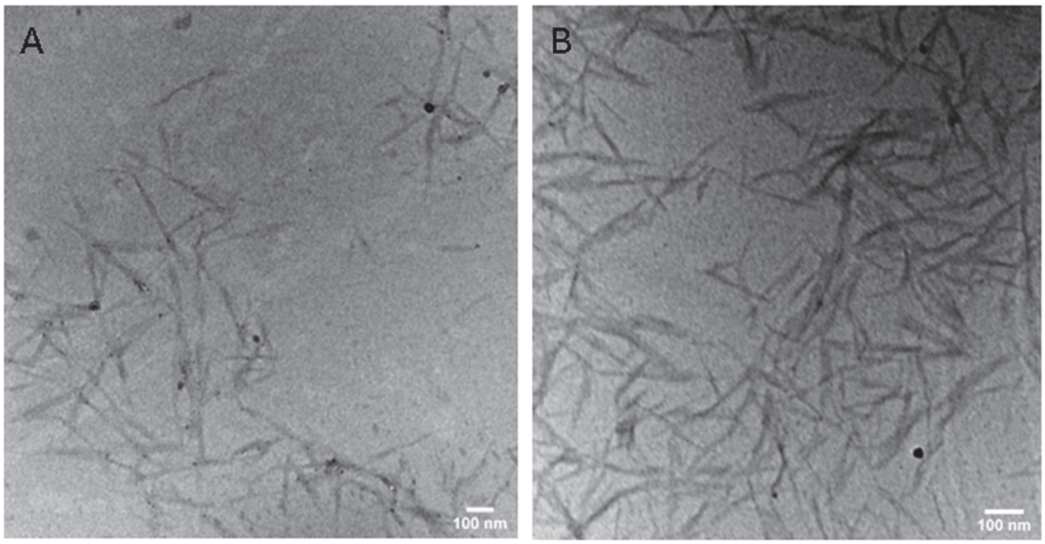

Figure 3-5. TEM images of A) unmodified CNCs, and B) CNC-TA. Scale bars are 100 nm.

3.3.2.4 Fourier Transform Infrared Spectroscopy (FTIR)

FTIR was employed to assess the chemical composition of the CNC-TA nanoparticles. FTIR spectra for CNC and tannic acid were also measured for comparative purposes. As shown in Figure 3-6, the spectrum for unmodified CNCs exhibited IR peaks characteristic of cellulosic functional groups at 3100 to 3600 cm^{-1}, and 900-1100 cm^{-1}, which correspond to -OH and –C-O-C stretching vibrations respectively. The spectrum for tannic acid showed a peak at 755 cm^{-1}, which correspond to the vibration of C=C in the benzene rings [78]. The spectrum for CNC-TA did not have any notable changes when compared to unmodified CNCs. A small peak was observed at 1600-1700 cm^{-1}, which could be attributed to the C=O stretch from the formation of quinones. However, the FTIR data did not show any conclusive evidence

of CNC modification. This might indicate that the deposition of tannic acid on CNC is largely due to physical adsorption.

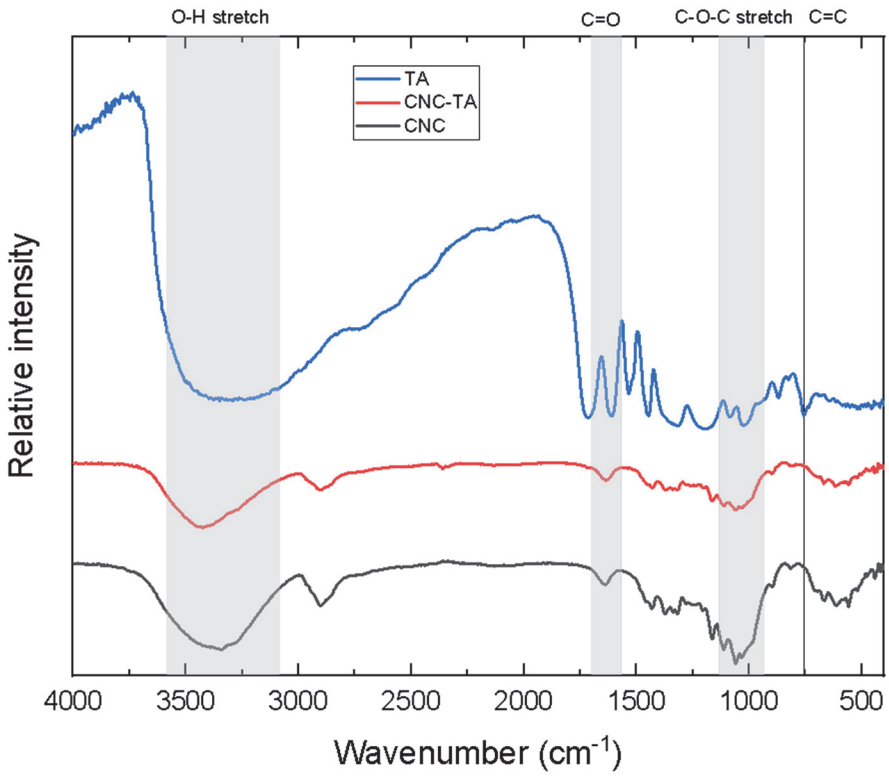

Figure 3-6. FTIR spectra of CNC, tannic acid, and CNC-TA

3.4 Conclusions

The fabrication and characterization of CNC-TA nanoparticles by a simple, green one-pot method was described. Tannic acid was successfully deposited onto CNCs and the mass ratio for the synthesis was optimized at 20:1 CNC:TA. The CNC-TA nanoparticles exhibited excellent colloidal stability in water with a zeta potential of -35 mV and an average particle size of about 200 nm, which is suitable for penetration of the mucous membrane [12]. TEM

analysis showed that the CNCs maintained their rod morphology after modification, and an increase in their cross-section indicated successful coating of tannic acid. UV-Vis spectra confirmed oxidation of some of the hydroxyl groups of tannic acid to quinones. Both these groups are able to interact with interact with mucin by the formation of hydrogen bonds. The modification of CNCs with tannic acid is expected to strengthen their interaction with mucin. The enhancement in the mucoadhesive properties as well as the mechanism of interaction will be described in Chapter 5.

Chapter 4. Optimized Synthesis of Catechol-functionalized Cellulose Nanocrystals (CPC-cat)

4.1 Introduction

Cellulose nanocrystals (CNCs) are abundant and renewable nanomaterials that possess attractive properties for drug delivery applications. They have a high surface area for drug loading and display excellent dispersability in water due to their negative surface charge [81]. CNCs are biocompatible and non-toxic, making them ideal for use in marine drug delivery as they would have minimal environmental impact. Furthermore, the hydroxyl groups on their surface show potential to interact with the mucosa via the formation of hydrogen bonds [10]. However, the mucoadhesive abilities of CNCs and methods to enhance their interactions with mucous have not been extensively explored.

On the other hand, chitosan (CS) is a well-established first generation mucoadhesive that has been extensively studied due to its strong mucoadhesive properties. CS is known as one of the only natural cationic polymers used in mucoadhesive drug delivery due to its ability to induce electrostatic interactions with negatively-charged mucin proteins [82]. However, the application of CS in drug delivery is limited by its low solubility above pH 6.5 where the positive charge is lost due to the de-protonation of primary amines. Therefore, several modification strategies have been explored to improve the solubility in alkaline environments as well as enhance the mucoadhesive properties of CS.

The catechol groups on the side chain of L-3,4-dihydroxyphenylalinine (DOPA) have been utilized to modify CS, promoting an enhancement in the mucoadhesive properties and solubility at alkaline pH [38]. DOPA is an amino acid crucial to the underwater adhesion of mussels. The catechol groups of mussels can bind to various types of surfaces due to the two

hydroxyl groups on the benzene ring. Furthermore, catechol is found in nature and is highly biocompatible, making it an excellent candidate for marine drug delivery.

Catechol-functionalized chitosan (CS-cat) has been established as a novel mucoadhesive polymer with tremendous potential for biomedical applications due to its long-lasting mucoadhesive properties [39]. The driving forces for the interaction of CS-cat and mucin are highly pH dependent, which is an important factor to consider when designing a MDDS. Below pH 6.5, catechol groups are un-oxidized and the primary driving force is electrostatic interactions between the positively charged amine groups and negatively charged mucin. However, at pH above 6.5, the catechol groups are oxidized to o-quinones, which can form irreversible covalent bonds with the amine and thiol groups of mucin. This allows the polymer to remain adhered to the mucus layer for prolonged periods, promoting controlled drug release.

There are several examples in the literature on the approaches used to conjugate catechol onto chitosan. One of the most common approaches to prepare CS-cat is to utilize EDC chemistry to conjugate hydrocaffeic acid (HCA) onto the chitosan backbone through the formation of an amide linkage. However, the synthetic protocols tend to vary between publications, making it challenging to reproduce and replicate protocols. Narkar et al. [83] studied the accuracy of existing protocols, identified critical parameters, and prepared an optimized protocol for the synthesis of CS-cat. Key parameters that were considered included the pH at which the reaction should occur as well as the pH of the dialysis medium. The focus of the study was to make changes that would prevent the formation of undesirable catechol oxidation products, as was highly likely in published protocols. Oxidation of catechol occurs

due to prolonged exposure to pH>5. This can lead to the formation of intrapolymeric adducts between the catechol groups and amine groups during the reaction, making the catechol groups unavailable for interactions with mucin.

In this chapter, we first synthesized CS-cat following the optimized protocol and then coated it onto CNCs via electrostatic gelation to fabricate a CNC-based mucoadhesive with an enhanced capacity to interact with mucosa through electrostatic interactions and covalent bonds. This is in stark contrast to the work done in Chapter 3, where the focus was to introduce groups on CNCs that interact with the mucosa through hydrogen bonding. The synthetic conditions, colloidal behavior and morphology of the modified CNCs is discussed in detail. The addition of PDADMAC was also explored as a strategy to increase the positive surface charge and colloidal stability of the nanoparticles at alkaline pH.

4.2 Materials and Methods

4.2.1 Materials

Low M_w chitosan (50k-190kDa with 75%-85% deacetylated), EDC (N-(3-dimethylaminopropyl)-N′-ethylcarbodiimide hydrochloride, hydrochloric acid (ACS reagent, 37%), sodium hydroxide (NaOH) pellets, polydiallyldimethylammonium chloride (pDADMAC, 20 wt% in water), and potassium bromide (anhydrous, powder, 99.95% metals basis) were purchased from Sigma Aldrich. 3,4-dihydroxyhydrocinnamic acid (hydrocaffeic acid, HCA 98+%) was purchased from Alfa Aesar. Cellulose nanocrystals (CNCs) were supplied by Celluforce Inc.

4.2.2 Synthesis of CS-cat

Chitosan (CS) was functionalized with the catechol group (cat) using EDC chemistry as shown in Figure 4-1. 45.5 mL of Milli-Q water was adjusted to pH 1.6 using 1M HCl, and 0.5g of chitosan powder was added. The pH was readjusted to 1.6 with 1M HCl. The colloid was stirred at 400 rpm until a clear, pale yellow dispersion was obtained. 1M NaOH was added slowly drop-wise to raise the pH to 5.4 under stirring, resulting in a cloudy colloid. 591 mg of HCA was added and stirred till it was clear, and a pale yellow colloid was obtained again. EDC (1244.8 mg) was dissolved in 50 mL of 1:1 v/v solution of ethanol and Milli-Q water. The EDC solution was added drop-wise to the colloid containing HCA and chitosan under stirring at 400 rpm. The pH was adjusted to 4.6 using 1M HCl and maintained for 1 hour under vigorous stirring. Unreacted compounds were removed by dialyzing against deionized water adjusted to pH 3 for 3 days and the purified solution was freeze-dried to obtain powder.

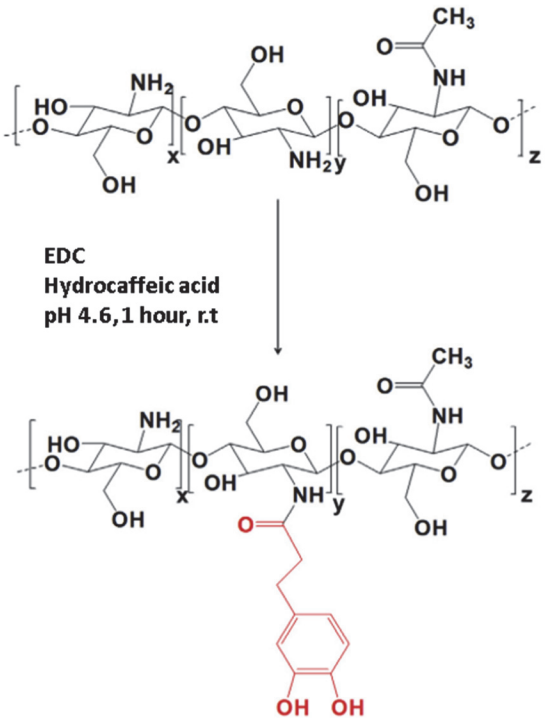

Figure 4-1. Synthesis of CS-cat (adapted from Kim et al. [39])

4.2.3 Synthesis of CNC/CS-cat (CC-cat)

0.5 wt% CNC solutions were prepared by dispersing CNCs in Milli-Q water by probe sonication for five minutes. CS-cat solutions (various concentrations) were prepared by stirring overnight at 200 rpm. 5 mL of each CS-cat solution was slowly injected into the CNC solutions at 1.5 mL/min using a syringe pump under probe sonication to prepare CC-cat solutions with varying CNC:CS-cat mass ratios.

4.2.4 Synthesis of CNC-PDADMAC-CS-cat (CPC-cat)

PDADMAC was introduced to the CC-cat nanoparticles to improve the colloidal stability at physiological pH. The previously optimized CNC:CS-cat mass ratio was

maintained for the synthesis of CPC-cat. PDADMAC solutions were prepared at various concentrations to vary the PDADMAC:CS-cat mass ratio. CS-cat solutions (2.5 mL) were mixed with PDADMAC solutions (2.5 mL) and slowly injected into CNC solutions (5 mL) at 1.5 mL/min by a syringe pump under probe sonication.

4.2.5 UV-Visible Spectra

UV-Visible spectroscopy was used to detect the presence of the catechol groups in CS-cat, CC-cat and CPC-cat samples. A stock solution of hydrocaffeic acid (200 ppm) was prepared in Milli-Q water at pH 5. The stock solution was diluted to prepare various concentrations of hydrocaffeic acid for preparing the calibration curve. A Cary 100 Bio spectrophotometer was used to obtain the spectra for hydrocaffeic acid (10 to 100 ppm), chitosan, CS-cat, CNC, CS-cat, and CPC-cat at pH 5 and room temperature. All samples were prepared in Milli-Q water at 0.1 wt% concentration, and probe sonicated for 2 minutes prior to the measurements. The concentration of catechol groups in each sample was calculated using the generated calibration curve based on absorbance at 280 nm.

4.2.6 Hydrodynamic Size and Zeta Potential

The hydrodynamic sizes and zeta potentials of CC-cat (various CNC:CS-cat mass ratios) and CPC-cat nanoparticles (various CS-cat:PDADMAC mass ratios) were measured to evaluate the colloidal stability and optimize the mass ratio for further characterization. The samples with optimized mass ratio were further evaluated for colloidal stability from pH 2 to 10. Solutions were diluted to a 0.1 mg/mL concentration with Milli-Q water and bath sonicated for 2 minutes prior to the measurements. All measurements were performed using the Malvern

Nano-ZS90 Zetasizer at room temperature. Four measurements (15 runs each) were taken for each sample and the average is presented.

4.2.7 Transmission Electron Microscopy (TEM)

The morphologies and size of CC-cat and CPC-cat nanoparticles were analyzed using a Philips CM 10 transmission electron microscope at an accelerating voltage of 60 kV. The samples were diluted to a concentration of 0.01 wt% in Milli-Q water and bath sonicated for 5 minutes to ensure complete dispersion. 20 μL of sample was dropped onto a carbon-coated copper grid (200 mesh) and left to dry overnight in ambient conditions. Image analysis was performed using ImageJ software. The particle sizes presented were obtained from the analysis of a minimum of 100 particles.

4.2.8 Fourier Transform Infrared Spectroscopy (FTIR)

A Bruker Tensor 27 FTIR spectrometer was used to detect the presence of specific functional groups in chitosan, hydrocaffeic acid, CS-cat, CC-cat, and CPC-cat. Powdered samples of CS-cat, CC-cat, and CPC-cat were obtained by freeze-drying. Small amounts of each material were ground in a mortar with potassium bromide and compressed using a hydraulic press to produce homogenous pellets. The FTIR spectra were recorded between 4000 cm^{-1} and 400 cm^{-1} at a resolution of 4 cm^{-1} with 32 scans performed at each wavenumber.

4.3 Results and Discussion

4.3.1 Synthesis of CS-cat

The first step in preparing the CPC-cat nanoparticles involved conjugating the primary amine groups of chitosan (CS) with hydrocaffeic acid (HCA) using EDC chemistry. EDC is a

water-soluble carbodiimide that is well-established as a coupling agent between carboxylic acids and primary amines. During the reaction, EDC first reacts with the carboxylic acid group of HCA to form an active O-acylisourea intermediate that is then easily displaced by a nucleophilic attack from primary amine groups in the reaction mixture. An amide bond is formed between the amine and carboxyl groups and a soluble urea derivative is formed as a by-product. Reactions involving EDC have been shown to be most efficient in acidic conditions. This, in addition to the low solubility of chitosan and the oxidation of catechol (cat) groups at higher pH meant that pH control was critical to the preparation of CS-cat.

The optimized protocol adopted for the functionalization of chitosan with catechol was developed by Narkar et al. [83]. The synthetic scheme for the reaction is described in Figure 4-1 and the different stages of the synthesis are shown in Figure 4-2. To ensure chitosan was completely dissolved, the pH was adjusted to 1.6 before and after the addition of chitosan. The colloid was stirred vigorously until a clear pale yellow dispersion (Figure 4-2A) was obtained. Next, the pH was slowly raised to 5.4 by drop-wise addition of 1M NaOH, that yielded a cloudy dispersion (Figure 4-2B). Previous protocols involved the dissolution of HCA in deionized water prior to the addition to the chitosan. However, given that the pH of the water was around 6.5, there was a high probability that the catechol groups would be oxidized to form quinones [39]. Therefore, HCA was added in powder form and the colloid was stirred until it turned clear, pale yellow again. The pH at the end of this step was 3.5. The EDC solution was then added slowly drop-wise under constant stirring to initiate the coupling reaction. The pH after the addition of EDC was around 4.8. A few drops of 1M HCl were added to lower the pH to 4.6, where the reaction is most efficient, and the reduced state of catechol could be ensured.

During the 1 hour reaction, the pH was monitored closely and maintained at 4.6, and the final solution is shown in Figure 4-2C.

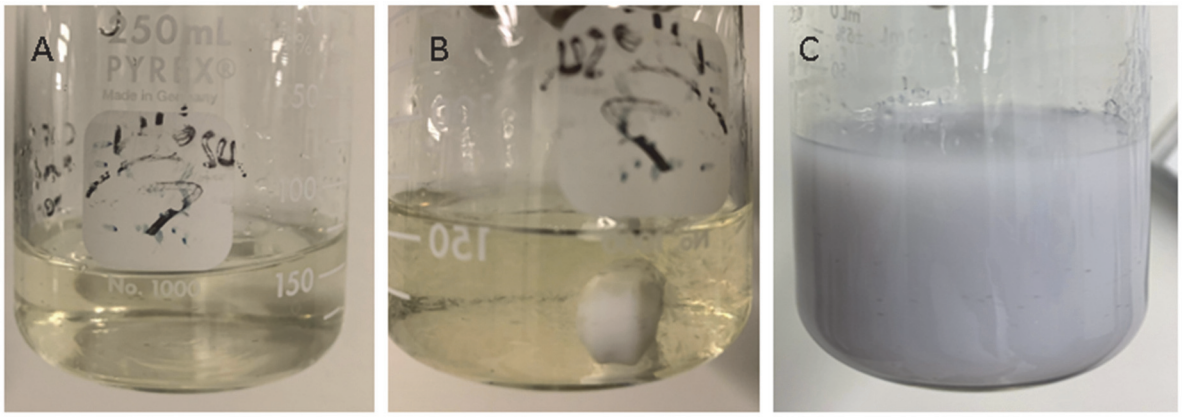

Figure 4-2. Different stages of the synthesis of CS-cat: A) Clear pale yellow colloid obtained on dissolving chitosan, B) Cloudy colloid obtained on addition of NaOH, and C) Final solution after addition of EDC/HCA and 1 hour stirring.

The reaction by-product and unreacted compounds were removed by dialysis against deionized water for 3 days. The pH of the dialysis medium was adjusted to 3 each day to ensure that oxidation did not occur. Dried CS-cat (Figure 4-3A) was obtained by freeze-drying. The white color of the product confirmed that the catechol groups were in their reduced state. The CS-cat powder was re-dispersed at pH 7 (Figure 4-3B) by overnight stirring to yield a white dispersion, which turned brown (Figure 4-3C) over several days as the catechol groups started to oxidize. To avoid this, all stock solutions for further experimentation were prepared at pH ≤ 5.

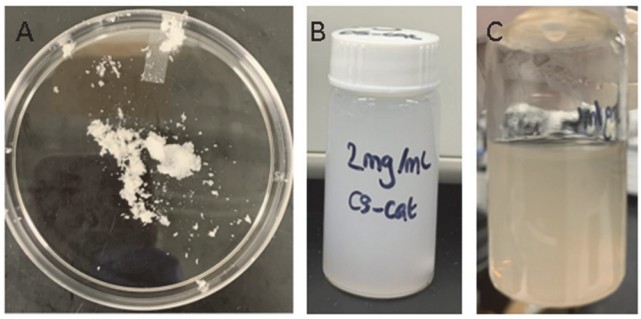

Figure 4-3. A) Freeze-dried CS-cat powder, B) 2 mg/mL re-dispersed CS-cat (pH 7), and C) Oxidation of CS-cat solution after several days

4.3.2 Characterization of CS-cat

The successful grafting of the catechol groups on the chitosan backbone was confirmed by UV-Visible spectroscopy and FTIR. The benzene ring of phenolic compounds has a distinct UV absorbance peak at 280 nm. The amount of catechol grafted could therefore be determined using the Beer-Lambert law, where the absorbance of HCA at 280 nm is proportional to the concentration of HCA solutions. UV-Vis spectra of HCA solutions (pH 5) with concentrations ranging from 10 to 100 ppm (Figure 4-4A) were used to prepare a calibration curve. The slope of the calibration curve (Figure 4-4B) corresponds to the absorptivity coefficient, which was determined to be 0.0167. The calibration curve could be used to determine the concentration of catechol in CS-cat from 10 to 100 ppm.

UV-Vis spectra of the un-grafted and grafted CS are shown in Figure 4-5. The samples were prepared in Milli-Q water adjusted to pH 5 owing to the low solubility of chitosan at higher pH values. The spectrum for CS showed no absorbance at 280 nm, while CS-cat had a distinct absorbance peak at 280 nm, indicating successful grafting.

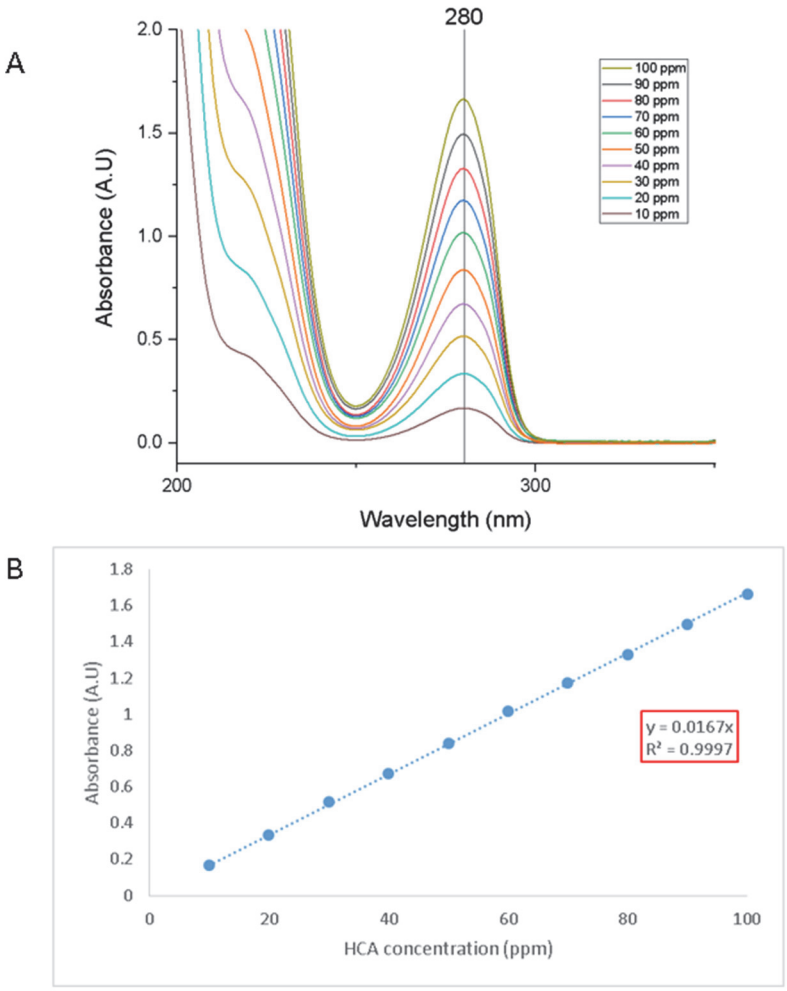

Figure 4-4. A) UV-Visible Spectra of HCA (10 to 100 ppm), and B) HCA calibration curve based on absorbance at 280 nm

A notable difference between the spectrum of pure HCA and the CS-cat was the rising baseline observed in the CS-cat spectrum. This can be attributed to Rayleigh scattering caused by the presence of small particles in the solution. The scattering was found to persist despite several attempts to obtain a flat baseline. Therefore, in order to estimate the grafting percentage, the baseline was corrected using the Origin software prior to determining the peak height. The peak height was determined to be 0.175, corresponding to a catechol concentration

of 10.46 ppm. The grafting percentage was calculated by dividing the number of moles of catechol by the moles of potential grafting sites (1 per repeat unit of CS). The percentage of deacetylation was taken into account for the calculation with a lower limit of 75% and upper limit of 85%. The grafting percentage was estimated to be between 11.7% and 11.9%, which is in good agreement with the literature regarding catechol-modified chitosan [39]. Higher degrees of catechol conjugation have been shown to form aggregates during the EDC reaction and have reduced solubility at pH 7 [84].

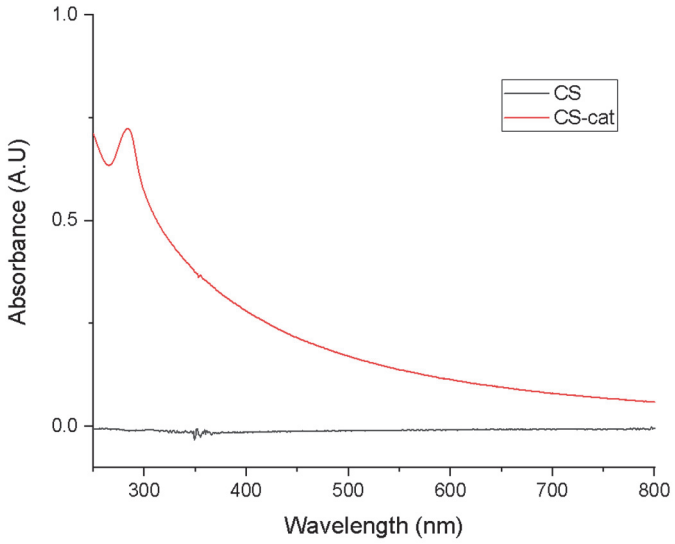

Figure 4-5. UV-Vis spectra of CS and CS-cat at pH 5

FTIR spectra (Figure 4-6) of CS, HCA, and CS-cat were measured to confirm the successful grafting of catechol. The O-H and N-H stretching vibration appeared in all the spectra as a broad peak from 3100 to 3600 cm^{-1}. The carboxylic acid of HCA had a peak around 1700 cm^{-1}. Grafting was confirmed by the peak observed around 1650 cm^{-1} in the CS-cat spectrum, corresponding to the amide linkage formed between the carboxylic acid of HCA and

the primary amines of CS. This peak is absent from the HCA and CS spectra, indicating successful modification of CS with the catechol group.

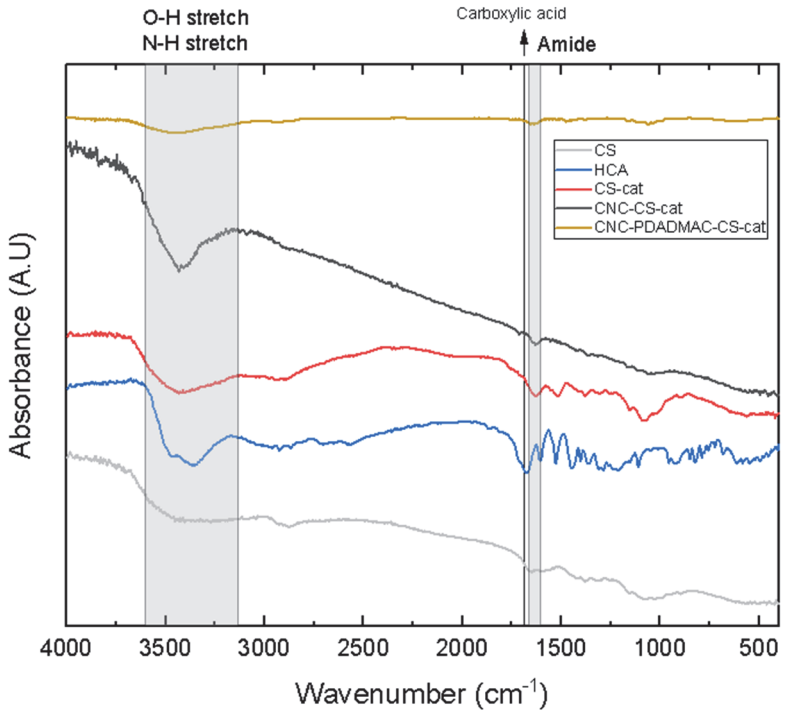

Figure 4-6. FTIR spectra of CS, HCA, CS-cat, CC-cat, and CPC-cat

4.3.3 Optimized Synthesis and Characterization of CC-cat nanoparticles

CC-cat nanoparticles were prepared using a facile synthesis method based on electrostatic gelation between the positively charged CS-cat and negatively charged CNCs. When the CS-cat solutions were first introduced to the 0.5 wt% CNC dispersions, a thick aggregated gel was formed due to the strong electrostatic interactions as observed in Figure 4-7A. Bath sonication was found to be insufficient to disperse the aggregated complex. Therefore, a syringe pump was used to slowly inject the CS-cat solutions into the CNC solution while employing probe sonication to ensure the prepared nanoparticles were well-dispersed

and had a reduced particle size. CC-cat nanoparticles prepared with the probe sonicator (Figure 4-7B) appeared colloidally stable. The positively charged CS-cat coating on the surface of the CNCs caused the nanoparticles to bind to the surface of the negatively charged glass vial. Both the colloidal stability and positive charge are important characteristics for the eventual application in drug delivery. The CS-cat coating is expected to introduce electrostatic interactions with negatively charged mucin proteins to enhance the weak mucoadhesion of CNCs. The mechanism of interaction is investigated in detail in Chapter 5.

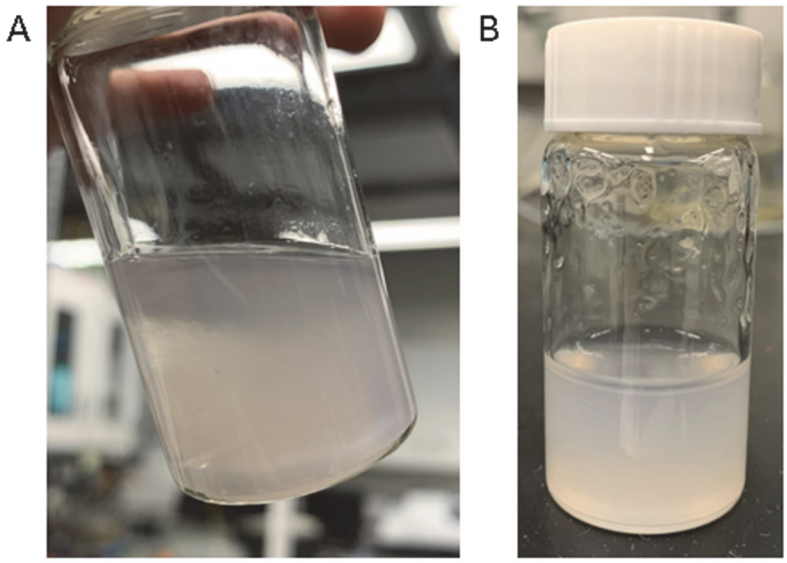

Figure 4-7. A) Ionic gelation of CNCs and CS-cat, and B) CC-cat nanoparticles binding to glass.

CC-cat was synthesized at various mass ratios (CNC:CS-cat w/w) to determine the optimized synthesis condition. The concentration of the CNC solution was maintained at 0.5 wt% while CS-cat solutions containing different amounts of catechol groups were introduced. The colloidal behaviour was evaluated by measuring the particle size and zeta potential at each condition as depicted in Figure 4-8. Results showed that the mass ratio played a significant

role in controlling the colloidal properties of the system. The CC-cat nanoparticles at all the mass ratios had sizes greater than pristine CNC (~100 nm), indicating the successful coating of CS-cat onto the surface. At a mass ratio of 40:1 CNC:CS-cat, the zeta potential was about -40 mV, similar to the zeta potential of pristine CNCs. While the CC-cat synthesized at this condition was colloidally stable, the negative zeta potential indicated that the CS-cat had not fully coated the surface of the CNCs. As more CS-cat was introduced, it was observed that the zeta potential began to increase gradually but remained negative up to a mass ratio of 10:1. Further addition of CS-cat caused the system to aggregate, with average particle sizes of 4-6 μm and zeta potentials close to 0 mV due to the loss of electrostatic repulsion. Beyond a mass ratio of 1:1, the colloidal system was stabilized again, with high positive zeta potentials and particle sizes in the nanometer range. This indicated that the CS-cat had fully coated the CNC surface as required. Interestingly, an increase in the particle size was observed at mass ratios of 1:2 and 1:3 with sizes about 500-600 nm despite a zeta potential of +50 mV. The diffusivity of mucoadhesive particles is highly dependent on size [12] and smaller particle sizes are preferred for better penetration. Therefore, a mass ratio of 1:1 was chosen as the optimized synthesis condition. CC-cat nanoparticles prepared at this mass ratio had the smallest particle size of about 380 nm in addition to a zeta potential of +40 mV, which was deemed sufficient for electrostatic interaction with mucin proteins.

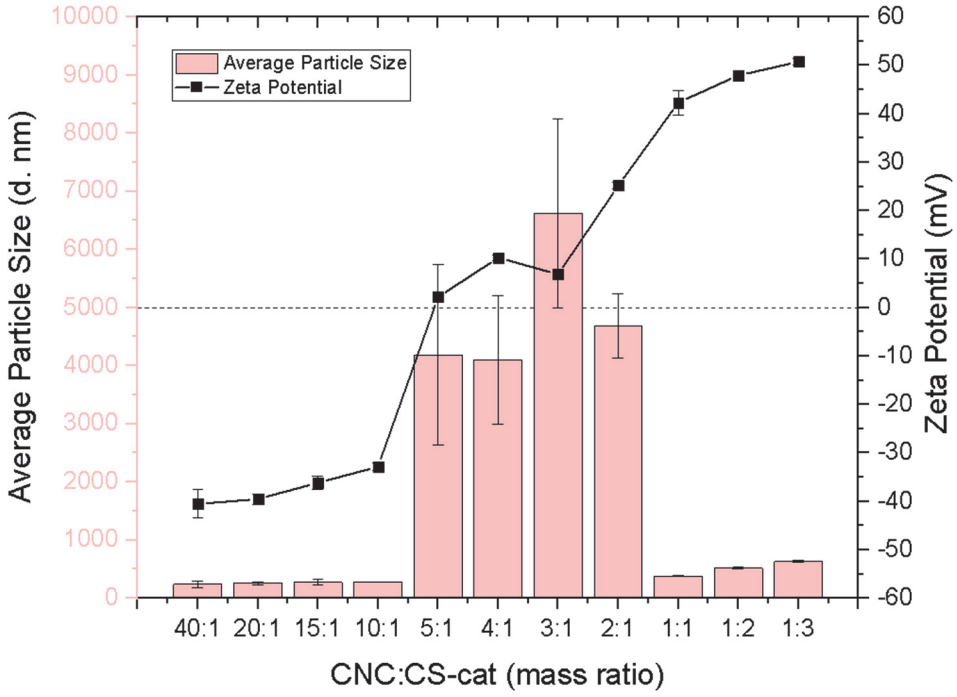

Figure 4-8. Average particle sizes and zeta potentials of CC-cat at various CNC:CS-cat mass ratios.

The presence of the catechol groups in the optimized CC-cat nanoparticles was detected using UV-Visible spectroscopy and FTIR. The UV-Vis spectrum for 1:1 CC-cat at pH 5 displayed a distinct peak around 280 nm, which is characteristic of catechol. The Rayleigh scattering seen in the spectrum for CS-cat was observed as well. The FTIR spectrum for 1:1 CC-cat (Figure 4-6) also showed a peak around 1650 cm^{-1}, corresponding to the amide linkage from the CS-cat.

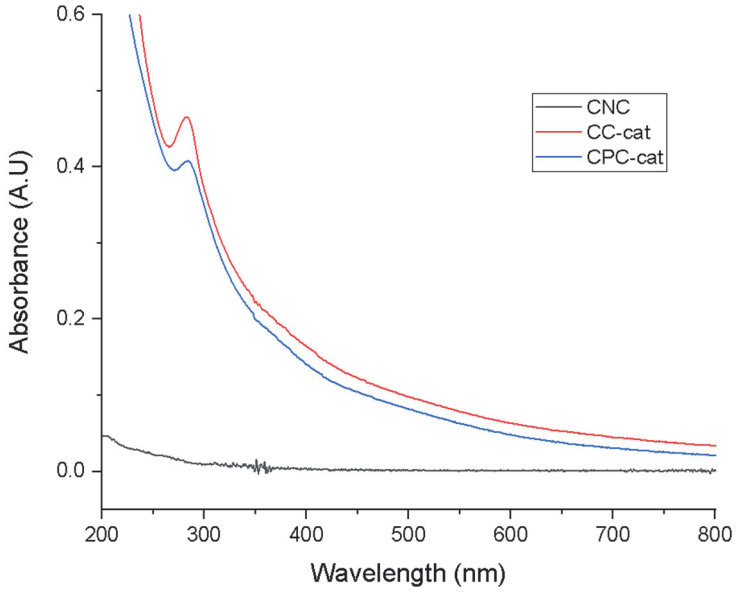

Figure 4-9. UV-Vis spectra of CNC, CC-cat, and CPC-cat at pH 5

The morphology of the CC-cat nanoparticles at the optimal mass ratio was observed using TEM (Figure 4-10). Rod-shaped particles were observed with thicker cross-sections compared to pristine CNCs, indicating that the CNCs had been coated with a layer of CS-cat. The electrostatic gelation can be observed as well, where gels comprising of many nanoparticles were formed. Particle sizes ranged from 400 to 800 nm, which is not in accordance with the data obtained from the Zetasizer. This could be explained by potential aggregation of the nanoparticles as they were drying on the TEM grid.

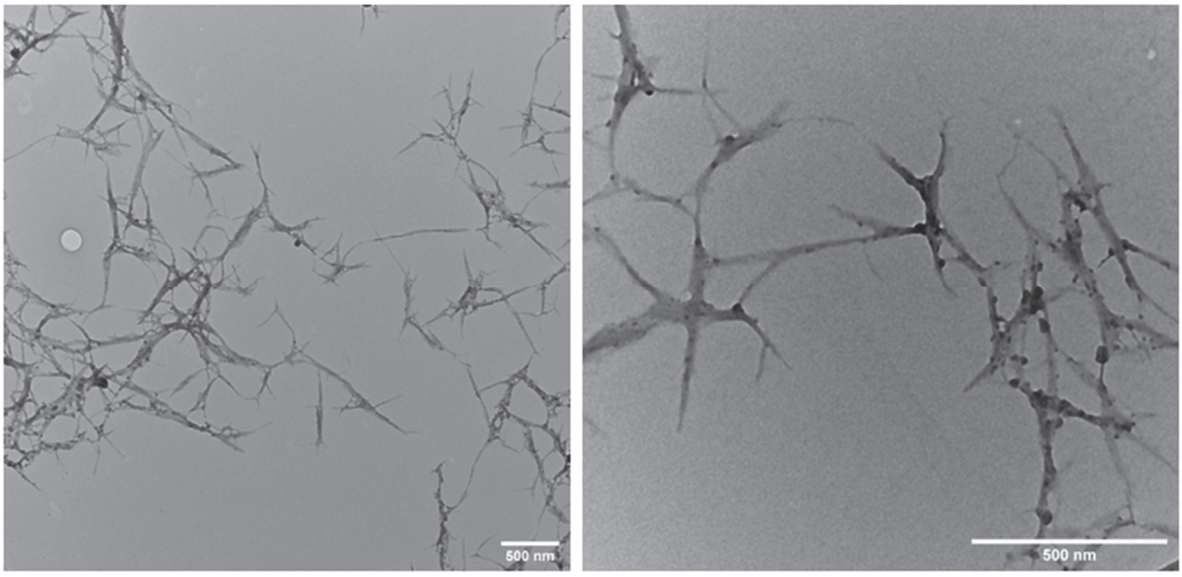

Figure 4-10. TEM images of CC-cat nanoparticles. Scale bars are 500 nm.

4.3.4 Limitations of CC-cat

The pKa of the primary amine of chitosan is around 6.5, which results in limited solubility at higher pH. The purpose of conjugating catechol groups on chitosan was to improve the solubility and mucoadhesive properties at physiological pH values. Additionally, coating the modified chitosan onto CNCs was expected to produce colloidally stable nanoparticles that could have enhanced interactions with mucin via electrostatic interactions and covalent bonding. However, due to the relatively low degree of catechol functionalization (~12%), the presence of free amines on the chitosan backbone could still limit the mucoadhesive application of CC-cat nanoparticles.

Therefore, it was necessary to evaluate the colloidal behavior of the optimized CC-cat nanoparticles at different pH values. The average particle sizes and zeta potentials of 1:1 CC-cat from pH 2 to 10 are shown in Figure 4-11. The nanoparticles were stable up to pH 5 with

small particle sizes and high zeta potentials of +40 to +50 mV. However, at pH 6, the zeta potential decreased to about +28 mV, which borders on colloidal instability. Raising the pH beyond 6 caused the system to lose its colloidal stability as the amine groups were de-protonated, with zeta potentials close to 0 mV being observed at pH 7 and 8. Without the electrostatic repulsion of the positively charged amines, the nanoparticles formed large aggregates. The system was re-stabilized beyond pH 9, as further de-protonation resulted in an overall negative surface charge close to -40 mV.

The colloidal behavior of CC-cat beyond pH 6 was a cause for concern. Physiological pH as well as the pH of the ocean range from pH 7 to pH 8, where the system was shown to be unstable. Maintaining a positive surface charge at these pH values was essential to induce electrostatic interactions with mucosal membranes. To address this, PDADMAC was introduced to increase the positive surface charge and improve the colloidal stability of CC-cat as discussed in the next section.

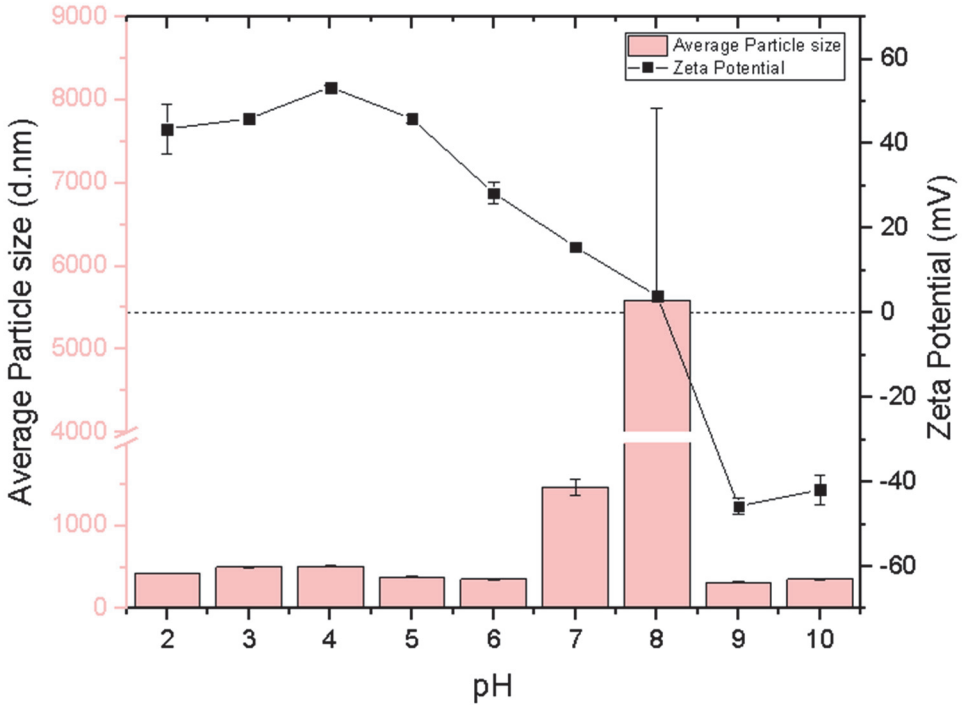

Figure 4-11. Average particle sizes and zeta potentials of CC-cat at different pH values

4.3.5 Optimized Synthesis and Characterization of CPC-cat

PDADMAC was introduced to the CC-cat nanoparticles to improve their colloidal stability and mucoadhesive properties. PDADMAC is a synthetic cationic polymer that has been approved by the Food and Drug Administration for use as an antimicrobial agent [85], making it a good candidate for drug delivery applications. The quaternary ammonium group of PDADMAC was hypothesized to increase the positive surface charge of the nanoparticles at the required pH for stabilization of the colloidal system. Additionally, the positive charge would enhance the interactions with the negatively charged mucus membrane.

CPC-cat nanoparticles were synthesized by a similar electrostatic gelation technique as that used for the CC-cat synthesis. PDADMAC is capable of adhering to the negatively-

charged CNCs by the formation of strong electrostatic interactions. Dong et al. [85] previously prepared PDADMAC-coated CNCs for glucose sensing, by blending PDADMAC and CNC solutions by sonication, and then stirring. The synthesized CNC-PDADMAC nanoparticles had excellent colloidal stability with a zeta potential of +50 mV. We prepared CPC-cat at various mass ratios of CS-cat:PDADMAC using a similar method with slight modifications. The CNC:CS-cat ratio was maintained at 1:1 and various concentrations of PDADMAC were introduced to determine the optimal synthesis condition. CS-cat solutions (2.5 mL) and PDADMAC solutions (2.5 mL) were mixed well before combined addition to the CNC dispersion under probe sonication. It was expected that both CS-cat and PDADMAC polymer coatings would be present on the surface of the CNCs.

The CPC-cat solutions prepared at various mass ratios are shown in Figure 4-12. The particle size and zeta potential of each solution was measured to elucidate the colloidal behavior of CPC-cat and determine the optimal mass ratio for their application in MDDS. As shown in Figure 4-13A, increasing the amount of PDADMAC resulted in higher positive zeta potentials. At mass ratios of 15:1 and 10:1 CS-cat to PDADMAC, the measured zeta potentials were below +30 mV, which falls under colloidal instability. All mass ratios above 10:1 showed excellent colloidal stability, with the highest zeta potentials of +40 mV being observed at mass ratios of 1:2 and 1:5. Average particle sizes at all the mass ratios ranged from 300 to 400 nm. However, the slight increase in the particle size from 1:2 to 1:5 prompted the selection of 1:2 as the optimized synthesis condition. Further characterization such as pH studies, UV-Visible spectroscopy, FTIR, and TEM were conducted using the 1:2 CPC-cat nanoparticles.

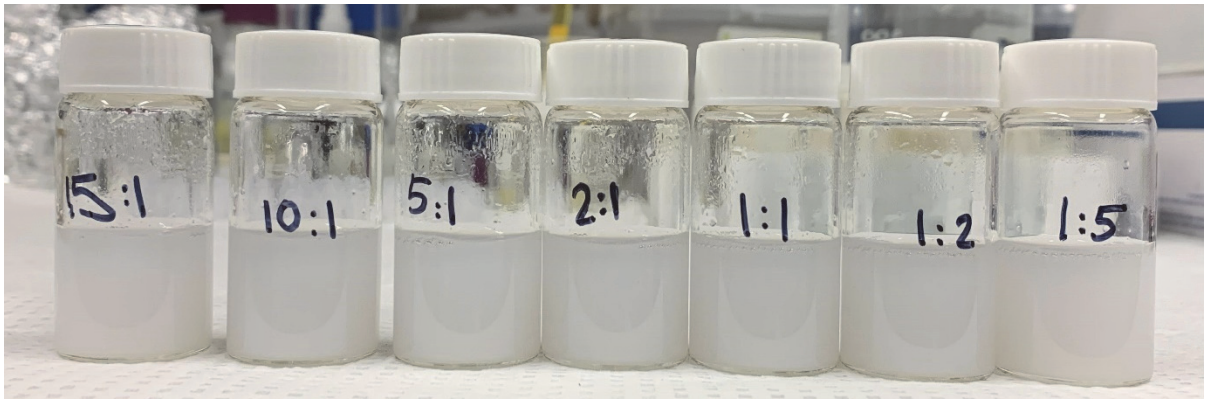

Figure 4-12. CPC-cat synthesized at various CS-cat:PDADMAC mass ratios

To determine whether the addition of PDADMAC had a positive effect on the colloidal stability at pH 7 and 8, the particle sizes and zeta potentials were measured from pH 2 to 10 (Figure 4-13B), similar to what was done previously for CC-cat (Figure 4-11). CPC-cat was found to be colloidally stable from pH 2 to 10, with zeta potentials ranging from +30 to +55 mV. While the zeta potential did decrease at higher pH due to de-protonation of the amine groups, the addition of PDADMAC ensured that the overall positive surface charge was maintained and the system remained stable. At pH 9 and 10, a positive zeta potential was observed for CPC-cat compared to the negative zeta potential for the CC-cat nanoparticles.

The optimized CPC-cat nanoparticles were characterized by UV-Visible spectroscopy and FTIR to confirm the presence of the catechol groups, which are essential to enhance the mucoadhesive properties. The UV-Vis spectrum for 1:2 CPC-cat at pH 5 (Figure 4-9) had an absorbance peak at 280 nm, which had a similar peak height to CC-cat. This corroborated that the CC-cat and CPC-cat nanoparticles had the same CNC:CS-cat mass ratio of 1:1. Additionally, the FTIR spectrum for CPC-cat (Figure 4-6) had a peak corresponding to the

amide linkage at 1650 cm^{-1}, confirming the presence of the catechol-modified chitosan (CS-cat).

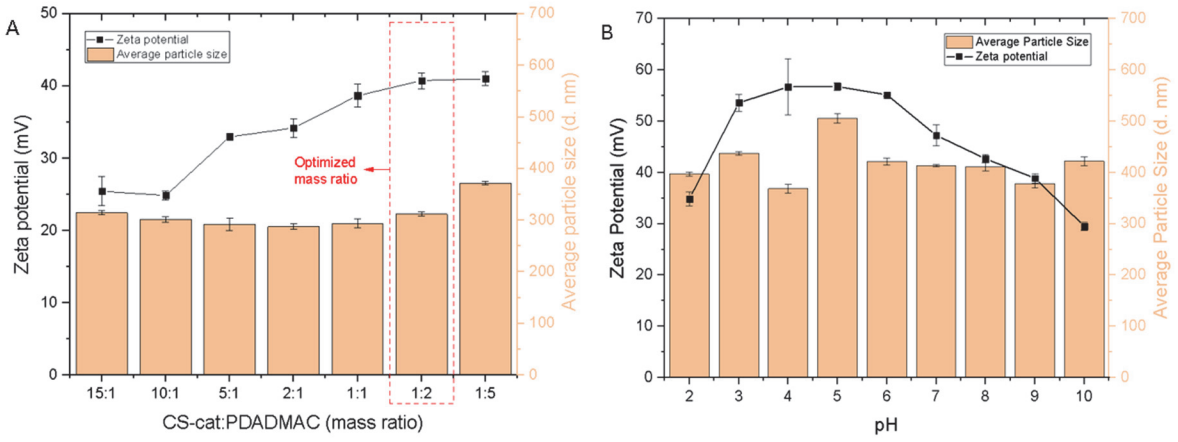

Figure 4-13. Zeta potential and average particle sizes of CPC-cat at A) different mass ratios (CS-cat-PDADMAC w/w), and B) different pH values (optimized mass ratio)

The morphology of the CPC-cat nanoparticles was observed by TEM (Figure 4-14). The CNCs maintained their rod morphology after the modification and appeared thicker than pristine CNCs (Figure 3-5) due to the presence of PDADMAC and CS-cat coatings. The mean length of the particles was about 300 nm, which agreed well with the size results obtained from the Zetasizer. The CPC-cat nanoparticles also exhibited a more uniform shape and size distribution compared to the CC-cat nanoparticles (Figure 4-10). Interestingly, black dots were observed on the CPC-cat nanoparticles, which were not observed in TEM images for CC-cat. This suggests the successful incorporation of PDADMAC into the system. Similar black dots were observed by Dong et al. [85] on CNC-PDADMAC nanoparticles.

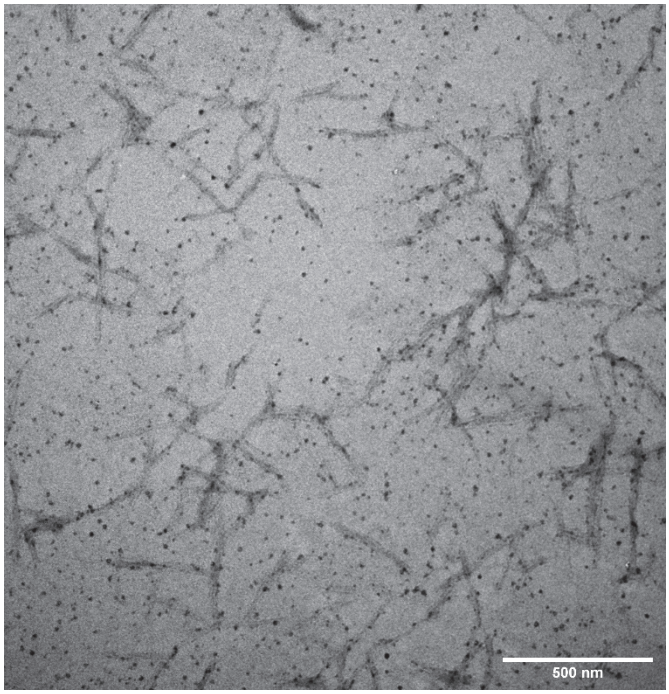

Figure 4-14. TEM image of CPC-cat nanoparticles (scale bar is 500 nm)

4.4 Conclusions

The novel mucoadhesive polymer, CS-cat was coated onto CNCs to enhance their mucoadhesive capabilities. CC-cat nanoparticles were prepared by a simple electrostatic gelation technique under probe sonication, and the optimal CNC:CS-cat mass ratio was found to be 1:1. However, the CC-cat nanoparticles exhibited poor colloidal stability above pH 6, which limits their applications in marine drug delivery. This was addressed by introducing PDADMAC, a synthetic cationic polymer, to increase the positive surface charge and improve the colloidal stability. The optimal CS-cat:PDADMAC mass ratio for synthesis of CPC-cat nanoparticles was found to be 1:2, with a particle size of about 300 nm and zeta potential of +40 mV. CPC-cat had a positive surface charge and was stable from pH 2 to 10, ensuring it

would be able to interact electrostatically with mucin. Furthermore, the presence of the catechol group is expected to induce strong covalent bonds with the thiol and amine groups of mucin. The mechanism of the interaction and the enhancement in mucoadhesive ability of CNC due to CS-cat and PDADMAC coatings is investigated in Chapter 5.

Chapter 5. Mucoadhesive Properties of CNC-TA and CPC-cat Nanoparticles

5.1 Introduction

The development of controlled drug delivery systems has advanced the controlled release of active compounds, allowing the desired therapeutic effects to be achieved at a lower drug dosage [14]. Cellulose nanocrystals (CNCs) have been explored for controlled drug delivery due to their desirable characteristics such as high surface area, excellent water dispersibility, and ease of surface modification [86]. However, the success of controlled drug delivery systems is limited by the short residence time at the target sites. The phenomenon of mucoadhesion offers a way to prolong the residence time by achieving an intimate contact between the drug carrier and the absorption sites [16]. Mucoadhesive drug carriers can be developed using mucoadhesive polymers that interact with mucosal sites by various types of bonding.

A recent study by Lin et al. [10] revealed that CNCs can interact with mucous in simulated gastric and intestinal conditions via the formation of hydrogen bonds. The mucoadhesive capabilities of CNCs were found to be comparable to well-known mucoadhesive polymers such as pectin and Carbomer, but weak when compared to second generation mucoadhesives such as thiolated polymers that can form specific bonds with mucin. The surface modifications described in Chapters 3 and 4 were performed to enhance the mucoadhesive capabilities of CNCs by introducing functional groups that can interact more strongly with mucin.

The interactions of the modified CNCs with mucin are described in this chapter. Turbidity titrations, rheology, and adhesive force measurements were employed to evaluate the mucoadhesive capabilities of CNC, CNC-TA, and CPC-cat. The modified CNCs were

compared with pristine CNCs to evaluate the enhancement in their mucoadhesive properties. The primary mechanisms of mucoadhesion for each material were also investigated by the addition of chemical blockers such as urea and salt.

5.2 Materials and Methods

5.2.1 Materials

Mucin from porcine stomach (PGM) type II, Urea (ACS reagent, 99.0-100.5%), hydrochloric acid (ACS reagent, 37%), and sodium chloride (ACS reagent, ≥ 99.0%) were purchased from Sigma Aldrich. Phosphate buffered saline (PBS) tablets (biotechnology grade) were purchased from VWR Life Science. Cellulose nanocrystals (CNC) were supplied by Celluforce Inc. CNC-TA and CPC-cat powders were obtained by freeze-drying as outlined in the previous chapters.

5.2.2 Turbidimetric Titrations

The turbidity of the colloids upon the addition of increasing amounts of polymer (CNC, CNC-TA, and CPC-cat) was evaluated using a Cary 100 Bio UV-Vis Spectrophotometer. Briefly, 1 mg/mL solutions of mucin and each polymer were prepared in PBS buffer (pH 7.4). The polymer solutions were added to mucin solutions at various ratios (g/g) of polymer to mucin (Table 2). The mixtures were allowed to equilibrate for 10 seconds and the absorbance was recorded at 600 nm.

Table 2. Polymer/mucin ratios for turbidity measurements

Polymer/mucin (g/g)	Volume of mucin (pH 7.4)	Volume of polymer (pH 7.4)
0	1 mL	0 µL
0.2	1 mL	200 µL
0.4	1 mL	400 µL
0.6	1 mL	600 µL
0.8	1 mL	800 µL
1	1 mL	1 mL

5.2.3 Zeta Potential and Size Measurements

The mechanism of interaction between CPC-cat and mucin was investigated by measuring the zeta potential and size of aggregates formed during the turbidimetric titrations. The CPC-cat/mucin mixtures were transferred to disposable sizing cuvettes and folded capillary cells for the size and zeta potential measurements respectively. Measurements were performed using a Malvern Nano-ZS90 Zetasizer at room temperature. The refractive index was set to 1.150 and measurements were repeated 3 times (10 runs each), with the average presented.

5.2.4 Rheology Measurements

The rheological properties of polymer and mucin mixtures were measured to evaluate their interactions with mucin in an aqueous environment. Briefly, a 10 wt% solution of porcine gastric mucin, and 1 wt% solutions of CNC, CNC-TA, and CPC-cat were prepared by stirring

overnight at room temperature. Polymer solutions were individually mixed with mucin solutions in a 1:1 ratio (5 mL each). The mixtures were placed on a rolling mixer for three days to ensure they were well mixed. A 5 wt% mucin solution and 0.5 wt% solutions of each polymer were also prepared by diluting with Milli-Q water. A Malvern Kinexus Ultra+ rheometer was used for all the rheological measurements at 25 °C, using the cup geometry for the less viscous solutions and the cone-plate geometry for the more viscous mixtures. The shear viscosity of all solutions was measured from shear rate 0.1 to 1000 s^{-1}, with a ramp time of 2 minutes. The viscosity enhancements due to mucoadhesion were calculated using the following equation at shear rates of 4 s^{-1} and 10 s^{-1}:

$$\eta_{enhancement} = \eta_{mixture} - \left(\eta_{5\%mucin} + \eta_{0.5\%polymer}\right)$$

5.2.5 Addition of Chemical Blockers

The nature of the interactions between the synthesized nanoparticles and mucin was investigated using chemical blockers to shield the interactions. Urea was used to shield hydrogen bonds, and sodium chloride was used to shield electrostatic interactions. Turbidimetric titrations for CNC and CNC-TA were repeated with separate solutions prepared in 2M urea and PBS buffer. 10 mg/mL CNC and CNC-TA were titrated with 1 mg/mL mucin at polymer/mucin ratios of 0.2, 0.4, 2, 4, 8, and 16. Turbidimetric titrations for CPC-cat were repeated following the same procedure described in Section 5.2.2, with CPC-cat and mucin solutions prepared in 1M NaCl. The zeta potential and size of the CPC-cat/mucin mixtures were measured following the procedure outlined in Section 5.2.3. Viscosity measurements for the polymer-mucin mixtures were also repeated with solutions prepared in 1M NaCl for CPC-cat, and 2M and 5M urea for CNC and CNC-TA.

5.2.6 Adhesive Force Measurements

Films (0.5 mm thickness) of CNC, CNC-TA, and CPC-cat were prepared by casting 3 wt% solutions on petri dishes lined with Parafilm. The films were left to dry overnight in a fume hood under ambient conditions. Mucin powder was dispersed in Milli-Q water and stirred overnight to prepare a 5 wt% solution. The force of adhesion was measured using a DataPhysics DCAT 25 with a RG 2 Du Nouy ring. An immersion depth of 0.5 mm, motor speed of 0.05 mm/s, and surface detection of 2 mg were used for all measurements. The films were cut into small circles, taped to a glass slide with the help of double-sided tape, and placed on the sample holder. A droplet (3 µL) of mucin solution was carefully placed on the ring and inserted above the film. The measurements were repeated twice for each material and the average is presented.

5.3 Results and Discussion

5.3.1 Interactions of CNC, CNC-TA, and CPC-cat with mucin

The strength of the interactions of CNC, CNC-TA, and CPC-cat with mucin was evaluated and compared using turbidity titrations, rheology, and adhesive force measurements. Commercially available porcine gastric mucin (PGM) type II was used as a substitute for fresh mucin or fresh mucosa. Commercial PGM has been widely used as it has been shown to provide reliable information on the mucoadhesive interactions. It is also more easily available and has reproducible quality [87].

5.3.1.1 Turbidimetric titrations

The interactions of pristine and modified CNCs with mucin were first studied by turbidimetric titration at pH 7.4 (Figure 5-1). The absorbance of polymer/mucin mixtures was recorded at 600 nm, and turbidity, τ was calculated according to Equation 3.

$$\tau = \frac{A}{L}\ln(10) \qquad (3)$$

where A is the absorbance at 600 nm, and L is the path length (1.2 cm).

The addition of pristine CNCs to mucin was accompanied by a linear increase in the turbidity with increasing CNC concentrations. The increasing turbidity of the mixture was due to the aggregation of mucin particles upon the polymer adsorption on the surface. Similar increases in turbidity were observed for both CNC-TA and CPC-cat, indicating their ability to interact with mucin. The aggregates observed upon the addition of the modified CNCs were large enough to be visible to the naked eye, indicating that these interactions were stronger than the interaction with CNC.

The relative strength of the interactions was also assessed by the maximum turbidity observed in each case. Compared to CNC, CNC-TA showed a steeper increase in turbidity, with the maximum turbidity of 1.68 cm^{-1} being observed at a polymer/mucin mass ratio of 0.8. Further addition of polymer caused a slight decrease in turbidity, indicating the CNC-TA was in excess. It is expected that exceeding a polymer/mucin mass ratio of 1.0 would cause a linear decrease in the turbidity due to further dilution of the mucin aggregates [88]. Compared to CNC-TA, CPC-cat showed an even steeper initial increase in turbidity as the negatively charged mucin formed complexes with the positively charged polymer. The maximum turbidity for CPC-cat was 1.99 cm^{-1} at a polymer/mucin mass ratio of 0.4, after which a slow

decline was observed. Previous studies have shown that catechol can form strong covalent bonds with mucin when it has been oxidized to quinones, which typically occurs above pH 6.7 [83]. However, the oxidation process takes several days and it is likely that these covalent bonds were not formed during the turbidity titrations. This is addressed in more detail in the following sections.

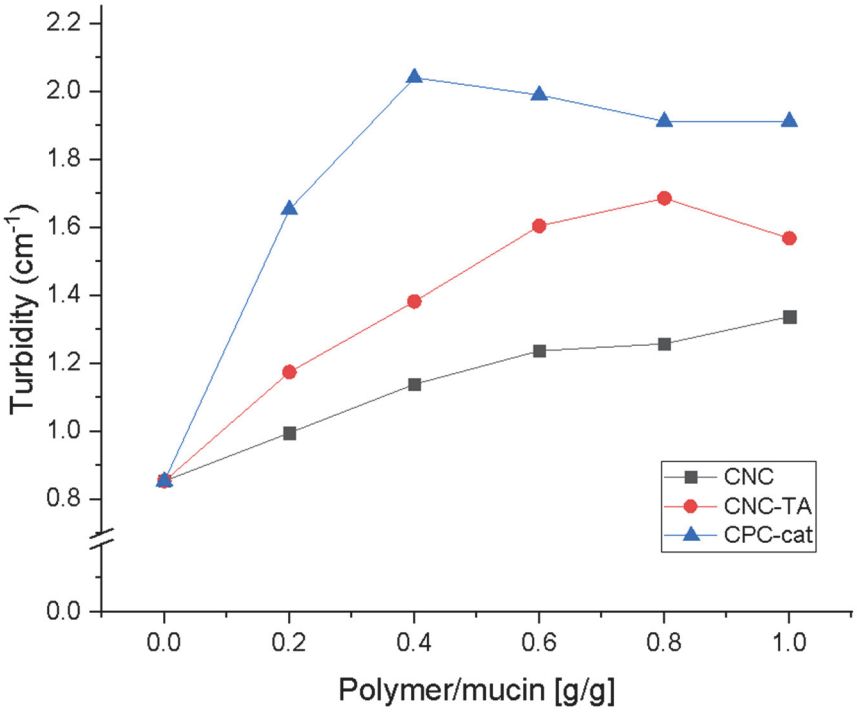

Figure 5-1. Turbidimetric titrations of 1 mg/mL mucin by 1 mg/mL solutions of CNC, CNC-TA, and CPC-cat. All solutions were prepared in PBS (pH 7.4)

5.3.1.2 Rheology

The strength of mucoadhesive interactions can also be assessed using rheological measurements. Physical and chemical bond energies in mucin-polymer interactions can be transformed into mechanical energy or work, which alters the shape or arrangement of

macromolecules and is the basis for changes in viscosity [57]. In the absence of any interaction, the viscosity of a polymer-mucin mixture is simply the sum of the viscosities of the components. However, when a mucoadhesive polymer is mixed with mucin, a synergistic increase in viscosity is typically observed. A greater viscosity synergism is indicative of a stronger polymer-mucin reaction [64].

The viscosities of CNC, CNC-TA, CPC-cat, mucin, and their mixtures with mucin are shown in Figure 5-2A. The viscosities of the mixtures were higher compared to the viscosities of the individual solutions, confirming that all three nanomaterials display mucoadhesive properties. The relative strengths of the interaction were assessed by the calculation of $\eta_{enhancement}$ and $\eta_{relative}$, which relate the expected and observed viscosities according to the following equations:

$$\eta_{enhancement} = \eta_{observed} - \eta_{expected}$$

$$\eta_{relative} = \eta_{observed}/\eta_{expected}$$

where $\eta_{expected}$ is the sum of the individual viscosities of mucin and polymer, and $\eta_{observed}$ is the measured viscosity of the polymer-mucin mixture.

The viscosity enhancements for each material are summarized in Figure 5-2B. The trend observed was similar to the turbidity titrations, where the modified CNCs had a greater viscosity enhancement than pristine CNCs at both shear rates, indicating enhanced mucoadhesive properties. A notable difference here is the extent of the enhancement for CPC-cat, which was significantly greater than the enhancement for CNC-TA. This could be explained by the presence of covalent bonding between the oxidized catechol and the amines and thiols of mucin. As discussed previously, catechol was oxidized above pH 6.7 with the

process taking several days to occur. It is likely that the catechol was oxidized to quinones during the three day mixing process, enabling the mucoadhesive interaction to be greatly strengthened by the introduction of strong covalent bonds.

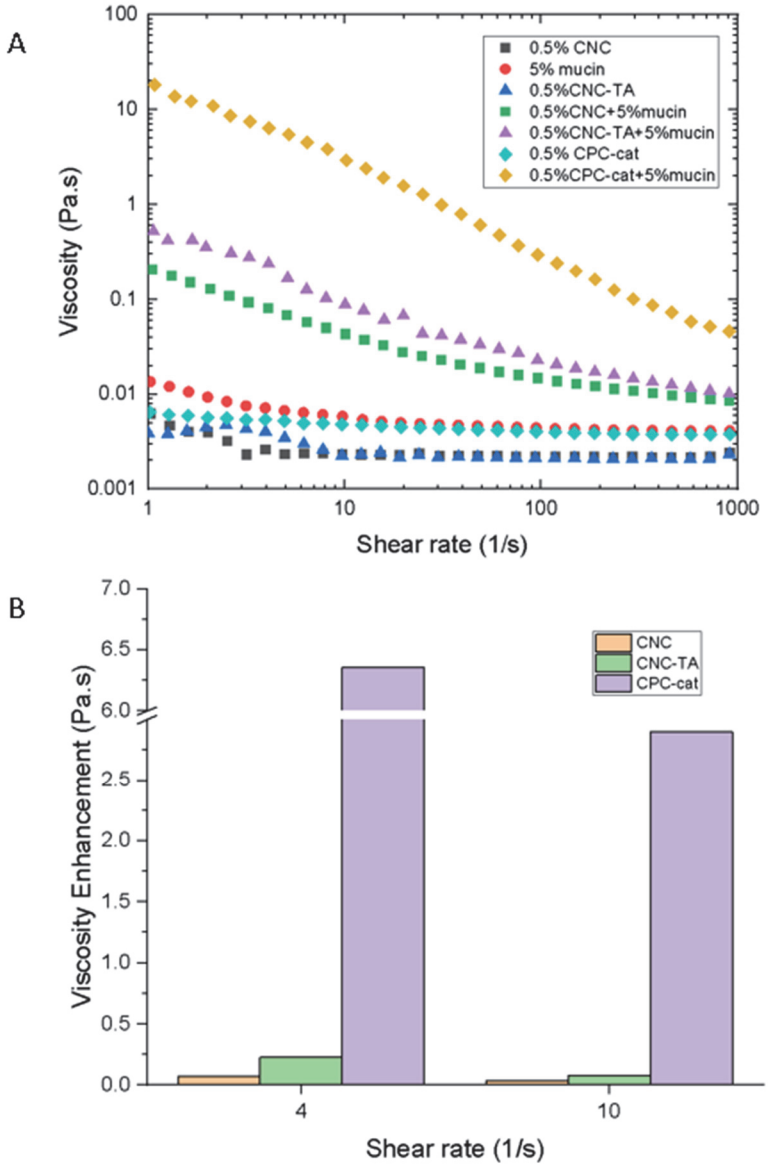

Figure 5-2. A) Viscosities of 0.5% CNC, CNC-TA, and CPC-cat and their mixtures with 5% mucin, and B) Viscosity enhancements of CNC, CNC-TA, and CPC-cat at shear rates 4 s^{-1} and 10 s^{-1}.

The magnitude of the rheology synergism is better described by the $\eta_{relative}$, or relative viscosity enhancement, which allows the enhancement to be expressed as a proportion of the viscosities of the unmixed materials. A $\eta_{relative} = 1$ is indicative of no interaction, while higher values are associated with mucoadhesive interactions. The calculated $\eta_{relative}$ for CNC, CNC-TA, and CPC-cat are summarized in Table 3. Pristine CNCs showed an 8-fold enhancement in viscosity at a shear rate of 4 s^{-1} when mixed with mucin. Modification of CNCs with tannic acid strengthened the interactions with mucin slightly, with a 21-fold enhancement being observed, while CPC-cat displayed the strongest mucoadhesion, with a 500-fold enhancement in viscosity. For all three materials, the $_{enhancement}$ and $\eta_{relative}$ were reduced at higher shear rates, indicating shear thinning behavior. The increase in shear rate disrupted the interactions with mucin, causing the relative viscosity enhancements to drop to 5.27, 10.90, and 273.11 for CNC, CNC-TA, and CPC-cat respectively.

Table 3. Expected and observed viscosities of polymer-mucin mixtures at shear rates $4s^{-1}$ and $10\ s^{-1}$

Sample	Viscosity (mPa.s)	
	Shear rate = 4 s^{-1}	**Shear rate = 10 s^{-1}**
0.5% CNC + 5% mucin		
$\eta_{expected}$	9.82	8.22
$\eta_{observed}$	81.71	43.34
$\eta_{relative}$	8.32	5.27
0.5% CNC-TA + 5% mucin		
$\eta_{expected}$	11.23	8.12
$\eta_{observed}$	273.6	88.54
$\eta_{relative}$	21.16	10.90
0.5 % CPC-cat + 5 % mucin		
$\eta_{expected}$	12.60	10.66
$\eta_{observed}$	6371.00	2911.33
$\eta_{relative}$	505.63	273.11

5.3.1.3 Adhesive Force Measurements

The mucoadhesive capabilities of pristine CNCs were compared with the modified CNCs by measuring the adhesive force between a droplet of mucin and films of each material. As shown in Figure 5-3, both CNC-TA and CPC-cat had larger adhesive forces with mucin compared to pristine CNCs. The enhancement in the adhesive force was about 1.5 times for both the modified CNCs. While these results indicate enhanced mucoadhesion compared to CNCs, the trend observed did not exhibit a similar enhancement compared to the rheology and turbidity titration results, where the CPC-cat had a significantly larger enhancement compared to CNC-TA. During the measurements, it was observed that the full droplet was not lifted off the films due to the adhesion between the mucin and polymer. Therefore, these results might

not be a good representation of the mucoadhesive properties. Adjustments, such as reducing the penetration depth were attempted to rectify the issue, however, parts of the droplet still remained on the films. Additionally, there was no literature to refer to, as this method has not previously been used to characterize mucoadhesion. Based on these issues, the data obtained using this method was treated as supporting information for results obtained by rheology and turbidity titrations. Further improvements would be required for this method to be utilized as a stand-alone method for measuring mucoadhesive forces. It may also be useful to perform a control experiment with a water droplet to evaluate the extent of the interaction with the mucin protein.

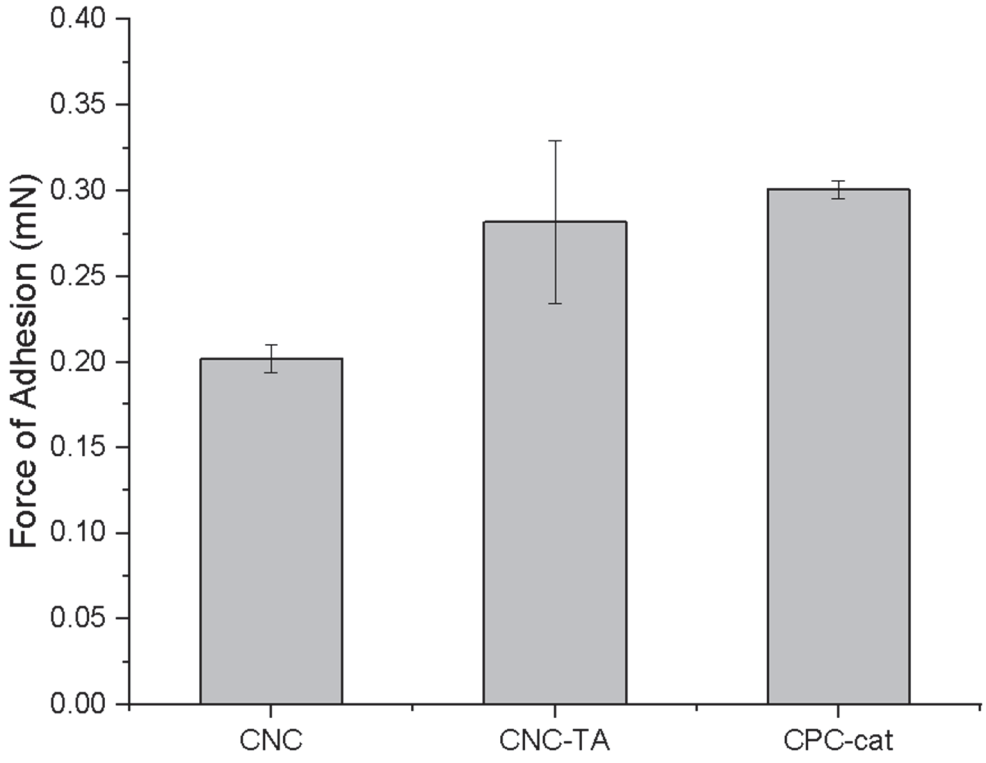

Figure 5-3. Force of adhesion between 5% mucin and films of CNC, CNC-TA, and CPC-cat.

5.3.2 Mechanisms of mucoadhesion

5.3.2.1 Hydrogen Bonding

The primary mechanism of mucoadhesion for CNCs and CNC-TA was expected to be hydrogen bonding. The hydroxyl and carboxylic acid groups of mucin can form hydrogen bonds with the hydroxyl groups of CNC. Coating the CNCs with tannic acid was expected to strengthen the interaction by the introduction of more hydroxyl groups that can participate in hydrogen bond formation. Additionally, during the synthesis, some of the hydroxyl groups were oxidized to quinones, which can form hydrogen bonds due to the lone pairs on the oxygen atom. The enhanced mucoadhesive capabilities were confirmed in Section 5.3.1.

To establish that the interaction was due to hydrogen bonding, turbidimetric titrations for CNC and CNC-TA were repeated in the presence of urea. Urea is known to act as a strong competitor for hydrogen bonds, and its presence in mucin dispersions can cause partial disruption of the intraparticle hydrogen bonds that hold the mucin particles together [89]. As shown in Figure 5-4, when the titrations were carried out in 2M urea, both CNCs and CNC-TA showed a decrease in turbidity as polymer concentration was increased. This indicates that there was no aggregation or formation of mucin-polymer complexes, and the addition of polymer solution simply diluted the mucin dispersion, resulting in reduced turbidity.

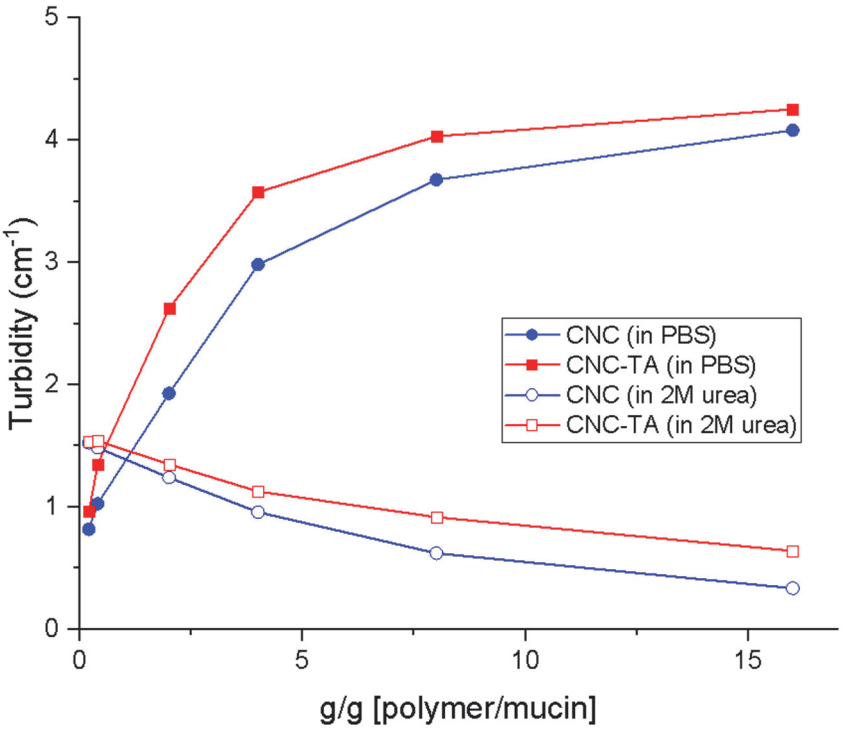

Figure 5-4. Turbidimetric titrations of 1 mg/mL mucin by 10 mg/mL solutions of CNC and CNC-TA

Repeating the rheology measurements in 2M and 5M urea displayed similar results as shown in Figure 5-5. The viscosity curves for the polymer-mucin mixtures were shifted downwards with the addition of urea, as the hydrogen bonds were disrupted and the interactions became weaker. For CNCs, at a shear rate of 4 s^{-1}, a 2-fold decrease was observed in the viscosity enhancement compared to a 6-fold decrease for CNC-TA with the addition of 2M urea. Similar to previous observations, at a shear rate of 10 s^{-1}, the enhancement in all conditions was reduced due to shear thinning. Increasing the concentration of urea to 5M further weakened the interactions, with the viscosity enhancements being decreased further. Interestingly, there is still a significant enhancement in viscosity with 5M urea, which reveals there are still mucoadhesive interactions present. This may either suggest the presence of other

types of bonding such as hydrophobic interactions between the nanoparticles and the mucin, or that a greater concentration of urea is required for complete shielding of the hydrogen bonds.

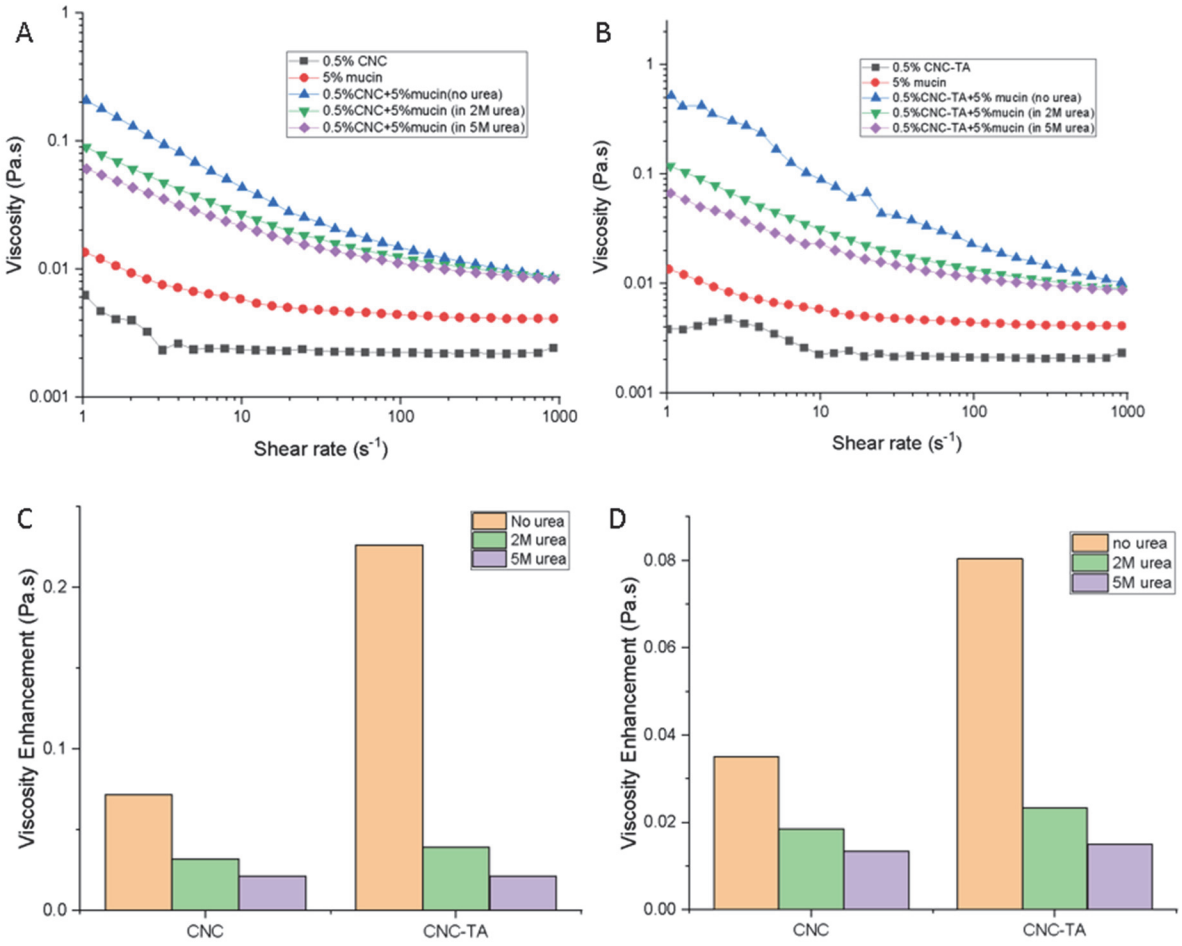

Figure 5-5. Effects of adding 2M and 5M urea. A,B) Viscosities of CNC-mucin (A) and CNC-TA mucin (B) mixtures, and C,D) Viscosity enhancements for CNC and CNC-TA at shear rate 4 s^{-1} (C) and shear rate 10 s^{-1} (D)

5.3.2.2 Electrostatic interactions

Coating CNCs with PDADMAC and CS-cat caused the surface charge of the CNCs to change from negative to positive. As a result, CPC-cat nanoparticles were expected to bind

electrostatically with negatively charged mucin proteins, forming stronger mucoadhesive bonds than pristine CNCs. The role of electrostatic interactions between the oppositely charged polymers and mucin was studied in the presence of 1M NaCl, which screens the Coulomb forces. As shown in Figure 5-6A, the turbidity of the mucin dispersion after the addition of CPC-cat increased slightly even in the presence of the salt, but to a much lesser extent than the measurements performed in PBS, indicating that interactions were weakened. The maximum turbidity of 1.06 cm^{-1} in 1M NaCl was observed at a polymer/mucin mass ratio of 0.4, after which it began to decrease due to dilution of the mucin aggregates. This result confirmed the presence of electrostatic interactions between CPC-cat and mucin.

Particle size and zeta potential measurements were performed to further probe the affinity of the CPC-cat particles to mucin. As shown in Figure 5-6B, mucin prepared at pH 7.4 had an average particle size of about 400 nm. Addition of CPC-cat at a polymer/mucin mass ratio of 0.2 resulted in a large increase in the particle size as the particles adsorbed onto the mucin, forming large aggregates. The trend in the particle size as a function of the polymer/mucin mass ratio was generally in accordance with the turbidimetric titration (Figure 5-6A), that is the maximum particle size was observed at lower ratios followed by a decrease, thus confirming that the changes in turbidity were due to changes in the particle size of the dispersion. When the measurements were repeated in 1M NaCl, a similar trend was observed, but the average size of the aggregates was smaller, indicating less polymer adhered to the mucin due to partial shielding of the electrostatic interactions.

The surface charge of the aggregates in Milli-Q water and NaCl was studied by zeta potential analysis (Figure 5-6C). At pH 7.4, mucin had a negative surface charge of about -15

mV. This can be attributed to the deprotonated carboxylic acid groups (pKa~4) [83]. When CPC-cat was added at a ratio of 0.2, the surface charge became less negative as the positively charged particles adhered to the mucin. The charge reversal of the mucin particles occurred around a mass ratio of 0.4, which corresponds to the maximum turbidity. Beyond this, the positive surface charge increased up to the final mass ratio of 1.0. The decrease in the aggregate size after a ratio of 0.6 (Figure 5-6B) can be explained by the increasing zeta potential, which results in electrostatic repulsion and disaggregation. In contrast, the surface charge remained negative at all the mass ratios for titrations performed in NaCl, indicating fewer positively charged particles were adhering to mucin. This further confirms the electrostatic forces between CPC-cat and mucin.

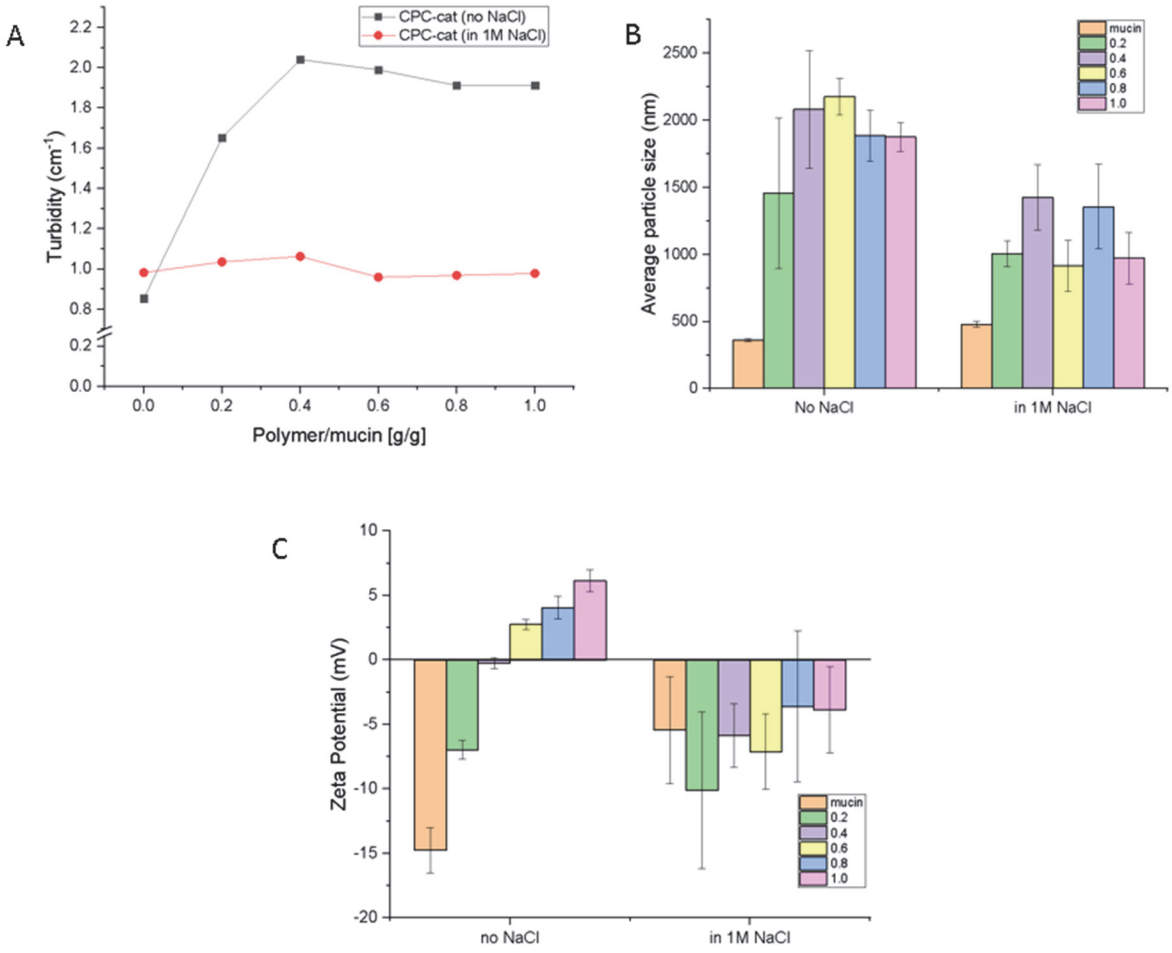

Figure 5-6. Effects of NaCl screening on A) Turbidity of CPC-cat-mucin mixtures, B) Size of CPC-cat-mucin complexes, and C) Zeta potential of CPC-cat-mucin complexes

The presence of electrostatic interactions was also confirmed by rheology. Mixtures of 0.5% CPC-cat and 5% mucin were prepared in Milli-Q water and 1M NaCl and the viscosity enhancements were compared. The mixtures were initially prepared in glass vials (Figure 5-7A), but due to the strong electrostatic interactions, the positively charged aggregates bound to the negatively charged glass. Interestingly, the binding was less pronounced in the NaCl,

indicating weaker interactions due to the shielding. However, since the aggregates were no longer within the solution, the viscosity measurements were not an accurate representation of the enhanced mucoadhesive properties. To rectify this, mixtures were prepared in falcon tubes (Figure 5-7B). The interactions between CPC-cat and mucin were clearly visible in Milli-Q water whereas no such observation was made in NaCl. This further indicated that there were electrostatic interactions at play.

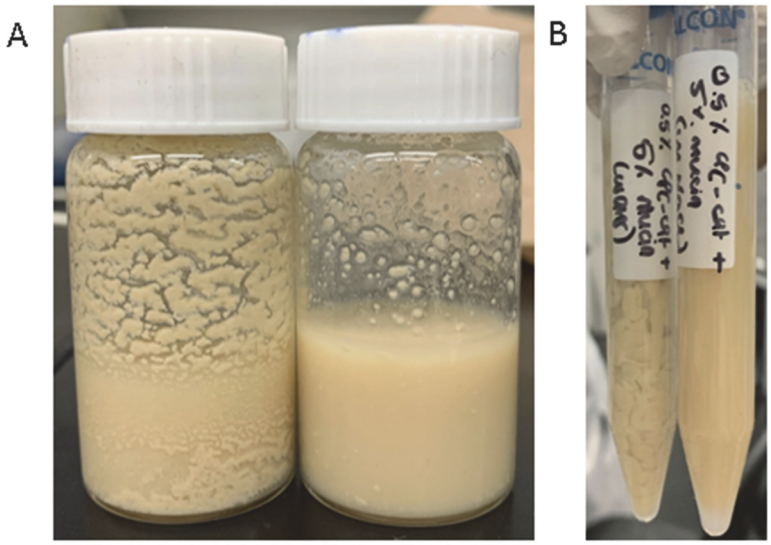

Figure 5-7. A, B) CPC-cat-mucin mixtures prepared in Milli-Q water (left) and 1M NaCl (right)

Quantitative proof of the decrease in mucoadhesive interactions was obtained through the viscosity measurements (Figure 5-8A) and the subsequent calculations of the viscosity enhancement (Figure 5-8B). About an 80-fold reduction was observed in the viscosity enhancements at shear rates of 4 s^{-1} and 10 s^{-1}. The large decrease indicated that electrostatic interactions were the primary mechanism of mucoadhesion. However, a small enhancement

remained even after screening, which suggested that other types of interactions such as hydrogen bonding may be involved.

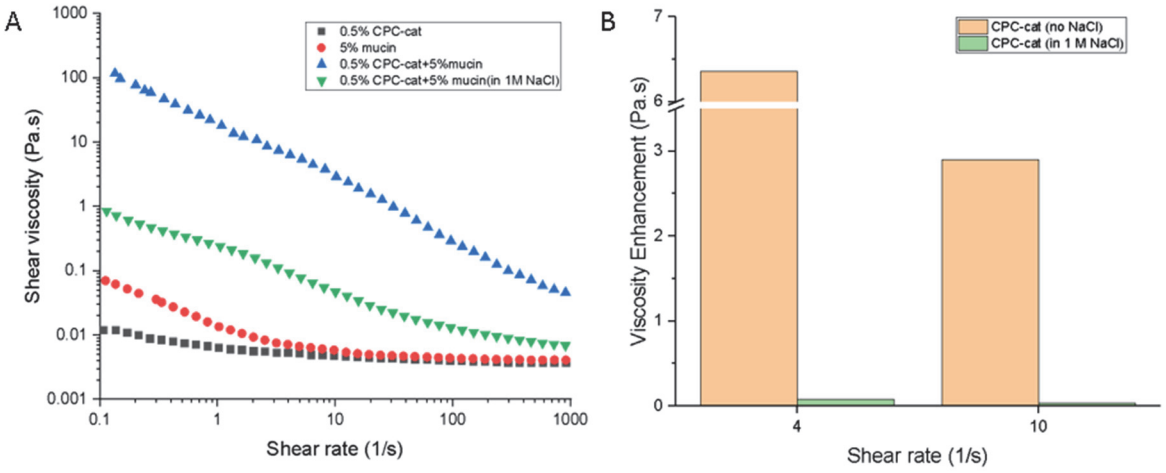

Figure 5-8. Effects of NaCl screening on A) Viscosities of CPC-cat mixtures, and B) Viscosity enhancements for CPC-cat at shear rates $4s^{-1}$ and $10s^{-1}$.

5.4 Conclusions

The enhancement in the mucoadhesive capabilities of CNCs modified with tannic acid (CNC-TA) and catechol (CPC-cat) was evaluated. Turbidity titrations and rheology experiments revealed that both the modified CNCs had stronger interactions with mucin compared to pristine CNCs. The primary mechanism for the interaction of CNC and CNC-TA with mucin was hydrogen bonding, which was confirmed by repeating measurements in urea. CPC-cat nanoparticles primarily interacted with mucin via electrostatic interactions due to their positive surface charge and this was confirmed by screening with sodium chloride. The catechol groups of CPC-cat can also form covalent bonds with mucin when oxidized. While

the presence of these bonds was not studied in detail, the differences in the extent of enhancement measured by turbidity titrations and rheology suggested that covalent bonding was involved. The differences in the nature of the interactions resulted in the catechol-functionalized CNCs displaying stronger mucoadhesion compared to CNCs coated with tannic acid.

Chapter 6. Conclusions and Recommendations for Future Work

In summary, cellulose nanocrystals (CNCs) were successfully modified with phenolic compounds including tannic acid (CNC-TA) and catechol (CPC-cat). The optimal synthesis conditions, colloidal stability and morphology of each material were studied in detail. The optimal mass ratio for the preparation of CNC-TA was determined as 20:1 (CNC:TA). The CNC-TA nanoparticles maintained the rod morphology of CNCs, and were stable at pH 7. The optimal mass ratios for preparation of CPC-cat were 1:1:2 (CNC:CS-cat:PDADMAC). The addition of PDADMAC ensured that CPC-cat was colloidally stable at pH 7 and maintained a positive surface charge for electrostatic interactions with mucin. Both the modified CNCs had a small particle size, which would enable good mucopenetration. The mucoadhesive capabilities of the modified CNCs were evaluated by turbidity titrations, rheology, and adhesive force measurements and compared with the mucoadhesive capability of CNCs. All three methods showed that the modifications enhanced the interactions of CNC with mucin. CPC-cat nanoparticles interacted with mucin by electrostatic interactions and covalent bonding, while CNC-TA nanoparticles interacted by forming hydrogen bonds with mucin.

While this study has demonstrated the ability of CNC-TA and CPC-cat to interact with mucin, there are several aspects that need to be investigated. Firstly, the mucoadhesive capabilities should be evaluated using direct methods with fresh mucosal tissues. The use of fresh tissue would allow for a more comprehensive evaluation of the mucoadhesive capabilities as it more closely mimics real systems. Possible tests could include performing tensile assays to measure the maximum detachment force and total work of adhesion. These assays would provide a more accurate assessment of the mucoadhesive forces compared to the method used in this work. Additionally, flow assays or the rotating cylinder method could be used to

determine the residence time of CNC-TA and CPC-cat on mucosa. All the aforementioned methods have been reported in the literature and data obtained through these tests would allow us to compare our systems to other well-known mucoadhesive materials as well as evaluate whether further improvement is required.

Furthermore, this study focused solely on determining the primary forces of interaction between the modified CNCs and mucin. However, there may be other driving forces such as hydrophobic interactions at play. The presence of several types of interactions could help ensure mucoadhesive capabilities are not diminished in different environmental conditions. This is particularly important in the case of CPC-cat, since electrostatic interactions could be shielded in the presence of salt in the oceans. Experiments should be conducted to confirm the presence of more than one type of binding, specifically hydrophobic interactions for both materials and hydrogen bonding for CPC-cat.

These materials were designed to be incorporated in mucoadhesive drug delivery systems for the treatment of sea lice in salmon farms. Future work should be directed at more closely mimicking the conditions these materials would be used in. While criteria such as particle size, stability, and surface functionalities were considered, there are other factors that could be taken into consideration. For instance, since the temperature and pH of the ocean are not constant across regions as well as throughout the year, it would be useful to conduct the mucoadhesive tests at a wider range of temperature (18 – 25 ^{o}C) and pH values (7-8). Additionally, tests could be conducted in sea water or simulated conditions that mimic those on the farms. This would ensure the particles could be used to treat fish existing in different environments. Additionally, tests should be performed using mucin/mucous from fish as

opposed to the porcine mucin used in this work. The mucosa of fish is subject to constant change, and the composition depends on various factors including the presence of infections. It may also vary across different species of fish. Therefore, performing tests using mucin extracted directly from fish subjected to different conditions could help evaluate whether these particles can be applied more widely.

Future work should also consider the challenges that may be faced when using these materials at a larger scale. This can include the cost and efficiency of manufacturing at a larger scale. The efficacy of the treatment using these particles should be compared with current efficacy using in-feed treatments to ensure value is being added. Drugs used for sea lice treatment currently, such as emamectin benzoate, could be used to evaluate the drug loading and encapsulation efficiencies of the particles in addition to conducting drug release studies. The release studies in particular would help to determine how frequently the particles would need to be administered. This is an important consideration, keeping in mind the level of stress fish are subjected to, which can have negative implications on their overall health. Conducting field studies may also prove helpful in this regard. Finally, toxicity studies should also be conducted to evaluate the safety of using these particles for fish treatment.

References

[1] A. I. S. Luis, E. V. R. Campos, J. L. de Oliveira, and L. F. Fraceto, “Trends in aquaculture sciences: from now to use of nanotechnology for disease control,” *Rev. Aquac.*, vol. 11, no. 1, pp. 119–132, 2019.

[2] S. N. Carmichael *et al.*, “Salmon lice (Lepeophtheirus salmonis) showing varying emamectin benzoate susceptibilities differ in neuronal acetylcholine receptor and GABA-gated chloride channel mRNA expression,” *BMC Genomics*, vol. 14, no. 1, pp. 1–16, 2013.

[3] L. M. Collier and E. H. Pinn, “An assessment of the acute impact of the sea lice treatment ivermectin on a benthic community,” *J. Exp. Mar. Bio. Ecol.*, vol. 230, no. 1, pp. 131–147, 1998.

[4] M. Crane, M. Gross, D. S. Maycock, A. Grant, and B. H. Fossum, “Environmental quality standards for a deltamethrin sea louse treatment in marine finfish aquaculture based on survival time analyses and species sensitivity distributions,” *Aquac. Res.*, vol. 42, no. SUPPL. 1, pp. 68–72, 2011.

[5] R. Gautam, R. Vanderstichel, A. S. Boerlage, C. W. Revie, and K. L. Hammell, “Evaluating bath treatment effectiveness in the control of sea lice burdens on Atlantic salmon in New Brunswick, Canada,” *J. Fish Dis.*, vol. 40, no. 7, pp. 895–905, 2017.

[6] P. F. Neto *et al.*, “Emamectin benzoate in tilapia: Alternative method for drug incorporation into feed and associated residual depletion study,” *Food Res. Int.*, vol. 119, no. January, pp. 524–529, 2019.

[7] B. R. Shah and J. Mraz, “Advances in nanotechnology for sustainable aquaculture and fisheries,” *Rev. Aquac.*, pp. 1–18, 2019.

[8] N. Grishkewich, N. Mohammed, J. Tang, and K. C. Tam, “Current Opinion in Colloid & Interface Science Recent advances in the application of cellulose nanocrystals,” *Curr. Opin. Colloid Interface Sci.*, vol. 29, pp. 32–45, 2017.

[9] A. B. Seabra, J. S. Bernardes, W. J. Fávaro, A. J. Paula, and N. Durán, “Cellulose nanocrystals as carriers in medicine and their toxicities: A review,” *Carbohydr. Polym.*, vol. 181, no. December 2017, pp. 514–527, 2018.

[10] Y. J. Lin, J. A. Shatkin, and F. Kong, “Evaluating mucoadhesion properties of three types of

nanocellulose in the gastrointestinal tract in vitro and ex vivo," *Carbohydr. Polym.*, vol. 210, no. January, pp. 157–166, 2019.

[11] S. Naskar, K. Koutsu, and S. Sharma, "Chitosan-based nanoparticles as drug delivery systems: a review on two decades of research," *J. Drug Target.*, vol. 27, no. 4, pp. 379–393, 2019.

[12] H. M. Yildiz, C. A. McKelvey, P. J. Marsac, and R. L. Carrier, "Size selectivity of intestinal mucus to diffusing particulates is dependent on surface chemistry and exposure to lipids," *J. Drug Target.*, vol. 23, no. 7–8, pp. 768–774, 2015.

[13] F. Laffleur and V. Keckeis, "Advances in drug delivery systems: Work in progress still needed?," *Int. J. Pharm. X*, vol. 2, no. March, 2020.

[14] S. Muppalaneni, D. Mastropietro, and H. Omidian, "Mucoadhesive Drug Delivery Systems," *Eng. Polym. Syst. Improv. Drug Deliv.*, vol. 9781118098, pp. 319–342, 2013.

[15] J. K. Vasir, K. Tambwekar, and S. Garg, "Bioadhesive microspheres as a controlled drug delivery system," vol. 255, pp. 13–32, 2003.

[16] E. Perez and F. Pincet, "Bioadhesion," *Peyresq Lect. Nonlinear Phenom.*, vol. 3, no. 2, pp. 241–278, 2012.

[17] R. P. Brannigan and V. V Khutoryanskiy, "Progress and Current Trends in the Synthesis of Novel Polymers with Enhanced Mucoadhesive Properties," vol. 1900194, pp. 1–11, 2019.

[18] E. A. Kharenko, N. I. Larionova, and N. B. Demina, "Mucoadhesive drug delivery systems (Review)," *Pharm. Chem. J.*, vol. 43, no. 4, pp. 200–208, 2009.

[19] V. V Khutoryanskiy, *Mucoadhesive Materials and Drug Delivery Systems*. John Wiley & Sons, Lrd.

[20] R. Bansil and B. S. Turner, "Mucin structure, aggregation, physiological functions and biomedical applications," *Curr. Opin. Colloid Interface Sci.*, vol. 11, no. 2–3, pp. 164–170, 2006.

[21] R. Bansil and B. S. Turner, "The biology of mucus: Composition, synthesis and organization," *Adv. Drug Deliv. Rev.*, vol. 124, pp. 3–15, 2018.

[22] B. Phanindra, B. Krishna Moorthy, and M. Muthukumaran, "Recent advances in mucoadhesive/bioadhesive drug delivery systems:," *Int. J. Pharma Med. Biol. Sci.*, vol. 1, pp.

1996–1998, 2003.

[23] S. Mansuri, P. Kesharwani, K. Jain, R. K. Tekade, and N. K. Jain, “Mucoadhesion: A promising approach in drug delivery system,” *React. Funct. Polym.*, vol. 100, pp. 151–172, 2016.

[24] A. Ahuja, R. K. Khar, J. Ali, A. Ahuja, R. K. Khar, and J. Ali, “Mucoadhesive Drug Delivery Systems Mucoadhesive Drug Delivery Systems,” vol. 9045, no. 1997, 2008.

[25] R. S. Kumar and K. Nuvati, “Mucosal Drug Delivery Systems : An Overview,” vol. 9, no. 4, pp. 629–634, 2019.

[26] N. A. N. Hanafy, S. Leporatti, and M. A. El-Kemary, “Mucoadhesive hydrogel nanoparticles as smart biomedical drug delivery system,” *Appl. Sci.*, vol. 9, no. 5, 2019.

[27] T. Osmałek *et al.*, “Recent Advances in Polymer-Based Vaginal Drug Delivery Systems,” *Pharmaceutics*, vol. 13, no. 6, p. 884, 2021.

[28] M. I. Ugwoke, R. U. Agu, N. Verbeke, and R. Kinget, “Nasal mucoadhesive drug delivery: Background, applications, trends and future perspectives,” *Adv. Drug Deliv. Rev.*, vol. 57, no. 11, pp. 1640–1665, 2005.

[29] A. Ludwig, “The use of mucoadhesive polymers in ocular drug delivery,” *Adv. Drug Deliv. Rev.*, vol. 57, no. 11, pp. 1595–1639, 2005.

[30] H. Patil, R. V. Tiwari, and M. A. Repka, “Recent advancements in mucoadhesive floating drug delivery systems: A mini-review,” *J. Drug Deliv. Sci. Technol.*, vol. 31, pp. 65–71, 2016.

[31] S. Roy, K. Pal, A. Anis, K. Pramanik, and B. Prabhakar, “Polymers in mucoadhesive drug-delivery systems: A brief note,” *Des. Monomers Polym.*, vol. 12, no. 6, pp. 483–495, 2009.

[32] R. Anand and A. Kumar, “Significant biopolymers and their applications in buccal mediated drug delivery,” *J. Biomater. Sci. Polym. Ed.*, vol. 32, no. 9, pp. 1203–1218, 2021.

[33] V. Zargar, M. Asghari, and A. Dashti, “A Review on Chitin and Chitosan Polymers: Structure, Chemistry, Solubility, Derivatives, and Applications,” *ChemBioEng Rev.*, vol. 2, no. 3, pp. 204–226, 2015.

[34] A. Bernkop-Schnürch, A. H. Krauland, V. M. Leitner, and T. Palmberger, “Thiomers: Potential excipients for non-invasive peptide delivery systems,” *Eur. J. Pharm. Biopharm.*,

vol. 58, no. 2, pp. 253–263, 2004.

[35] A. Anitha, N. Deepa, K. P. Chennazhi, S. V Nair, H. Tamura, and R. Jayakumar, "Development of mucoadhesive thiolated chitosan nanoparticles for biomedical applications," *Carbohydr. Polym.*, vol. 83, no. 1, pp. 66–73, 2011.

[36] R. Sharma and M. Ahuja, "Thiolated pectin: Synthesis, characterization and evaluation as a mucoadhesive polymer," *Carbohydr. Polym.*, vol. 85, no. 3, pp. 658–663, 2011.

[37] S. Khalid *et al.*, "Thiolated sodium alginate conjugates for mucoadhesive and controlled release behavior of metformin microspheres," *Int. J. Biol. Macromol.*, vol. 164, pp. 2691–2700, 2020.

[38] H. Lee, S. M. Dellatore, W. M. Miller, and P. B. Messersmith, "Mussel-Inspired Surface Chemistry for Multifunctional Coatings," *Science (80-.).*, vol. 318, no. OCTOBER, pp. 426–431, 2007.

[39] K. Kim, K. Kim, J. Hyun, and H. Lee, "Biomaterials Chitosan-catechol : A polymer with long-lasting mucoadhesive properties," *Biomaterials*, vol. 52, pp. 161–170, 2015.

[40] N. Sahatsapan, T. Ngawhirunpat, T. Rojanarata, P. Opanasopit, and P. Patrojanasophon, "Catechol-Functionalized Alginate Nanoparticles as Mucoadhesive Carriers for Intravesical Chemotherapy," *AAPS PharmSciTech*, vol. 21, no. 6, pp. 1–9, 2020.

[41] C. Pornpitchanarong, T. Rojanarata, P. Opanasopit, T. Ngawhirunpat, and P. Patrojanasophon, "Catechol-modified chitosan/hyaluronic acid nanoparticles as a new avenue for local delivery of doxorubicin to oral cancer cells," *Colloids Surfaces B Biointerfaces*, vol. 196, no. May, p. 111279, 2020.

[42] M. Davidovich-Pinhas and H. Bianco-Peled, "Novel mucoadhesive system based on sulfhydryl-acrylate interactions," *J. Mater. Sci. Mater. Med.*, vol. 21, no. 7, pp. 2027–2034, 2010.

[43] M. Davidovich-Pinhas and H. Bianco-Peled, "Alginate-PEGAc: A new mucoadhesive polymer," *Acta Biomater.*, vol. 7, no. 2, pp. 625–633, 2011.

[44] X. Liang, M. Trentle, V. Kozlovskaya, E. Kharlampieva, and M. Bonizzoni, " Carbohydrate Sensing Using Water-Soluble Poly(methacrylic acid)- co -3-(Acrylamido)phenylboronic Acid Copolymer ," *ACS Appl. Polym. Mater.*, vol. 1, no. 6, pp. 1341–1349, 2019.

[45] S. Liu *et al.*, “Phenylboronic acid modified mucoadhesive nanoparticle drug carriers facilitate weekly treatment of experimentallyinduced dry eye syndrome,” *Nano Res.*, vol. 8, no. 2, pp. 621–635, 2015.

[46] O. M. Kolawole, W. M. Lau, and V. V. Khutoryanskiy, “Synthesis and Evaluation of Boronated Chitosan as a Mucoadhesive Polymer for Intravesical Drug Delivery,” *J. Pharm. Sci.*, vol. 108, no. 9, pp. 3046–3053, 2019.

[47] N. Sahatsapan, T. Rojanarata, T. Ngawhirunpat, P. Opanasopit, and P. Tonglairoum, “6-Maleimidohexanoic acid-grafted chitosan: A new generation mucoadhesive polymer,” *Carbohydr. Polym.*, vol. 202, no. May, pp. 258–264, 2018.

[48] Y. Shtenberg, M. Goldfeder, A. Schroeder, and H. Bianco-Peled, “Alginate modified with maleimide-terminated PEG as drug carriers with enhanced mucoadhesion,” *Carbohydr. Polym.*, vol. 175, pp. 337–346, 2017.

[49] M. Jelkmann *et al.*, “Chitosan: The One and Only? Aminated Cellulose as an Innovative Option for Primary Amino Groups Containing Polymers,” *Biomacromolecules*, vol. 19, no. 10, pp. 4059–4067, 2018.

[50] E. Baloğlu, M. Özyazici, S. Y. Hizarcioğlu, and H. A. Karavana, “An in vitro investigation for vaginal bioadhesive formulations: Bioadhesive properties and swelling states of polymer mixtures,” *Farmaco*, vol. 58, no. 5, pp. 391–396, 2003.

[51] S. A. Mortazavi and J. D. Smart, “An investigation of some factors influencing the in vitro assessment of mucoadhesion,” *Int. J. Pharm.*, vol. 116, no. 2, pp. 223–230, 1995.

[52] S. Steininger, “Synthesis and characterisation of mucoadhesive thiolated polymers,” vol. 194, pp. 239–247, 2000.

[53] K. V. R. Rao and P. Buri, “A novel in situ method to test polymers and coated microparticles for bioadhesion,” *Int. J. Pharm.*, vol. 52, no. 3, pp. 265–270, 1989.

[54] E. P. Kakoulides, J. D. Smart, and J. Tsibouklis, “Azocrosslinked poly(acrylic acid) for colonic delivery and adhesion specificity: In vitro degradation and preliminary ex vivo bioadhesion studies,” *J. Control. Release*, vol. 54, no. 1, pp. 95–109, 1998.

[55] D. Patel, J. R. Smith, A. W. Smith, N. Grist, P. Barnett, and J. D. Smart, “An atomic force microscopy investigation of bioadhesive polymer adsorption onto human buccal cells,” *Int. J.*

Pharm., vol. 200, no. 2, pp. 271–277, 2000.

[56] C. M. Lehr, J. A. Bouwstra, J. J. Tukker, and H. E. Junginger, "Intestinal transit of bioadhesive microspheres in an in situ loop in the rat-A comparative study with copolymers and blends based on poly(acrylic acid)," *J. Control. Release*, vol. 13, no. 1, pp. 51–62, 1990.

[57] E. E. Hassan and J. M. Gallo, "A Simple Rheological Method for the in Vitro Assessment of Mucin-Polymer Bioadhesive Bond Strength," *Pharmaceutical Research: An Official Journal of the American Association of Pharmaceutical Scientists*, vol. 7, no. 5. pp. 491–495, 1990.

[58] M. M. Patel, J. D. Smart, T. G. Nevell, R. J. Ewen, P. J. Eaton, and J. Tsibouklis, "Mucin/poly(acrylic acid) interactions: A spectroscopic investigation of mucoadhesion," *Biomacromolecules*, vol. 4, no. 5, pp. 1184–1190, 2003.

[59] J. Xiang and X. Li, "Novel mucoadhesive polymer: Synthesis and mucoadhesion of poly[acrylic acid-co-poly(ethylene glycol) monomethylether monomethacrylate-co-dimethylaminoethyl methacrylate]," *J. Appl. Polym. Sci.*, vol. 94, no. 6, pp. 2431–2437, 2004.

[60] C. Li, P. P. Bhatt, and T. P. Johnston, "Evaluation of a mucoadhesive buccal patch for delivery of peptides: In vitro screening of bioadhesion," *Drug Dev. Ind. Pharm.*, vol. 24, no. 10, pp. 919–926, 1998.

[61] J. Shen, Y. Wang, Q. Ping, Y. Xiao, and X. Huang, "Mucoadhesive effect of thiolated PEG stearate and its modified NLC for ocular drug delivery," *J. Control. Release*, vol. 137, no. 3, pp. 217–223, 2009.

[62] M. Shin, K. Kim, W. Shim, J. W. Yang, and H. Lee, "Tannic Acid as a Degradable Mucoadhesive Compound," 2016.

[63] H. Hsein, G. Garrait, E. Beyssac, and V. Hoffart, "Whey protein mucoadhesive properties for oral drug delivery: Mucin-whey protein interaction and mucoadhesive bond strength," *Colloids Surfaces B Biointerfaces*, vol. 136, pp. 799–808, 2015.

[64] N. Thirawong, R. A. Kennedy, and P. Sriamornsak, "Viscometric study of pectin-mucin interaction and its mucoadhesive bond strength," *Carbohydr. Polym.*, vol. 71, no. 2, pp. 170–179, 2008.

[65] A. Chakrabarty and Y. Teramoto, "Recent advances in nanocellulose composites with polymers: A guide for choosing partners and how to incorporate them," *Polymers (Basel).*,

vol. 10, no. 5, 2018.

[66] M. R. Vakili *et al.*, “Development of mucoadhesive hydrogels based on polyacrylic acid grafted cellulose nanocrystals for local cisplatin delivery,” *Carbohydr. Polym.*, vol. 255, no. October 2020, p. 117332, 2021.

[67] K. Kim *et al.*, “TAPE: A medical adhesive inspired by a ubiquitous compound in plants,” *Adv. Funct. Mater.*, vol. 25, no. 16, pp. 2402–2410, 2015.

[68] J. M. McRae and J. A. Kennedy, “Wine and grape tannin interactions with salivary proteins and their impact on astringency: A review of current research,” *Molecules*, vol. 16, no. 3, pp. 2348–2364, 2011.

[69] M. Shin, J. H. Ryu, J. P. Park, K. Kim, J. W. Yang, and H. Lee, “DNA/tannic acid hybrid gel exhibiting biodegradability, extensibility, tissue adhesiveness, and hemostatic ability,” *Adv. Funct. Mater.*, vol. 25, no. 8, pp. 1270–1278, 2015.

[70] M. Tavares-dias, “Living Resources Current knowledge on use of essential oils as alternative treatment against fi sh parasites,” 2018.

[71] K. L. Shephard, “Mucus on the epidermis of fish and its influence on drug delivery,” *Adv. Drug Deliv. Rev.*, vol. 11, no. 3, pp. 403–417, 1993.

[72] A. C. d. S. Costa *et al.*, “Mucoadhesive nanoparticles: A new perspective for fish drug application,” *J. Fish Dis.*, vol. 39, no. 4, pp. 503–506, 2016.

[73] I. Charlie-Silva *et al.*, “Nanoparticle mucoadhesive system as a new tool for fish immune system modulation,” *Fish Shellfish Immunol.*, vol. 80, no. January, pp. 651–654, 2018.

[74] A. L. Ferreira *et al.*, “Chitosan-coated zein nanoparticles containing eugenol potentiates anesthesia in Nile tilapia,” *Aquaculture*, vol. 529, no. April, p. 735659, 2020.

[75] S. Kitiyodom *et al.*, “Modulation of the mucosal immune response of red tilapia (Oreochromis sp.) against columnaris disease using a biomimetic-mucoadhesive nanovaccine,” *Fish Shellfish Immunol.*, vol. 112, no. December 2020, pp. 81–91, 2021.

[76] J. Ji, D. Torrealba, À. Ruyra, and N. Roher, “Nanodelivery systems as new tools for immunostimulant or vaccine administration: Targeting the fish immune system,” *Biology (Basel).*, vol. 4, no. 4, pp. 664–696, 2015.

[77] P. Phanthong, P. Reubroycharoen, X. Hao, G. Xu, A. Abudula, and G. Guan, “Nanocellulose: Extraction and application,” *Carbon Resour. Convers.*, vol. 1, no. 1, pp. 32–43, 2018.

[78] Z. Hu, R. M. Berry, R. Pelton, and E. D. Cranston, “One-Pot Water-Based Hydrophobic Surface Modi fi cation of Cellulose Nanocrystals Using Plant Polyphenols,” 2017.

[79] P. B. Messersmith, T. S. Sileika, D. G. Barrett, R. Zhang, and K. H. A. Lau, “Colorless Multifunctional Coatings Inspired by Polyphenols Found in Tea, Chocolate, and Wine,” 2013.

[80] Z. Fu and R. Chen, “Study of complexes of tannic acid with Fe(III) and Fe(II),” *J. Anal. Methods Chem.*, vol. 2019, 2019.

[81] S. P. Akhlaghi, R. C. Berry, and K. C. Tam, “Surface modification of cellulose nanocrystal with chitosan oligosaccharide for drug delivery applications,” *Cellulose*, vol. 20, no. 4, pp. 1747–1764, 2013.

[82] A. Bernkop-schnürch and S. Dünnhaupt, “European Journal of Pharmaceutics and Biopharmaceutics Chitosan-based drug delivery systems,” vol. 81, pp. 463–469, 2012.

[83] A. R. Narkar, E. Cannon, H. Yildirim-Alicea, and K. Ahn, “Catechol-Functionalized Chitosan: Optimized Preparation Method and Its Interaction with Mucin,” *Langmuir*, vol. 35, no. 48, pp. 16013–16023, 2019.

[84] K. Kim, J. H. Ryu, D. Y. Lee, and H. Lee, “Bio-inspired catechol conjugation converts water-insoluble chitosan into a highly water-soluble, adhesive chitosan derivative for hydrogels and LbL assembly,” *Biomater. Sci.*, vol. 1, no. 7, pp. 783–790, 2013.

[85] L. Dong *et al.*, “Poly(diallyldimethylammonium chloride)-cellulose nanocrystals supported Au nanoparticles for nonenzymatic glucose sensing,” *RSC Adv.*, vol. 6, no. 8, pp. 6436–6442, 2016.

[86] S. Parinaz, A. Richard, and K. C. Tam, “Surface modification of cellulose nanocrystal with chitosan oligosaccharide for drug delivery applications,” pp. 1747–1764, 2013.

[87] J. Wang, Y. Tabata, D. Bi, and K. Morimoto, “Evaluation of gastric mucoadhesive properties of aminated gelatin microspheres,” *J. Control. Release*, vol. 73, no. 2–3, pp. 223–231, 2001.

[88] B. Á. Szilágyi, A. Mammadova, B. Gyarmati, and A. Szilágyi, “Mucoadhesive interactions between synthetic polyaspartamides and porcine gastric mucin on the colloid size scale,” *Colloids Surfaces B Biointerfaces*, vol. 194, no. June, p. 111219, 2020.

[89] Y. A. Albarkah, R. J. Green, and V. V. Khutoryanskiy, “Probing the Mucoadhesive Interactions between Porcine Gastric Mucin and Some Water-Soluble Polymers,” *Macromol. Biosci.*, vol. 15, no. 11, pp. 1546–1553, 2015.